Mathematics and Computers in Simulation 249 (2026) 744–783

Contents lists available at ScienceDirect

Mathematics and Computers in Simulation

journal homepage: www.elsevier.com/locate/matcom

Original articles

Well-posedness and adaptive mesh FEM for the blow-up solution to the time-fractional Keller–Segel system

Dingding Cao [a,b], Changpin Li [a,*], Paul Andries Zegeling [b]

[a] Department of Mathematics, Shanghai University, Shanghai 200444, China
[b] Department of Mathematics, Utrecht University, 3584 CD Utrecht, The Netherlands

ARTICLE INFO

Keywords:
Caputo–Hadamard derivative
Keller–Segel system
Blow-up
Adaptive mesh method
Moving mesh
Fractional chemotaxis system

ABSTRACT

This paper deals with well-posedness and blow-up of Caputo–Hadamard time-fractional Keller–Segel system. In order to enhance the simulation of the blow-up solution, two adaptive mesh methods are proposed, where the intrinsic characteristics of solutions to single-point and multi-point two-dimensional blow-up problems are incorporated. By constructing auxiliary functions and employing moving mesh strategies, adaptive meshes can be pre-generated and adjusted. Numerical experiments show the effectiveness of the methods.

1. Introduction

Chemotaxis is the directed movement of a group of cells or a population in response to chemical gradients. The Keller–Segel model, first proposed in the 1970s by Keller and Segel [1], plays a foundational role in the mathematical modeling of chemotaxis. It characterizes the movement and aggregation behavior of organisms such as slime molds in response to chemical gradients. The solution of the Keller–Segel system can develop sharp structures and may exhibit finite time blow-up patterns within small regions of the domain. Chemical attractants can either be sourced from the environment or generated internally within organisms [2]. However, the assumption of an instantaneous response to stimuli in this model overlooks the possibility of memory effects and delayed reactions, which are common in biological processes.

Increasing attention has been directed toward fractional derivatives in recent mathematical modeling, as they effectively describe memory-related behavior and spacial non-locality. By extending the order of differentiation and integration to real and even complex numbers, fractional calculus offers an efficient tool for capturing memory effects, non-local interactions, and anomalous diffusion in complex systems [3–5]. These features are especially relevant in chemotaxis, where cellular responses to chemical signals depend on both present and past stimuli. The development of fractional analysis for the Keller–Segel model, together with its variants, is driven by both the mathematical analysis and its potential importance for enhancing our understanding of certain biological processes.

In this paper, we consider the Caputo–Hadamard time-fractional Keller–Segel model

$$\begin{cases} {}_{C\!H}\mathrm{D}^{\alpha}_{a,t}u = \Delta u - \nabla\cdot(u\nabla v), & x\in\Omega,\ t>a>0,\\ {}_{C\!H}\mathrm{D}^{\alpha}_{a,t}v = \Delta v - \gamma v + u, & x\in\Omega,\ t>a>0, \end{cases} \tag{1.1}$$

in a bounded domain $\Omega\subseteq\mathbb{R}^N$, $N\geq 2$, with smooth boundary $\partial\Omega$, subject to the homogeneous Neumann boundary conditions

$$\frac{\partial u}{\partial \mathbf{n}} = \frac{\partial v}{\partial \mathbf{n}} = 0, \quad x\in\partial\Omega,\ t>a>0 \tag{1.2}$$

* Corresponding author.
E-mail address: lcp@shu.edu.cn (C. Li).

https://doi.org/10.1016/j.matcom.2026.05.040
Received 23 November 2025; Received in revised form 23 May 2026; Accepted 29 May 2026
Available online 6 June 2026
0378-4754/© 2026 International Association for Mathematics and Computers in Simulation (IMACS). Published by Elsevier B.V. All rights are reserved, including those for text and data mining, AI training, and similar technologies.

and the initial conditions

$$u(\mathrm{x},a)=u_a(\mathrm{x}),\quad v(\mathrm{x},a)=v_a(\mathrm{x}),\quad \mathrm{x}\in\Omega, \tag{1.3}$$

where $\frac{\partial}{\partial \mathbf{n}}$ denotes the exterior normal derivative on $\partial\Omega$, and $a\in\mathbb{R}^+$ is the starting time. The operator ${}_{CH}\mathrm{D}^{\alpha}_{a,t}$ is the Caputo–Hadamard fractional derivative one of order $\alpha\in(0,1)$, which will be introduced later. The parameter $\gamma\geq 0$ is the decay rate of attractant, and the term $-\gamma v$ denotes the degradation of the attractant, $u(\mathrm{x},t)$ represents the density of cells at the point $\mathrm{x}\in\Omega$ at time t, while $v(\mathrm{x},t)$ is the concentration of the chemoattractant. The first equation includes a diffusion term representing the random Brownian motion of cells and a chemotactic drift term accounting for directed movement along chemical gradients. The terms in the second equation express the diffusion and production of attractant over time. For detailed background and derivation, see [1,6].

As far as we know, studies of fractional chemotaxis models appeared in the last decade. Azevedo et al. [7] proved an existence result of the time-fractional Keller–Segel system with small initial data in Besov-Morrey spaces. Self-similar solution was obtained, and asymptotic behavior was also analyzed. Cuevas et al. [8] studied the global existence, regularity, and long-time behavior of the solution to the Caputo time-fractional Keller–Segel model. Akilandeeswari and Tyagi [9] proved the existence of nonnegative weak solutions for the time-fractional Keller–Segel system under Dirichlet boundary conditions within a bounded domain. Tuan et al. [10] considered the time-fractional Keller–Segel model (in a bounded domain) and the space–time fractional Keller–Segel model (in $\mathbb{R}^N$), and established the global well-posedness of the solution in a Besov space, as well as the existence and uniqueness of a mild solution in a Hilbert space. Costa et al. [11] investigated the well-posedness and blow-up behavior of the time-fractional Keller–Segel chemotaxis model in Lebesgue and Besov spaces, considering homogeneous Neumann boundary conditions in a smooth domain. Jiang and Wang [12] studied the Cauchy problem for time–space fractional Keller–Segel–Navier–Stokes model in $\mathbb{R}^N$ ($N\geq 2$), and established the existence and the asymptotic in L^p space. Gao et al. [13] investigated the global existence and uniform boundedness in L^∞ of weak solutions to a space–time fractional parabolic–elliptic Keller–Segel system with logistic source terms. However, there are few relevant literature on numerical methods for fractional chemotaxis models, especially for the model with the time-fractional Caputo–Hadamard derivative. This paper is devoted to the theoretical analyzing and numerical computing model (1.1) with initial and boundary conditions (1.2) and (1.3).

Solving the Keller–Segel system on a uniform mesh may not be a good choice due to the presence of sharp gradients in certain regions of the physical domain. Therefore, employing the adaptive mesh method is essential for solving this type of partial differential equations (PDEs) more efficiently. The moving mesh method is one of adaptive mesh methods, where a critical aspect of mesh adaptation involves controlling the shape, size, and orientation of mesh elements, thereby controlling the error in the physical solution of PDEs [14]. It can be used as the response to some structure of the solution of a PDE [15]. The moving mesh method involves constructing a mapping from a computational (or logical) domain to the physical domain. In this process, the calculation typically begins with a uniform mesh, and the mesh points are subsequently adjusted during the solution process, while maintaining the mesh topology and the total number of mesh points. The locations or velocities of the mesh points are then determined by solving a system of moving mesh equations.

The movement strategies primarily lie in two aspects: defining the optimal mesh geometry (shape) and determining how to adjust the mesh to achieve this ideal shape. Optimal mesh geometry is often characterized using equidistribution measures derived from the PDE-based monitor functions or via variational principles. When employing these strategies, it is essential to carefully avoid mesh tangling while maintaining mesh regularity and isotropy. These techniques enable the movement of mesh points to align with the natural structures of the physical equations [15]. For one-dimensional problems, both the theory and practical techniques for generating meshes and solving PDEs on moving grids have become well-developed and widely adopted. However, in the higher-dimensional case, significant challenges still remain regarding mesh movement and the discretization of PDEs.

If the initial data are radially symmetric in $\mathbb{R}^2$, the solution of the Keller–Segel system tends to preserve this symmetry. This allows for the early identification of blow-up locations based on initial conditions. From this insight, we design two moving mesh methods for single-point and multi-point blow-up problems. One method involves the use of moving graded meshes, which are characterized by their alignment along the spacial coordinate directions. Another method employs auxiliary functions and the rezoning approach [14] to generate adaptive meshes. In this approach, an adaptive mesh is constructed through a coordinate transformation from the computational domain Ω to the physical domain Ω_c. This transformation is designed to minimize a meshing functional, thereby optimizing the mesh. One benefit of this approach is the ability to incorporate mesh qualities like smoothness, flexibility, and alignment into the functional formulation [16]. Additionally, auxiliary functions are utilized to replace solutions of physical equations, improving the flexibility and efficiency of the traditional moving mesh method.

The remainder of this paper is structured as follows. Section 2 introduces the essential definitions and properties of fractional derivatives, with an emphasis on the Caputo–Hadamard type, and details the L1 discretization scheme employed in our numerical method. In Section 3, we prove the existence and uniqueness of L^q-mild solution to the Caputo–Hadamard fractional Keller–Segel system. Moreover, we characterize the conditions of the appearance of the finite time blow-up solution. Section 4 is devoted to the computational method and numerical calculations: the first part conducts a finite element analysis on the fixed spatial meshes, while the second part develops two moving mesh strategies and outlines the discretization of the system on these adaptive meshes. Section 5 presents numerical experiments to validate the accuracy and efficiency of the proposed methods and to examine the key factors affecting the blow-up time.

2. Preliminaries

In the current section, several necessary definitions are introduced. The Hadamard-type (fractional) integral and derivatives are introduced as follows.

Definition 2.1 ([4,5]). The Hadamard integral of order α ($\alpha > 0$) of a given function $f(x) \in L^1(a,b)$ with $a > 0$ is defined as

$$ {}_H\mathrm{D}_{a,t}^{-\alpha} f(t) = \frac{1}{\Gamma(\alpha)} \int_a^t (\log t - \log \tau)^{\alpha-1} f(\tau) \frac{\mathrm{d}\tau}{\tau}, \ t > a. $$

Here, log is the natural logarithm (same below).

Definition 2.2 ([4,5]). The Hadamard derivative of order $\alpha \in (0,1)$ of a given function $f(t) \in AC_\delta^1[a,b]$ with $a > 0$ is defined as

$$ {}_H\mathrm{D}_{a,t}^{\alpha} f(t) = \frac{1}{\Gamma(1-\alpha)} \delta \int_a^t \left(\log \frac{t}{\tau}\right)^{-\alpha} f(\tau) \frac{\mathrm{d}\tau}{\tau}, \ t > a, $$

where $\delta = t\frac{\mathrm{d}}{\mathrm{d}t}$.

Definition 2.3 ([4,5]). The Caputo–Hadamard derivative of order $\alpha \in (0,1)$ of a given function $f(t) \in AC_\delta^1[a,b]$ with $a > 0$ is defined as

$$ {}_{CH}\mathrm{D}_{a,t}^{\alpha} f(t) = \frac{1}{\Gamma(1-\alpha)} \int_a^t \left(\log \frac{t}{\tau}\right)^{-\alpha} \delta f(\tau) \frac{\mathrm{d}\tau}{\tau}, \ t > a, $$

where $\delta = \tau\frac{\mathrm{d}}{\mathrm{d}\tau}$.

The Hadamard and Caputo–Hadamard derivatives are not equivalent either. From an application aspect, the Caputo–Hadamard derivatives are often used in the evolution equations to characterize superslow diffusion [5]. The Laplace transform of the Caputo–Hadamard fractional derivative will be presented below, which will be employed in the derivation of the mild solution to the system of equations.

Definition 2.4 ([17]). For $|f(t)| \le M t^{\log \frac{\gamma}{a}}$, where M is a positive constant and $\gamma > a\,(>0)$, the amended Laplace transform and the inverse amended Laplace transform of $f(t)$ as follows,

$$ \bar{f}(\omega) = \mathscr{L}_a[f(t),\omega] := \int_a^\infty \mathrm{e}^{-\log \frac{\omega}{a} \log \frac{t}{a}} f(t) \frac{\mathrm{d}t}{t}, \quad a > 0, \ \mathrm{Re}(\omega) > \gamma, $$

$$ f(t) = \mathscr{L}_a^{-1}[\bar{f}(\omega),t] := \frac{1}{2\pi i} \int_{c-i\infty}^{c+i\infty} \mathrm{e}^{\log \frac{\omega}{a} \log \frac{t}{a}} \bar{f}(\omega) \frac{\mathrm{d}\omega}{\omega}, \quad a > 0, \ c = \mathrm{Re}(\omega) > \gamma. $$

Here, e denotes the base of the natural logarithm, and we use this notation consistently throughout the paper.

The convolution of $f(t)$ and $g(t)$ is defined as

$$ f(t) * g(t) = \int_a^t f\left(a\frac{t}{\tau}\right) g(\tau) \frac{\mathrm{d}\tau}{\tau}, $$

then

$$ \mathscr{L}_a\{f(t) * g(t)\} = \mathscr{L}_a[f(t),\omega]\mathscr{L}_a[g(t),\omega] = \bar{f}(\omega)\bar{g}(\omega). $$

It immediately follows that

$$ \mathscr{L}_a\left[{}_H\mathrm{D}_{a,t}^{-\alpha} f(t),\omega\right] = \mathscr{L}_a\left[\frac{1}{\Gamma(\alpha)}\left(\log\frac{t}{a}\right)^{\alpha-1} * f(t),\omega\right] = \left(\log\frac{\omega}{a}\right)^{-\alpha} \bar{f}(\omega). $$

And it is not difficult to get the amended Laplace transform of the Caputo–Hadamard derivative of order $\alpha \in (0,1)$ of $f(t)$ as follows

$$ \begin{aligned} \mathscr{L}_a\left[{}_{CH}\mathrm{D}_{a,t}^{\alpha} f(t),\omega\right] &= \mathscr{L}_a\left[{}_H\mathrm{D}_{a,t}^{-(1-\alpha)} \delta f(t),\omega\right] \\ &= \left(\log\frac{\omega}{a}\right)^{\alpha} \bar{f}(\omega) - \left(\log\frac{\omega}{a}\right)^{\alpha-1} f(a). \end{aligned} $$

The Mittag-Leffler function has the expression

$$ E_{\alpha,\beta}(z) := \sum_{k=0}^{\infty} \frac{z^k}{\Gamma(\alpha k + \beta)}, \quad z \in \mathbb{C}, $$

where $\alpha > 0$ and $\beta \in \mathbb{R}$ are arbitrary constants. Obviously, $E_{\alpha,1}(z) = E_\alpha(z)$. For $\eta \ge 0$ and $0 < \alpha < 1$, $E_{\alpha,\alpha}(-\eta) \ge 0$.

The amended Laplace transform of the Mittag-Leffler function was given in [17]

$$\int_a^{\infty} \mathrm{e}^{-\log\frac{\omega}{a}\log\frac{s}{a}} \left(\log\frac{s}{a}\right)^{\alpha k+\beta-1} E_{\alpha,\beta}^{(k)}\left(\pm\xi\left(\log\frac{s}{a}\right)^{\alpha}\right)\frac{\mathrm{d}s}{s} = \frac{k!\left(\log\frac{\omega}{a}\right)^{\alpha-\beta}}{\left(\left(\log\frac{\omega}{a}\right)^{\alpha}\mp\xi\right)^{k+1}}, \quad \mathrm{Re}(\omega) > |\xi|^{\frac{1}{\alpha}}.$$

Several approximation schemes for the Caputo–Hadamard fractional derivative have been developed, including the L1, L1-2, and L2-1$_\sigma$ formulas. We provide a discrete formula for the Caputo–Hadamard derivative with $0 < \alpha < 1$. For a given positive number $T > a$, we divide the interval $[a, T]$ into N subintervals such that $a = t_0 < t_1 < \cdots < t_{k-1} < t_k < \cdots < t_N = T$ with the uniform stepsize $\tau = t_k - t_{k-1}, 1 \le k \le N$.

At $t = t_k, 1 \le k \le N$, there holds:

$$\begin{aligned}
{}_{CH}\mathrm{D}_{a,t}^{\alpha} g(t)\Big|_{t=t_k} &= \frac{1}{\Gamma(1-\alpha)}\int_a^{t_k}\left(\log\frac{t_k}{s}\right)^{-\alpha}\delta g(s)\frac{\mathrm{d}s}{s} \\
&= \frac{1}{\Gamma(1-\alpha)}\sum_{j=1}^{k}\int_{t_{j-1}}^{t_j}\left(\log\frac{t_k}{s}\right)^{-\alpha}\delta g(s)\frac{\mathrm{d}s}{s} \\
&= \frac{1}{\Gamma(1-\alpha)}\sum_{j=1}^{k}\frac{g\left(t_j\right)-g\left(t_{j-1}\right)}{\log\frac{t_j}{t_{j-1}}}\int_{t_{j-1}}^{t_j}\left(\log\frac{t_k}{s}\right)^{-\alpha}\frac{\mathrm{d}s}{s} + R^k \\
&= \sum_{j=1}^{k} a_{j,k}\left(g\left(t_j\right)-g\left(t_{j-1}\right)\right) + R^k \\
&= \sum_{j=0}^{k} b_{k-j,k}\, g\left(t_j\right) + R^k,
\end{aligned} \tag{2.1}$$

where

$$a_{j,k} = \frac{1}{\Gamma(2-\alpha)}\frac{1}{\log\frac{t_j}{t_{j-1}}}\left(\left(\log\frac{t_k}{t_{j-1}}\right)^{1-\alpha} - \left(\log\frac{t_k}{t_j}\right)^{1-\alpha}\right),$$

$$b_{k-j,k} = \begin{cases} -a_{1,k}, & j = 0, \\ a_{j,k} - a_{j+1,k}, & j = 1, 2, \ldots, k-1, \\ a_{k,k}, & j = k, \end{cases}$$

and

$$R^k = \frac{1}{\Gamma(1-\alpha)}\sum_{j=1}^{k}\int_{t_{j-1}}^{t_j}\left(\log\frac{t_k}{s}\right)^{-\alpha}\left(\delta g(s) - \frac{g\left(t_j\right)-g\left(t_{j-1}\right)}{\log\frac{t_j}{t_{j-1}}}\right)\frac{\mathrm{d}s}{s}.$$

We denote

$${}_{CH}\mathfrak{D}_{a,t}^{\alpha} g(t) = \sum_{j=0}^{k} b_{k-j,k}\, g\left(t_j\right). \tag{2.2}$$

Then, this can be regarded as an L1 formula for Caputo–Hadamard derivative. Here, we use the font ${}_{CH}\mathfrak{D}_{a,t}^{\alpha}$ to strictly distinguish the discrete operator from the continuous derivative ${}_{CH}\mathrm{D}_{a,t}^{\alpha}$.

Lemma 2.1 ([18]). *For $0 < \alpha < 1$, the coefficients $a_{j,k} (1 \le j \le k, 1 \le k \le N)$ in (2.1) satisfy*

$$a_{k,k} > a_{k-1,k} > \cdots > a_{j,k} > a_{j-1,k} > \cdots > a_{1,k} > 0.$$

Lemma 2.2 ([18]). *If $0 < \alpha < 1$, $g(t) \in C^2[a, T]$, then the local truncation error for (2.1) is given by*

$$\left|R^k\right| \le C\tau^{2-\alpha}.$$

3. Solution and its properties

We consider the negative Neumann Laplacian $-\Delta$ in a bounded domain $\Omega \subseteq \mathbb{R}^N$. For $p \in (1, \infty)$, let A be the realization of the operator $-\Delta$ with the homogeneous Neumann boundary condition in $L^p(\Omega)$ [19], i.e.

$$D(A) = \left\{\phi \in W^{2,p}(\Omega);\ \frac{\partial\phi}{\partial\mathbf{n}} = 0 \text{ on } \partial\Omega\right\} := W_N^{2,p}(\Omega),$$
$$A\phi = -\Delta\phi \text{ for } \phi \in W_N^{2,p}(\Omega).$$

For $p \in (1,\infty)$, the sectorial operator $-A$ generates an analytic semigroup $\{G(s) := e^{-sA}\}_{s\geq 0}$. The semigroup $\{G(s)\}_{s\geq 0}$ and its several $L^p - L^q$ estimates serve as a fundamental basis for developing the existence theory. Let $1 \leq p \leq q \leq \infty$ and $u \in L^p(\Omega)$, we have

$$\|G(s)u\|_{L^q(\Omega)} \leq Cs^{-\frac{N}{2}(\frac{1}{p}-\frac{1}{q})}\|u\|_{L^p(\Omega)}, \quad s \in (0,1). \tag{3.1}$$

Here, s represents a generic time variable for the semigroup, distinct from the physical time variable $t > a$ in model (1.1). We have also that

$$\|G(s)u\|_{L^q(\Omega)} \leq C\left(1 + s^{-\frac{N}{2}\left(\frac{1}{p}-\frac{1}{q}\right)}\right)\|u\|_{L^p(\Omega)}, \quad s > 0. \tag{3.2}$$

It is indeed important to highlight that the divergence operator $\nabla\cdot$ does generally not commute with the exponential operator $e^{s\Delta}$. For all $w \in L^p(\Omega)$ and $1 < p \leq q < \infty$, one has

$$\|G(s)\nabla\cdot w\|_{L^q(\Omega)} \leq C\left(1 + s^{-\frac{1}{2}-\frac{N}{2}\left(\frac{1}{p}-\frac{1}{q}\right)}\right)e^{-\lambda_1 s}\|w\|_{L^p(\Omega)}, \quad s > 0, \tag{3.3}$$

where $\lambda_1 > 0$ denotes the first nonzero eigenvalue of $-\Delta$ with homogeneous Neumann boundary conditions. Let $1 \leq p \leq q \leq +\infty$. Then, for all $u \in L^p(\Omega)$, we have

$$\|\nabla G(s)u\|_{L^q(\Omega)} \leq C\left(1 + s^{-\frac{N}{2}\left(\frac{1}{p}-\frac{1}{q}\right)-\frac{1}{2}}\right)e^{-\lambda_1 s}\|u\|_{L^p(\Omega)}, \quad s > 0. \tag{3.4}$$

Let $w \in W^{1,p}(\Omega)$. If $2 \leq p < \infty$, then

$$\|\nabla G(s)w\|_{L^p(\Omega)} \leq Ce^{-\lambda_1 s}\|\nabla w\|_{L^p(\Omega)}, \quad s > 0. \tag{3.5}$$

Estimates (3.1)–(3.5) and their proofs can be found in [11,20]. It should be noted that the variable $s \in (0,1)$ in the above inequalities will merely act as a generic variable. In the subsequent proofs, it will be replaced by the logarithmic term $\log(t/a)$, and these substitutions are rigorously justified.

3.1. L^q-mild solution

We first derive the mild solution of the system (1.1) through integral transformation. Applying the Hadamard integral of order α on both sides of Eq. (1.1), one gets

$$\begin{cases} u(t) = u_a + \dfrac{1}{\Gamma(\alpha)}\displaystyle\int_a^t \left(\log\frac{t}{s}\right)^{\alpha-1}\Delta u(s)\frac{\mathrm{d}s}{s} - \frac{1}{\Gamma(\alpha)}\int_a^t \left(\log\frac{t}{s}\right)^{\alpha-1}\nabla\cdot(u\nabla v)(s)\frac{\mathrm{d}s}{s}, \\ v(t) = v_a + \dfrac{1}{\Gamma(\alpha)}\displaystyle\int_a^t \left(\log\frac{t}{s}\right)^{\alpha-1}\Delta v(s)\frac{\mathrm{d}s}{s} - \frac{1}{\Gamma(\alpha)}\int_a^t \left(\log\frac{t}{s}\right)^{\alpha-1}(\gamma v - u)(s)\frac{\mathrm{d}s}{s}. \end{cases}$$

Through the modified Laplace transform, one obtains

$$\begin{cases} \mathscr{L}_a(u)(\lambda) = \dfrac{u_a}{\log\frac{\lambda}{a}} + \left(\log\frac{\lambda}{a}\right)^{-\alpha}\Delta\mathscr{L}_a(u)(\lambda) - \left(\log\frac{\lambda}{a}\right)^{-\alpha}\mathscr{L}_a(\nabla\cdot(u\nabla v))(\lambda), \\ \mathscr{L}_a(v)(\lambda) = \dfrac{v_a}{\log\frac{\lambda}{a}} + \left(\log\frac{\lambda}{a}\right)^{-\alpha}(\Delta-\gamma)\mathscr{L}_a(v)(\lambda) + \left(\log\frac{\lambda}{a}\right)^{-\alpha}\mathscr{L}_a u(\lambda). \end{cases}$$

By arranging the equations, one has

$$\begin{cases} \mathscr{L}_a(u)(\lambda) = \left(\log\frac{\lambda}{a}\right)^{\alpha-1}\left[\left(\log\frac{\lambda}{a}\right)^{\alpha} - \Delta\right]^{-1}u_a - \left[\left(\log\frac{\lambda}{a}\right)^{\alpha} - \Delta\right]^{-1}\mathscr{L}_a(\nabla\cdot(u\nabla v))(\lambda), \\ \mathscr{L}_a(v)(\lambda) = \left(\log\frac{\lambda}{a}\right)^{\alpha-1}\left[\left(\log\frac{\lambda}{a}\right)^{\alpha} - (\Delta-\gamma)\right]^{-1}v_a + \left[\left(\log\frac{\lambda}{a}\right)^{\alpha} - (\Delta-\gamma)\right]^{-1}\mathscr{L}_a u(\lambda). \end{cases}$$

Applying the modified inverse Laplace transform gives

$$\begin{cases} u(t) = E_\alpha\left(\left(\log\frac{t}{a}\right)^{\alpha}\Delta\right)u_a - \displaystyle\int_a^t\left(\log\frac{t}{s}\right)^{\alpha-1}\nabla\cdot E_{\alpha,\alpha}\left(\left(\log\frac{t}{s}\right)^{\alpha}\Delta\right)(u\nabla v)(s)\frac{\mathrm{d}s}{s}, \\ v(t) = E_\alpha\left(\left(\log\frac{t}{a}\right)^{\alpha}(\Delta-\gamma)\right)v_a - \displaystyle\int_a^t\left(\log\frac{t}{s}\right)^{\alpha-1}E_{\alpha,\alpha}\left(\left(\log\frac{t}{s}\right)^{\alpha}(\Delta-\gamma)\right)u(s)\frac{\mathrm{d}s}{s}. \end{cases} \tag{3.6}$$

Consider the Wright-type function [19,21]

$$M_\alpha(z) := \sum_{n=0}^{\infty}\frac{(-z)^n}{n!\Gamma(-\alpha n + 1 - \alpha)} = \frac{1}{\pi}\sum_{n=1}^{\infty}\frac{(-z)^n}{(n-1)!}\Gamma(n\alpha)\sin(n\pi\alpha), \quad z \in \mathbb{C}.$$

For $0 < \alpha < 1$, the Wright-type function satisfies the following properties:

$$M_\alpha(\theta) \geq 0, \quad \theta > 0,$$

$$\int_0^\infty M_\alpha(\theta)\mathrm{d}\theta = 1,$$

and

$$\int_0^\infty \theta^r M_\alpha(\theta)\mathrm{d}\theta = \frac{\Gamma(1+r)}{\Gamma(1+\alpha r)}, \quad -1 < r < \infty. \tag{3.7}$$

The Mittag-Leffler operators can be expressed as the following integral formulas,

$$\begin{aligned}
E_\alpha\left((\log\tfrac{t}{a})^\alpha \Delta\right) &= \int_0^\infty M_\alpha(s) G\left(s(\log\tfrac{t}{a})^\alpha\right)\mathrm{d}s,\\
E_{\alpha,\alpha}\left((\log\tfrac{t}{a})^\alpha \Delta\right) &= \int_0^\infty \alpha s M_\alpha(s) G\left(s(\log\tfrac{t}{a})^\alpha\right)\mathrm{d}s,\\
E_\alpha\left((\log\tfrac{t}{a})^\alpha (\Delta-\gamma)\right) &= \int_0^\infty M_\alpha(s) G_\gamma\left(s(\log\tfrac{t}{a})^\alpha\right)\mathrm{d}s,\\
E_{\alpha,\alpha}\left((\log\tfrac{t}{a})^\alpha (\Delta-\gamma)\right) &= \int_0^\infty \alpha s M_\alpha(s) G_\gamma\left(s(\log\tfrac{t}{a})^\alpha\right)\mathrm{d}s.
\end{aligned}$$

Here, $G_\gamma(t) = \mathrm{e}^{-t\gamma}G(t)$ for $t > 0$ denotes the damped heat semigroup. These operators are strongly continuous in $L^r(\Omega)$ for $1 \leq r < \infty$. The corresponding proofs will be provided in the next section.

Definition 3.1. A pair of continuous functions $(u, v) : [a, T] \to (L^q(\Omega))^2$ is called an L^q-mild solution to the time-fractional Keller–Segel model (1.1)–(1.3) if it satisfies (3.6).

3.2. Well-posedness and blow-up

Lemma 3.1. *The operator families* $\left(E_\alpha\left((\log\frac{t}{a})^\alpha\Delta\right)\right)_{t\geq a}$, $\left(E_\alpha\left((\log\frac{t}{a})^\alpha(\Delta-\gamma)\right)\right)_{t\geq a}$, $\left(\nabla E_\alpha\left((\log\frac{t}{a})^\alpha(\Delta-\gamma)\right)\right)_{t\geq a}$, $\left(E_{\alpha,\alpha}\left((\log\frac{t}{a})^\alpha(\Delta-\gamma)\right)\right)_{t\geq a}$ *and* $\left(\nabla E_{\alpha,\alpha}\left((\log\frac{t}{a})^\alpha(\Delta-\gamma)\right)\right)_{t\geq a}$ *are strongly continuous in* $L^r(\Omega)$, $1 \leq r < \infty$.

Proof. We only prove the statement for the first family. The other families can be proved in a similar manner and so the proofs are omitted here. Let $\varphi \in L^r(\Omega)$ with $1 \leq r < \infty$. According to integral formulas of the Mittag-Leffler operators and the properties of semigroup, one obtains that for $a \leq t_1 < t_2$,

$$\begin{aligned}
&\left\|E_\alpha\left((\log\tfrac{t_2}{a})^\alpha\Delta\right)\varphi - E_\alpha\left((\log\tfrac{t_1}{a})^\alpha\Delta\right)\varphi\right\|_{L^r(\Omega)}\\
\leq& C\int_0^\infty M_\alpha(s)\left\|G\left(s\left((\log\tfrac{t_2}{a})^\alpha - (\log\tfrac{t_1}{a})^\alpha\right)\right)\varphi - \varphi\right\|_{L^r(\Omega)}\mathrm{d}s.
\end{aligned}$$

Using the inequality (3.2), we obtain

$$M_\alpha(s)\left\|G\left(s\left((\log\tfrac{t_2}{a})^\alpha - (\log\tfrac{t_1}{a})^\alpha\right)\right)\varphi - \varphi\right\|_{L^r(\Omega)} \leq C M_\alpha(s)\|\varphi\|_{L^r(\Omega)}.$$

The integrand converges to zero pointwisely in $s > 0$ as $t_2 \to t_1^+$. Applying the Lebesgue dominated convergence theorem, the continuity of $E_\alpha\left((\log\frac{t}{a})^\alpha\Delta\right)\varphi$ in $L^r(\Omega)$ is obtained. This finishes the proof of Lemma 3.1. □

Lemma 3.2. *Let* $q \geq 1$, $q > \frac{N}{\rho}(\rho-1)$, $\beta = \frac{\alpha N}{2\rho q}(\rho-1)$ *and* $\rho > 2$. *If* u_a, $v_a \in L^q(\Omega)$, *then it holds that*

$$\lim_{t\to a^+}(\log\tfrac{t}{a})^\beta\left\|E_\alpha\left((\log\tfrac{t}{a})^\alpha\Delta\right)u_a\right\|_{L^{\rho q}(\Omega)} = 0, \tag{3.8}$$

$$\lim_{t\to a^+}(\log\tfrac{t}{a})^\beta\left\|E_\alpha\left((\log\tfrac{t}{a})^\alpha(\Delta-\gamma)\right)v_a\right\|_{L^{\rho q}(\Omega)} = 0. \tag{3.9}$$

Proof. Let $\varphi \in L^{\rho q}(\Omega)$. According to (3.2) and (3.7), we know that

$$\lim_{t\to a^+}(\log\tfrac{t}{a})^\beta\left\|E_\alpha\left((\log\tfrac{t}{a})^\alpha\Delta\right)\varphi\right\|_{L^{\rho q}(\Omega)} = 0,$$

and

$$\left\|E_\alpha\left((\log\tfrac{t}{a})^\alpha\Delta\right)\varphi\right\|_{L^{\rho q}(\Omega)} \leq C\|\varphi\|_{L^{\rho q}(\Omega)}, \quad t > a.$$

Analogously, we have

$$\lim_{t\to a^+}(\log\frac{t}{a})^{\beta}\left\|E_{\alpha}\left((\log\frac{t}{a})^{\alpha}(\Delta-\gamma)\right)\varphi\right\|_{L^{\rho q}(\Omega)}=0,$$

for all $\varphi\in L^{\rho q}(\Omega)$.

In the following, we prove that for all $\varphi\in L^{q}(\Omega)$ and all $t\in(a,ae)$,

$$(\log\frac{t}{a})^{\beta}\left\|E_{\alpha}\left((\log\frac{t}{a})^{\alpha}\Delta\right)\varphi\right\|_{L^{\rho q}(\Omega)}\le C\|\varphi\|_{L^{q}(\Omega)},\tag{3.10}$$

and

$$(\log\frac{t}{a})^{\beta}\left\|E_{\alpha}\left((\log\frac{t}{a})^{\alpha}(\Delta-\gamma)\right)\varphi\right\|_{L^{\rho q}(\Omega)}\le C\|\varphi\|_{L^{q}(\Omega)}.\tag{3.11}$$

The proofs of estimates (3.10) and (3.11) are similar, so we only prove inequality (3.10). Let $t\in(a,ae)$. We know that $q>\frac{N}{2\rho}(\rho-1)$, and then by using inequality (3.2) and equality (3.7), one can deduce that

$$\begin{aligned}\left\|E_{\alpha}\left((\log\frac{t}{a})^{\alpha}\Delta\right)\varphi\right\|_{L^{\rho q}(\Omega)}&\le C\int_0^{\infty}M_{\alpha}(s)\left(1+\left(s(\log\frac{t}{a})^{\alpha}\right)^{-\frac{N}{2\rho q}(\rho-1)}\right)\mathrm{d}s\|\varphi\|_{L^{q}(\Omega)}\\&=C\left(1+(\log\frac{t}{a})^{-\beta}\frac{\Gamma\left(1-\frac{\beta}{\alpha}\right)}{\Gamma(1-\beta)}\right)\|\varphi\|_{L^{q}(\Omega)}\\&\le C(\log\frac{t}{a})^{-\beta}\|\varphi\|_{L^{q}(\Omega)}.\end{aligned}$$

The smoothing property of the operator $E_{\alpha}((\log\frac{t}{a})^{\alpha}\Delta)$ provides a continuous embedding from $L^{q}(\Omega)$ into $L^{\rho q}(\Omega)$. Using the estimates (3.10) and (3.11), together with a density argument, yields (3.8) and (3.9). Therefore, Lemma 3.2 is proved. □

Lemma 3.3. *Let $\varphi\in L^{r}(\Omega)$ with $1\le r\le\infty$. Then, for all $t\in(a,ae)$, the following inequalities hold.*

$$\left\|E_{\alpha,\alpha}\left((\log\frac{t}{a})^{\alpha}\Delta\right)\nabla\cdot\varphi\right\|_{L^{r}(\Omega)}\le C(\log\frac{t}{a})^{-\frac{\alpha}{2}}\|\varphi\|_{L^{r}(\Omega)},\tag{3.12}$$

$$\left\|\nabla E_{\alpha}\left((\log\frac{t}{a})^{\alpha}(\Delta-\gamma)\right)\varphi\right\|_{L^{r}(\Omega)}\le C(\log\frac{t}{a})^{-\frac{\alpha}{2}}\|\varphi\|_{L^{r}(\Omega)},\tag{3.13}$$

$$\left\|\nabla E_{\alpha,\alpha}\left((\log\frac{t}{a})^{\alpha}(\Delta-\gamma)\right)\varphi\right\|_{L^{\infty}(\Omega)}\le C(\log\frac{t}{a})^{-\frac{\alpha}{2}\left(\frac{N}{r}+1\right)}\|\varphi\|_{L^{r}(\Omega)},\quad r>N,\tag{3.14}$$

$$\left\|\nabla E_{\alpha,\alpha}\left((\log\frac{t}{a})^{\alpha}(\Delta-\gamma)\right)\varphi\right\|_{L^{r}(\Omega)}\le C(\log\frac{t}{a})^{-\frac{\alpha}{2}}\|\varphi\|_{L^{r}(\Omega)},\tag{3.15}$$

$$\left\|E_{\alpha,\alpha}\left((\log\frac{t}{a})^{\alpha}(\Delta-\gamma)\right)\varphi\right\|_{L^{r}(\Omega)}\le C\|\varphi\|_{L^{r}(\Omega)}.\tag{3.16}$$

Proof. Using inequality (3.3) and Eq. (3.7), and keeping in mind that $0<a<t<ae$, one gets

$$\begin{aligned}\left\|E_{\alpha,\alpha}\left((\log\frac{t}{a})^{\alpha}\Delta\right)\nabla\cdot\varphi\right\|_{L^{r}(\Omega)}&\le C\int_0^{\infty}\alpha sM_{\alpha}(s)\left(1+s^{-\frac{1}{2}}(\log\frac{t}{a})^{-\frac{\alpha}{2}}\right)\mathrm{d}s\|\varphi\|_{L^{r}(\Omega)}\\&\le C\left(\frac{1}{\Gamma(1+\alpha)}+(\log\frac{t}{a})^{-\frac{\alpha}{2}}\frac{\Gamma\left(\frac{3}{2}\right)}{\Gamma\left(1+\frac{\alpha}{2}\right)}\right)\|\varphi\|_{L^{r}(\Omega)}\\&\le C(\log\frac{t}{a})^{-\frac{\alpha}{2}}\|\varphi\|_{L^{r}(\Omega)}\end{aligned}$$

The proofs of the estimates (3.13) and (3.15) are similar. We only show inequality (3.13). With the help of inequality (3.4) and Eq. (3.7), we get the estimate below

$$\begin{aligned}\left\|\nabla E_{\alpha}\left((\log\frac{t}{a})^{\alpha}(\Delta-\gamma)\right)\varphi\right\|_{L^{r}(\Omega)}&\le C\int_0^{\infty}M_{\alpha}(s)\mathrm{e}^{-s(\log\frac{t}{a})^{\alpha}\gamma}\left(1+\left(s(\log\frac{t}{a})^{\alpha}\right)^{-\frac{1}{2}}\right)\mathrm{d}s\|\varphi\|_{L^{r}(\Omega)}\\&\le C(\log\frac{t}{a})^{-\frac{\alpha}{2}}\|\varphi\|_{L^{r}(\Omega)}.\end{aligned}$$

In order to prove inequality (3.14), we should stress that $r > N$, and thereupon using Eq. (3.4) we get

$$\begin{aligned}\left\|\nabla E_{\alpha,\alpha}\left((\log\frac{t}{a})^{\alpha}(\Delta-\gamma)\right)\varphi\right\|_{L^{\infty}(\Omega)} &\le C\int_0^{\infty}\alpha s M_{\alpha}(s)\left(1+\left(s(\log\frac{t}{a})^{\alpha}\right)^{-\frac{1}{2}\left(\frac{N}{r}+1\right)}\right)\mathrm{d}s\|\varphi\|_{L^r(\Omega)}\\ &= C\alpha\left(\frac{1}{\Gamma(1+\alpha)}+(\log\frac{t}{a})^{-\frac{\alpha}{2}\left(\frac{N}{r}+1\right)}\frac{\Gamma\left(\frac{1}{2}\left(3-\frac{N}{r}\right)\right)}{\Gamma\left(1+\frac{\alpha}{2}\left(1-\frac{N}{r}\right)\right)}\right)\|\varphi\|_{L^r(\Omega)}\\ &\le C(\log\frac{t}{a})^{-\frac{\alpha}{2}\left(\frac{N}{r}+1\right)}\|\varphi\|_{L^r(\Omega)}.\end{aligned}$$

To prove inequality (3.16), we use Eq. (3.2) and proceed as follows:

$$\begin{aligned}\left\|E_{\alpha,\alpha}\left((\log\frac{t}{a})^{\alpha}(\Delta-\gamma)\right)\varphi\right\|_{L^r(\Omega)} &\le \int_0^{\infty}\alpha s M_{\alpha}(s)\left\|G\left(s(\log\frac{t}{a})^{\alpha}\right)\varphi\right\|_{L^r(\Omega)}\mathrm{d}s\\ &\le C\frac{1}{\Gamma(1+\alpha)}\|\varphi\|_{L^r(\Omega)}.\end{aligned}$$

This completes the proof. □

Remark 3.1. In Lemma 3.3 and inequality (3.10), the time variable is restricted to $t \in (a, ae)$. This specific choice ensures that $0 < \log(t/a) < 1$. Bounding the logarithmic term strictly away from infinity is mathematically necessary to control the exponents of the singular kernels when estimating the Mittag-Leffler operators and applying the contraction mapping principle.

The following is a generalization of Kato's lemma [22], which is useful in proving uniqueness.

Lemma 3.4. *Let X be a Banach space, and let $\psi : [a,T)$ to $\mathbb{R}$ be a differentiable function satisfying $\psi(a) = 0$ and $\psi(t) > 0$ for $t > a$. Suppose $f(\psi(s),\psi(t))$ is an X-valued continuous and bounded function for $0 < a < s < t < T \le \infty$. Let $\mu < 1$, $\nu < 1$. Define the function*

$$g(t) = \psi(t)^{\mu+\nu-1}\int_a^t \psi(s)^{-\mu}(\psi(t)-\psi(s))^{-\nu} f(\psi(s),\psi(t))\,\psi'(s)\,\mathrm{d}s, \quad a < t < T.$$

Then g belong to the space of bounded and continuous functions $BC((a,T);X)$. Furthermore, if the limit $\lim_{(s,t)\to(a,a)} f(\psi(s),\psi(t)) = \bar{f}$ exists, then g can be continuously extended to $[a,T)$, and

$$g(a) = \bar{f}\,\mathrm{B}(1-\mu,1-\nu),$$

where $\mathrm{B}(\cdot,\cdot)$ is the Beta function.

Proof. Introduce a new variable $\sigma = \frac{\psi(s)}{\psi(t)}$, where $\sigma \in (0,1)$, $s \in (a,t)$. Substitution in the integral yields

$$\begin{aligned}&\int_a^t \psi(s)^{-\mu}(\psi(t)-\psi(s))^{-\nu} f(\psi(s),\psi(t))\psi'(s)\,\mathrm{d}s\\ &= \psi(t)\int_0^1 (\psi(t)\sigma)^{-\mu}(\psi(t)(1-\sigma))^{-\nu} f(\psi(t)\sigma,\psi(t))\,\mathrm{d}\sigma.\end{aligned}$$

Thus, $g(t)$ becomes

$$\begin{aligned}g(t) &= \psi(t)^{\mu+\nu-1}\cdot\psi(t)\int_0^1 (\psi(t)\sigma)^{-\mu}(\psi(t)(1-\sigma))^{-\nu} f(\psi(t)\sigma,\psi(t))\,\mathrm{d}\sigma\\ &= \int_0^1 \sigma^{-\mu}(1-\sigma)^{-\nu} f(\psi(t)\sigma,\psi(t))\,\mathrm{d}\sigma.\end{aligned}$$

Since f is bounded,

$$\begin{aligned}\|g(t)\| &\le \int_0^1 \sigma^{-\mu}(1-\sigma)^{-\nu}\|f(\psi(t)\sigma,\psi(t))\|\,\mathrm{d}\sigma\\ &\le M\int_0^1 \sigma^{-\mu}(1-\sigma)^{-\nu}\,\mathrm{d}\sigma\\ &= M\cdot\mathrm{B}(1-\mu,1-\nu),\end{aligned}$$

where M is a positive constant. The Beta function $\mathrm{B}(1-\mu,1-\nu)$ is bounded because of $\mu,\nu < 1$. Hence, $g(t)$ is bounded.

For $t_0 \in (a,T)$, as $t \to t_0$, $\psi(t)\sigma \to \psi(t_0)\sigma$ and $\psi(t) \to \psi(t_0)$. By the continuity of f and the dominated convergence theorem, one gets

$$\lim_{t\to t_0} g(t) = \int_0^1 \sigma^{-\mu}(1-\sigma)^{-\nu}\lim_{t\to t_0} f(\psi(t)\sigma,\psi(t))\,\mathrm{d}\sigma = g(t_0).$$

Thus, $g(t)$ is continuous on (a,T).

As $t \to a^+$, $\psi(t) \to 0$. By the uniform convergence of $f(\psi(t)\sigma, \psi(t))$ to $\bar{f}$, one has

$$\begin{aligned}\lim_{t\to a} g(t) &= \int_0^1 \sigma^{-\mu}(1-\sigma)^{-\nu} \lim_{t\to a} f(\psi(t)\sigma, \psi(t))\,\mathrm{d}\sigma \\ &= \bar{f}\int_0^1 \sigma^{-\mu}(1-\sigma)^{-\nu}\,\mathrm{d}\sigma \\ &= \bar{f}\,\mathrm{B}(1-\mu, 1-\nu).\end{aligned}$$

Hence, g extends continuously to $[a, T)$. □

According to the Gronwall type inequalities with singular kernels in [23,24], we provide a version in the logarithmic sense.

Lemma 3.5. *Let $a > 0$, $b \geq 0$, $\beta > 0$, and let l be a nonnegative and nondecreasing function locally integrable on $a \leq t < T$ (for some $T \leq \infty$). Assume that u is a nonnegative function locally integrable on $[a, T)$ with*

$$u(t) \leq l(t) + b\int_a^t (\log\frac{t}{s})^{\beta-1} u(s)\frac{\mathrm{d}s}{s}, \quad a \leq t < T.$$

Then

$$u(t) \leq l(t) E_\beta\left(\theta(\log\frac{t}{a})^\beta\right), \quad a \leq t < T,$$

where $\theta = b\Gamma(\beta)$.

Theorem 3.1. *Let $u_a \in L^q(\Omega)$, where $q \geq 1$, $q > \frac{N}{\rho}(\rho-1)$, and $\rho > 2$. Set $\beta = \frac{\alpha N}{2\rho q}(\rho-1)$. Assume also that $v_a, \nabla v_a \in L^\infty(\Omega)$ so that $\|v_a\|_{L^\infty(\Omega)}$ is small enough. Given $R > 0$, there exists $T > a$ such that Eqs. (1.1)–(1.3) have an L^q-mild solution pair $(u, v) : [a, T] \to (L^q(\Omega))^2$ and u, v and ∇v belong to $C([a, T]; L^q(\Omega))$, with the following bounded properties:*

$$\sup_{t\in(a,T)} (\log\frac{t}{a})^\beta \|u(t)\|_{L^q(\Omega)} \leq CR, \tag{3.17}$$

$$\sup_{t\in(a,T)} (\log\frac{t}{a})^\beta \|v(t)\|_{L^q(\Omega)} \leq CR, \tag{3.18}$$

where C is a positive constant. Moreover,

$$(\log\frac{t}{a})^\beta \|u(t)\|_{L^q(\Omega)} \to 0, \ \text{as } t \to a^+, \tag{3.19}$$

$$(\log\frac{t}{a})^\beta \|v(t)\|_{L^q(\Omega)} \to 0, \ \text{as } t \to a^+. \tag{3.20}$$

This solution depends continuously on the initial value.

Proof. Let R be a positive number, and let $T \in (a, ae)$ be a parameter chosen later. We define a Banach space

$$\mathscr{X} = \left\{ u \in C((a, T]; L^{\rho q}(\Omega)) \mid \sup_{t\in(a,T)} \left(\log\frac{t}{a}\right)^\beta \|u(t)\|_{L^{\rho q}(\Omega)} < +\infty \right\}$$

and equip it with the norm $\|u\|_{\mathscr{X}} = \sup_{t\in(a,T)}(\log\frac{t}{a})^\beta \|u(t)\|_{L^{\rho q}(\Omega)}$. Let $\mathscr{B}_R$ be the closed ball of radius R in $\mathscr{X}$, centered at the origin. We note that $\beta + \frac{\alpha}{2} < 1$ and $q > \frac{N}{\rho}$. We then select a constant $C > 0$ as specified in Lemma 3.3 and choose $v_a \in L^\infty(\Omega)$ such that

$$\|v_a\|_{L^\infty(\Omega)} < \frac{1}{4C^2\mathrm{B}\left(1-\beta-\frac{\alpha}{2}, \frac{\alpha}{2}\right)}.$$

We select a sufficiently small T to ensure that

$$\sup_{t\in(a,T)} (\log\frac{t}{a})^\beta \left\| E_\alpha\left((\log\frac{t}{a})^\alpha \Delta\right) u_a \right\|_{L^{\rho q}(\Omega)} + \sup_{t\in(a,T)} (\log\frac{t}{a})^\beta \left\| E_\alpha\left((\log\frac{t}{a})^\alpha (\Delta-\gamma)\right) v_a \right\|_{L^{\rho q}(\Omega)} < \frac{R}{2}, \tag{3.21}$$

$$(\log\frac{T}{a})^{\frac{\alpha}{2}\left(2-\frac{N}{\rho q}\right)-\beta} < \frac{1}{4C^2 R\mathrm{B}\left(1-\beta, \frac{\alpha}{2}\left(1-\frac{N}{\rho q}\right)\right)\mathrm{B}\left(1-\beta-\frac{\alpha}{2}, \frac{\alpha}{2}\right)}, \tag{3.22}$$

and

$$C(\log\frac{T}{a})^\beta \mathrm{B}(1-\beta, \alpha) < \frac{1}{2}. \tag{3.23}$$

Given $u \in \mathscr{B}_R$, define v in Eq. (3.6). From inequalities(3.13) and (3.14) we have

$$\begin{aligned}
\sup_{t\in(a,T)} (\log \tfrac{t}{a})^{\frac{\alpha}{2}} \|\nabla v(t)\|_{L^\infty(\Omega)} &\le \sup_{t\in(a,T)} (\log \tfrac{t}{a})^{\frac{\alpha}{2}} \left\| \nabla E_\alpha \left((\log \tfrac{t}{a})^\alpha (\Delta - \gamma) \right) v_a \right\|_{L^\infty(\Omega)} \\
&\quad + C \sup_{t\in(a,T)} (\log \tfrac{t}{a})^{\frac{\alpha}{2}} \int_a^t (\log \tfrac{t}{s})^{\frac{\alpha}{2}\left(1-\frac{N}{\rho q}\right)-1} \|u(s)\|_{L^{\rho q}(\Omega)} \frac{\mathrm{d}s}{s} \\
&\le C \|v_a\|_{L^\infty(\Omega)} + C \sup_{t\in(a,T)} (\log \tfrac{t}{a})^{\frac{\alpha}{2}} \int_a^t (\log \tfrac{t}{s})^{\frac{\alpha}{2}\left(1-\frac{N}{\rho q}\right)-1} (\log \tfrac{s}{a})^{-\beta} \frac{\mathrm{d}s}{s} \|u\|_{\mathscr{X}} \\
&\le C \|v_a\|_{L^\infty(\Omega)} + C \sup_{t\in(a,T)} (\log \tfrac{t}{a})^{\frac{\alpha}{2}\left(2-\frac{N}{\rho q}\right)-\beta} \mathrm{B}\left(1-\beta, \frac{\alpha}{2}\left(1-\frac{N}{\rho q}\right)\right) R \\
&\le C \left(\|v_a\|_{L^\infty(\Omega)} + (\log \tfrac{T}{a})^{\frac{\alpha}{2}\left(2-\frac{N}{\rho q}\right)-\beta} \mathrm{B}\left(1-\beta, \frac{\alpha}{2}\left(1-\frac{N}{\rho q}\right)\right) R \right),
\end{aligned} \tag{3.24}$$

where $q > \frac{N}{\rho}(\rho - 1)$ and $\rho > 2$. Let

$$(\Phi u)(t) = E_\alpha \left((\log \tfrac{t}{a})^\alpha \Delta \right) u_a - \int_a^t (\log \tfrac{t}{s})^{\alpha-1} E_{\alpha,\alpha} \left((\log \tfrac{t}{s})^\alpha \Delta \right) \nabla \cdot (u \nabla v)(s) \frac{\mathrm{d}s}{s}. \tag{3.25}$$

The next step is to prove $\Phi u \in \mathscr{B}_R$. By virtue of (3.12), we can obtain the following estimate

$$\begin{aligned}
\|(\Phi u)(t)\|_{L^{\rho q}(\Omega)} &\le \left\| E_\alpha \left((\log \tfrac{t}{a})^\alpha \Delta \right) u_a \right\|_{L^{\rho q}(\Omega)} + C \int_a^t (\log \tfrac{t}{s})^{\frac{\alpha}{2}-1} \|(u\nabla v)(s)\|_{L^{\rho q}(\Omega)} \frac{\mathrm{d}s}{s} \\
&\le \left\| E_\alpha \left((\log \tfrac{t}{a})^\alpha \Delta \right) u_a \right\|_{L^{\rho q}(\Omega)} + C \int_a^t (\log \tfrac{t}{s})^{\frac{\alpha}{2}-1} \|u(s)\|_{L^{\rho q}(\Omega)} \|\nabla v(s)\|_{L^\infty(\Omega)} \frac{\mathrm{d}s}{s} \\
&\le \left\| E_\alpha \left((\log \tfrac{t}{a})^\alpha \Delta \right) u_a \right\|_{L^{\rho q}(\Omega)} \\
&\quad + C \int_a^t (\log \tfrac{t}{s})^{\frac{\alpha}{2}-1} (\log \tfrac{s}{a})^{-\beta-\frac{\alpha}{2}} \frac{ds}{s} \|u\|_{\mathscr{X}} \sup_{t\in(a,T)} (\log \tfrac{t}{a})^{\frac{\alpha}{2}} \|\nabla v(t)\|_{L^\infty(\Omega)}.
\end{aligned}$$

From (3.24), using (3.21) and (3.22), we obtain

$$\begin{aligned}
(\log \tfrac{t}{a})^\beta \|(\Phi u)(t)\|_{L^{\rho q}(\Omega)} &\le (\log \tfrac{t}{a})^\beta \left\| E_\alpha \left((\log \tfrac{t}{a})^\alpha \Delta \right) u_a \right\|_{L^{\rho q}(\Omega)} + C^2 \mathrm{B}\left(1-\beta-\frac{\alpha}{2}, \frac{\alpha}{2}\right) R \|v_a\|_{L^\infty(\Omega)} \\
&\quad + C^2 \mathrm{B}\left(1-\beta-\frac{\alpha}{2}, \frac{\alpha}{2}\right) \mathrm{B}\left(1-\beta, \frac{\alpha}{2}\left(1-\frac{N}{\rho q}\right)\right) R^2 (\log \tfrac{T}{a})^{\frac{\alpha}{2}\left(2-\frac{N}{\rho q}\right)-\beta} \\
&\le \frac{R}{2} + \frac{R}{2} = R.
\end{aligned}$$

Hence, Φ is a self-mapping in $\mathscr{B}_R$.

We just need to check the continuity of Φu. Given that $E_\alpha \left((\log \frac{t}{a})^\alpha \Delta \right)$ is strongly continuous (see Lemma 3.1), it suffices to focus on the continuity of the function

$$(\mathscr{T} u)(t) = \int_a^t (\log \tfrac{t}{s})^{\alpha-1} E_{\alpha,\alpha} \left((\log \tfrac{t}{s})^\alpha \Delta \right) \nabla \cdot (u \nabla v)(s) \frac{\mathrm{d}s}{s}.$$

For $a < t_1 < t_2 < T$, we split $\mathscr{T}(u)(t_2) - \mathscr{T}(u)(t_1)$ as

$$(\mathscr{T} u)(t_2) - (\mathscr{T} u)(t_1) = I_1 + I_2 + I_3,$$

where

$$\begin{aligned}
I_1 &= \int_{t_1}^{t_2} (\log \tfrac{t_2}{s})^{\alpha-1} E_{\alpha,\alpha} \left((\log \tfrac{t_2}{s})^\alpha \Delta \right) \nabla \cdot (u \nabla v)(s) \frac{\mathrm{d}s}{s}, \\
I_2 &= \int_a^{t_1} \left((\log \tfrac{t_2}{s})^{\alpha-1} - (\log \tfrac{t_1}{s})^{\alpha-1} \right) E_{\alpha,\alpha} \left((\log \tfrac{t_2}{s})^\alpha \Delta \right) \nabla \cdot (u \nabla v)(s) \frac{\mathrm{d}s}{s}, \\
I_3 &= \int_a^{t_1} (\log \tfrac{t_1}{s})^{\alpha-1} \left(E_{\alpha,\alpha} \left((\log \tfrac{t_2}{s})^\alpha \Delta \right) - E_{\alpha,\alpha} \left((\log \tfrac{t_1}{s})^\alpha \Delta \right) \right) \nabla \cdot (u \nabla v)(s) \frac{\mathrm{d}s}{s}.
\end{aligned}$$

From (3.12), the first and second terms can be estimated as follows,

$$\begin{aligned}
\|I_1\|_{L^{\rho q}(\Omega)} &\le \int_{t_1}^{t_2} (\log \tfrac{t_2}{s})^{\frac{\alpha}{2}-1} \|u(s)\|_{L^{\rho q}(\Omega)} \|(\nabla v)(s)\|_{L^\infty(\Omega)} \frac{\mathrm{d}s}{s} \\
&\le \int_{t_1}^{t_2} (\log \tfrac{t_2}{s})^{\frac{\alpha}{2}-1} (\log \tfrac{s}{a})^{-\beta-\frac{\alpha}{2}} \frac{\mathrm{d}s}{s} \|u\|_{\mathscr{X}} \sup_{t\in(a,T)} (\log \tfrac{t}{a})^{\frac{\alpha}{2}} \|(\nabla v)(t)\|_{L^\infty(\Omega)} \\
&\le (\log \tfrac{t_2}{a})^{-\beta} \|u\|_{\mathscr{X}} \sup_{t\in(a,T)} (\log \tfrac{t}{a})^{\frac{\alpha}{2}} \|(\nabla v)(t)\|_{L^\infty(\Omega)} \int_{\frac{\log \frac{t_1}{a}}{\log \frac{t_2}{a}}}^1 (1-s)^{\frac{\alpha}{2}-1} s^{-\beta-\frac{\alpha}{2}} \frac{\mathrm{d}s}{s},
\end{aligned}$$

$$\|I_2\|_{L^{\rho q}(\Omega)} \le \int_a^{t_1} \left|(\log\frac{t_2}{s})^{\alpha-1} - (\log\frac{t_1}{s})^{\alpha-1}\right| (\log\frac{t_2}{s})^{-\frac{\alpha}{2}} (\log\frac{s}{a})^{-\beta-\frac{\alpha}{2}} \frac{\mathrm{d}s}{s} \times R \sup_{t\in(a,T)} (\log\frac{t}{a})^{\frac{\alpha}{2}} \|(\nabla v)(t)\|_{L^\infty(\Omega)}.$$

By applying inequality (3.3), we derive the following upper bound

$$\begin{aligned}
\|I_3\|_{L^{\rho q}(\Omega)} \le& \int_a^{t_1} (\log\frac{t_1}{s})^{\alpha-1} \left\| \left(E_{\alpha,\alpha}\left((\log\frac{t_2}{s})^\alpha \Delta\right) - E_{\alpha,\alpha}\left((\log\frac{t_1}{s})^\alpha \Delta\right)\right) \nabla\cdot(u\nabla v)(s)\right\|_{L^{\rho q}(\Omega)} \frac{\mathrm{d}s}{s}\\
\le& \int_a^{t_1} (\log\frac{t_1}{s})^{\alpha-1} \int_0^\infty \alpha\tau M_\alpha(\tau) \left\| \left(G\left(\tau(\log\frac{t_2}{s})^\alpha\right) - G\left(\tau(\log\frac{t_1}{s})^\alpha\right)\right) \nabla\cdot(u\nabla v)(s)\right\|_{L^{\rho q}(\Omega)} \mathrm{d}\tau\frac{\mathrm{d}s}{s}\\
\le& C\int_a^{t_1} (\log\frac{t_1}{s})^{\alpha-1} \int_0^\infty \alpha\tau M_\alpha(\tau) \left\| \left(G\left(\tau(\log\frac{t_2}{s})^\alpha - (\log\frac{t_1}{s})^\alpha\right) - I\right) \nabla\cdot(u\nabla v)(s)\right\|_{L^{\rho q}(\Omega)} \mathrm{d}\tau\frac{\mathrm{d}s}{s}\\
\le& CR \sup_{t\in(a,T)} (\log\frac{t}{a})^{\frac{\alpha}{2}} \|(\nabla v)(t)\|_{L^\infty(\Omega)} \int_a^{t_1} (\log\frac{t_1}{s})^{\alpha-1} (\log\frac{s}{a})^{-\beta-\frac{\alpha}{2}}\\
&\times \int_0^\infty \alpha\tau M_\alpha(\tau)\left(1+\tau^{-\frac{1}{2}}(\log\frac{t_1}{s})^{-\frac{a}{2}}\right) \left\| G\left(\tau\left((\log\frac{t_2}{s})^\alpha - (\log\frac{t_1}{s})^\alpha\right)\right) - I\right\|_{\mathscr{B}(L^{\rho q}(\Omega))} \mathrm{d}\tau\frac{\mathrm{d}s}{s}.
\end{aligned}$$

Here, $\mathscr{B}(L^{\rho q}(\Omega))$ denotes the bounded linear operator space from $L^{\rho q}(\Omega)$ to itself. Consequently, it follows that $\|I_1\|_{L^{\rho q}(\Omega)} \to 0$, as $t_2 \to t_1^+$. Using the Lebesgue dominated convergence theorem, we get that $\|I_2\|_{L^{\rho q}(\Omega)}$, $\|I_3\|_{L^{\rho q}(\Omega)}$ converge to zero as $t_2 \to t_1^+$. Therefore, we conclude that $\mathscr{T}(u)$ is continuous.

We aim to prove that Φ is a contraction. Let $u^i \in \mathscr{B}_R$ and define v^i by Eq. (3.6), $i = 1, 2$. We then estimate $\|\Phi u^1 - \Phi u^2\|_{\mathscr{X}}$. To do so, we first write

$$\begin{cases}
\mathscr{J}_1^\alpha(t) = \displaystyle\int_a^t (\log\frac{t}{s})^{\alpha-1} E_{\alpha,\alpha}\left((\log\frac{t}{s})^\alpha\Delta\right)\nabla\cdot\left(\left(u^2-u^1\right)\nabla v^1\right)(s)\frac{\mathrm{d}s}{s},\\
\mathscr{J}_2^\alpha(t) = \displaystyle\int_a^t (\log\frac{t}{s})^{\alpha-1} E_{\alpha,\alpha}\left((\log\frac{t}{s})^\alpha\Delta\right)\nabla\cdot\left(u^2\nabla\left(v^2-v^1\right)\right)(s)\frac{\mathrm{d}s}{s}.
\end{cases} \tag{3.26}$$

From inequalities (3.12), (3.24), and (3.22), we obtain

$$\begin{aligned}
(\log\frac{t}{a})^\beta \left\|\mathscr{J}_1^\alpha(t)\right\|_{L^{\rho q}(\Omega)} &\le C\mathrm{B}\left(1-\beta-\frac{\alpha}{2},\frac{\alpha}{2}\right) \sup_{t\in(0,T)} (\log\frac{t}{a})^{\frac{\alpha}{2}} \left\|\nabla v^1(t)\right\|_{L^\infty(\Omega)} \left\|u^2-u^1\right\|_{\mathscr{X}}\\
&\le C^2\mathrm{B}\left(1-\beta-\frac{\alpha}{2},\frac{\alpha}{2}\right)\left(\|v_a\|_{L^\infty(\Omega)}\right.\\
&\quad \left.+(\log\frac{T}{a})^{\frac{\alpha}{2}\left(2-\frac{N}{\rho q}\right)-\beta}\mathrm{B}\left(1-\beta,\frac{\alpha}{2}\left(1-\frac{N}{\rho q}\right)\right)R\right)\left\|u^2-u^1\right\|_{\mathscr{X}}\\
&< \frac{1}{2}\left\|u^2-u^1\right\|_{\mathscr{X}}.
\end{aligned} \tag{3.27}$$

Next, taking into account the upper bound, we get

$$\sup_{t\in(a,T)} (\log\frac{t}{a})^{\frac{\alpha}{2}} \left\|\nabla\left(v^2-v^1\right)(t)\right\|_{L^\infty(\Omega)} \le C(\log\frac{T}{a})^{\frac{\alpha}{2}\left(2-\frac{N}{\rho q}\right)-\beta}\mathrm{B}\left(1-\beta,\frac{\alpha}{2}\left(1-\frac{N}{\rho q}\right)\right)\left\|u^2-u^1\right\|_{\mathscr{X}}.$$

From this, we infer that

$$\begin{aligned}
(\log\frac{t}{a})^\beta \left\|\mathscr{J}_2^\alpha\right\|_{L^{\rho q}(\Omega)} &\le C^2R(\log\frac{T}{a})^{\frac{\alpha}{2}\left(2-\frac{N}{\rho q}\right)-\beta}\mathrm{B}\left(1-\beta-\frac{\alpha}{2},\frac{\alpha}{2}\right)\mathrm{B}\left(1-\beta,\frac{\alpha}{2}\left(1-\frac{N}{\rho q}\right)\right)\left\|u^2-u^1\right\|_{\mathscr{X}}\\
&\le \frac{1}{4}\left\|u^2-u^1\right\|_{\mathscr{X}}.
\end{aligned} \tag{3.28}$$

Now, it follows from inequalities (3.27) and (3.28) that

$$\left\|\Phi u^2-\Phi u^1\right\|_{\mathscr{X}} \le \frac{3}{4}\left\|u^2-u^1\right\|_{\mathscr{X}},$$

for every $u^1, u^2 \in \mathscr{B}_R$. The contraction mapping principle yields the existence of a unique fixed-point u in $\mathscr{B}_R$. Next, we demonstrate that the pair (u, v) represents the unique solution provided by the theorem within the space $\mathscr{B}_R$. However, establishing the uniqueness of solutions in the entire space is significantly challenging, thus the problem remains open.

Note that v belongs to $\mathscr{B}_R$. Indeed, invoking inequalities (3.12), (3.21), and (3.23), one has

$$\begin{aligned}(\log\tfrac{t}{a})^{\beta}\|v(t)\|_{L^{\rho q}(\Omega)} &\le (\log\tfrac{t}{a})^{\beta}\left\|E_{\alpha}\left((\log\tfrac{t}{a})^{\alpha}(\Delta-\gamma)\right)v_a\right\|_{L^{\rho q}(\Omega)}\\ &\quad+(\log\tfrac{t}{a})^{\beta}\int_a^t(\log\tfrac{t}{s})^{\alpha-1}\left\|E_{\alpha,\alpha}\left((\log\tfrac{t}{s})^{\alpha-1}(\Delta-\gamma)\right)u(s)\right\|_{L^{\rho q}(\Omega)}\frac{\mathrm{d}s}{s}\\ &\le \frac{R}{2}+C(\log\tfrac{t}{a})^{\beta}\int_a^t(\log\tfrac{t}{s})^{\alpha-1}\|u\|_{L^{\rho q}(\Omega)}\frac{\mathrm{d}s}{s}\\ &\le \frac{R}{2}+C\|u\|_{\mathscr{X}}(\log\tfrac{T}{a})^{\beta}\int_a^t(\log\tfrac{t}{s})^{\alpha-1}(\log\tfrac{s}{a})^{-\beta}\frac{\mathrm{d}s}{s}\\ &\le \frac{R}{2}+CR(\log\tfrac{T}{a})^{\beta}\mathrm{B}(1-\beta,\alpha)\\ &\le \frac{R}{2}+\frac{R}{2}=R.\end{aligned}$$

Since u and v belong to $\mathscr{B}_R$, we immediately get the bounded properties (3.17) and (3.18).

We next prove the asymptotic profiles of u and v. Using Eq. (3.6) and inequality (3.12), we can estimate the L^q-norm of $u(t)$ as follows

$$\begin{aligned}\|u(t)\|_{L^q(\Omega)} &\le \left\|E_{\alpha}\left((\log\tfrac{t}{a})^{\alpha}\Delta\right)u_a\right\|_{L^q(\Omega)}+C\int_a^t(\log\tfrac{t}{s})^{\frac{\alpha}{2}-1}\|(u\nabla v)(s)\|_{L^q(\Omega)}\frac{\mathrm{d}s}{s}\\ &\le \left\|E_{\alpha}\left((\log\tfrac{t}{a})^{\alpha}\Delta\right)u_a\right\|_{L^q(\Omega)}+C\int_a^t(\log\tfrac{t}{s})^{\frac{\alpha}{2}-1}\|u(s)\|_{L^{\rho q}(\Omega)}\|(\nabla v)(s)\|_{L^{\frac{\rho q}{\rho-1}}(\Omega)}\frac{\mathrm{d}s}{s}\\ &\le \left\|E_{\alpha}\left((\log\tfrac{t}{a})^{\alpha}\Delta\right)u_a\right\|_{L^q(\Omega)}+C(\log\tfrac{t}{a})^{\frac{\alpha}{2}-\beta}\mathrm{B}\left(1-\beta,\tfrac{\alpha}{2}\right)\|u\|_{\mathscr{X}}\sup_{t\in(a,T)}\|(\nabla v)(t)\|_{L^{\frac{\rho q}{\rho-1}}(\Omega)}.\end{aligned}\tag{3.29}$$

From (3.5) and (3.15), we have

$$\begin{aligned}\sup_{t\in(a,T)}\|\nabla v(t)\|_{L^{\frac{\rho q}{\rho-1}}(\Omega)} &\le \sup_{t\in(a,T)}\left\|\nabla E_{\alpha}\left((\log\tfrac{t}{a})^{\alpha}(\Delta-\gamma)\right)v_a\right\|_{L^{\frac{\rho q}{\rho-1}}(\Omega)}\\ &\quad+\sup_{t\in(a,T)}\int_a^t(\log\tfrac{t}{s})^{\frac{\alpha}{2}-1}\|u(s)\|_{L^{\rho q}(\Omega)}\|u(s)\|_{L^{\frac{\rho q}{\rho-1}}(\Omega)}\frac{\mathrm{d}s}{s}\\ &\le C\sup_{t\in(a,T)}\left\|\nabla E_{\alpha}\left((\log\tfrac{t}{a})^{\alpha}(\Delta-\gamma)\right)v_a\right\|_{L^{\rho q}(\Omega)}\\ &\quad+C\sup_{t\in(a,T)}\int_a^t(\log\tfrac{t}{s})^{\frac{\alpha}{2}-1}\|u(s)\|_{L^{\rho q}(\Omega)}\frac{\mathrm{d}s}{s}\\ &\le C\left(\|\nabla v_a\|_{L^{\infty}(\Omega)}+CR\int_a^t(\log\tfrac{t}{s})^{\frac{\alpha}{2}-1}(\log\tfrac{s}{a})^{-\beta}\frac{\mathrm{d}s}{s}\right)\\ &\le C\left(\|\nabla v_a\|_{L^{\infty}(\Omega)}+CR(\log\tfrac{T}{a})^{\frac{\alpha}{2}-\beta}\mathrm{B}\left(1-\beta,\tfrac{\alpha}{2}\right)\right).\end{aligned}\tag{3.30}$$

Then, based on inequalities (3.29), (3.30), and Lemma 3.2, we conclude that u satisfies the convergence property (3.19). Considering Eq. (3.6) and inequality (3.16), we have

$$\begin{aligned}(\log\tfrac{t}{a})^{\beta}\|v(t)\|_{L^q(\Omega)} &\le (\log\tfrac{t}{a})^{\beta}\left\|E_{\alpha}\left((\log\tfrac{t}{a})^{\alpha}(\Delta-\gamma)\right)v_a\right\|_{L^q(\Omega)}\\ &\quad+C(\log\tfrac{t}{a})^{\beta}\int_a^t(\log\tfrac{t}{s})^{\alpha-1}\|u(t)\|_{L^q(\Omega)}\frac{\mathrm{d}s}{s}\\ &\le C(\log\tfrac{t}{a})^{\beta}\left\|E_{\alpha}\left((\log\tfrac{t}{a})^{\alpha}(\Delta-\gamma)\right)v_a\right\|_{L^{\rho q}(\Omega)}+C(\log\tfrac{t}{a})^{\alpha}\|u\|_{\mathscr{X}}.\end{aligned}$$

Utilizing Lemma 3.2, we get the convergence (3.20). Consequently, any solution $(u,v)\in\mathscr{X}\times\mathscr{X}$ to the integral Eq. (3.6) satisfies the convergent relations (3.19) and (3.20).

Next, we aim to show u, v, and $\nabla v\in C([a,T];L^q(\Omega))$. Using the method for proving inequality (3.29) leads to

$$\|u(t)-u_a\|_{L^q(\Omega)}\le\left\|E_{\alpha}\left((\log\tfrac{t}{a})^{\alpha}\Delta\right)u_a-u_a\right\|_{L^q(\Omega)}+C(\log\tfrac{t}{a})^{\frac{\alpha}{2}-\beta}.$$

Applying Lemma 3.1 yields

$$\lim_{t\to a^+}\|u(t)-u_a\|_{L^q(\Omega)}=0.$$

Therefore, we obtain $u\in C([a,T];L^q(\Omega))$.

The continuity of v follows from combining Lemma 3.1 with Lemma 3.4, where $\psi(t)=\log\frac{t}{a}$ and the parameters are chosen such that $\beta<\mu<\alpha$ and $\nu=1-\mu$. Define the function $f(\psi(s),\psi(t))=(\psi(s))^{\mu}(\psi(t)-\psi(s))^{\alpha-\mu}E_{\alpha,\alpha}((\psi(t)-\psi(s))^{\alpha}(\Delta-\gamma))u(s)$, for all $a<s<t\le T$. Firstly, f is an $L^{\rho q}(\Omega)$-valued continuous function. Secondly, it can be shown that $\sup_{a<s<t<T}\|f(\psi(s),\psi(t))\|_{L^{\rho q}(\Omega)}<+\infty$ and $f(\psi(s),\psi(t))\to 0$ as $(s,t)\to(a,a)$. Similarly, the continuity of ∇v can be shown by applying the same reasoning.

To prove continuous dependence on the initial data, we adopt an approach analogous to that used in the contraction mapping argument. Specifically, let (u^1, v^1) and (u^2, v^2) be $\mathscr{B}_R$-solutions of the integral equations defined by (3.6) with initial data (u_a^1, v_a^1) and (u_a^2, v_a^2), respectively. Utilizing the representation (3.6), Lemma 3.3, and inequalities (3.22) and (3.24), we obtain

$$\begin{aligned}\left\|u^1-u^2\right\|_{\mathscr{X}} \leq & C\left\|u_a^1-u_a^2\right\|_{L^q(\Omega)}+C \mathrm{B}\left(1-\beta-\frac{\alpha}{2}, \frac{\alpha}{2}\right) \sup_{t\in(a,T)}(\log \frac{t}{a})^{\frac{\alpha}{2}}\left\|\nabla v^1(t)\right\|_{L^{\infty}(\Omega)}\left\|u^1-u^2\right\|_{\mathscr{X}} \\ & +C R \mathrm{B}\left(1-\beta-\frac{\alpha}{2}, \frac{\alpha}{2}\right) \sup_{t\in(a,T)}(\log \frac{t}{a})^{\frac{\alpha}{2}}\left\|\nabla\left(v^1-v^2\right)(t)\right\|_{L^{\infty}(\Omega)} \\ \leq & C\left\|u_a^1-u_a^2\right\|_{L^q(\Omega)}+C^2 R \mathrm{B}\left(1-\beta-\frac{\alpha}{2}, \frac{\alpha}{2}\right)\left\|v_a^1-v_a^2\right\|_{L^{\infty}(\Omega)}+\frac{3}{4}\left\|u^1-u^2\right\|_{\mathscr{X}} .\end{aligned} \tag{3.31}$$

Employing Eq. (3.6), and inequalities (3.2) and (3.14) gives

$$\left\|v^1-v^2\right\|_{\mathscr{X}} \leq C\left\|v_a^1-v_a^2\right\|_{L^{\infty}(\Omega)}+\frac{1}{2}\left\|u^1-u^2\right\|_{\mathscr{X}} . \tag{3.32}$$

Then we get

$$\left\|u^1-u^2\right\|_{\mathscr{X}}+\left\|v^1-v^2\right\|_{\mathscr{X}} \leq C\left(\left\|u_a^1-u_a^2\right\|_{L^q(\Omega)}+\left\|v_a^1-v_a^2\right\|_{L^{\infty}(\Omega)}\right).$$

This closes the proof of Theorem 3.1. □

Theorem 3.2. *Under the hypotheses of Theorem 3.1, provided that (u, v) is an L^q-mild solution of Eqs. (1.1)–(1.3), then (u, v) can be uniquely continued up to maximal time $T_{\max} > T$. If $T_{\max} < +\infty$, then $\limsup_{t\to T_{\max}^-} \|u(t)\|_{L^{\rho q}(\Omega)} = \infty$.*

Proof (*Continuation of the Solution*).. Let $(u, v) : [a, T] \to (L^{\rho q}(\Omega))^2$ be the solution determined by Theorem 3.1 with $u, v \in \mathscr{B}_R$. For $\overline{T} > T$, we define the complete metric space

$$\mathscr{C}=\left\{\bar{u} \in C\left((a, \overline{T}]; L^{\rho q}(\Omega)\right) \mid \sup_{t\in[T,\overline{T}]}\|\bar{u}(t)-u(T)\|_{L^{\rho q}(\Omega)}<R, u \equiv \bar{u} \text{ in } [a, T]\right\}$$

with norm defined by

$$\|\bar{u}\|_{\mathscr{C}}=\sup_{t\in(a,\overline{T})}(\log \frac{t}{a})^{\beta}\|\bar{u}(t)\|_{L^{\rho q}(\Omega)}.$$

Let $\Phi : \mathscr{C} \to \mathscr{C}$ be given by Eq. (3.25).

Set $\bar{u} \in \mathscr{C}$, and define $\bar{v}$ as the function given by Eq. (3.6). A straightforward computation reveals that $\Phi\bar{u}(t) = u(t)$ for all $t \in [a, T]$. Using inequalities (3.3) and (3.4), we obtain

$$\left\|\nabla E_\alpha\left((\log \frac{t}{a})^\alpha(\Delta-\gamma)\right) f\right\|_{L^{\infty}(\Omega)} \leq C(\log \frac{t}{a})^{-\frac{\alpha}{2}}\left((\log \frac{t}{a})^{\frac{\alpha}{2}}+1\right)\|f\|_{L^{\infty}(\Omega)}, \quad t>a, \tag{3.33}$$

$$\left\|\nabla E_{\alpha,\alpha}\left((\log \frac{t}{a})^\alpha(\Delta-\gamma)\right) f\right\|_{L^{\infty}(\Omega)} \leq C\left(1+(\log \frac{t}{a})^{-\frac{\alpha}{2}\left(\frac{N}{\rho q}+1\right)}\right)\|f\|_{L^{\rho q}(\Omega)}, \quad t>a, \tag{3.34}$$

$$\left\|E_{\alpha,\alpha}\left((\log \frac{t}{a})^\alpha\Delta\right)\nabla\cdot f\right\|_{L^{\rho q}(\Omega)} \leq C\left(1+(\log \frac{t}{a})^{-\frac{\alpha}{2}}\right)\|f\|_{L^{\rho q}(\Omega)}, \quad t>a. \tag{3.35}$$

By using inequalities (3.33) and (3.34), we get

$$\sup_{t\in[a,\overline{T}]}(\log \frac{t}{a})^{\frac{\alpha}{2}}\|\nabla\bar{v}(t)\|_{L^{\infty}(\Omega)}<+\infty.$$

In fact, we also have the following inequalities:

$$\begin{aligned}(\log \frac{t}{a})^{\frac{\alpha}{2}}\|\nabla\bar{v}(t)\|_{L^{\infty}(\Omega)} \leq & C\left\|v_a\right\|_{L^{\infty}(\Omega)}+C(\log \frac{t}{a})^{\frac{\alpha}{2}}\int_a^t(\log \frac{t}{s})^{\alpha-1}\left\|\nabla E_{\alpha,\alpha}\left((\log \frac{t}{s})^\alpha(\Delta-\gamma)\right)u(s)\right\|_{L^{\infty}(\Omega)}\frac{\mathrm{d}s}{s} \\ \leq & C\left\|v_a\right\|_{L^{\infty}(\Omega)}+C(\log \frac{t}{a})^{\frac{\alpha}{2}}\int_a^t(\log \frac{t}{s})^{\alpha-1}\left(1+(\log \frac{t}{a})^{-\frac{\alpha}{2}\left(\frac{N}{\rho q}+1\right)}\right)\|\bar{u}(s)\|_{L^{\rho q}(\Omega)}\frac{\mathrm{d}s}{s} \\ \leq & C\left\|v_a\right\|_{L^{\infty}(\Omega)}+C\Big[(\log \frac{t}{a})^{\frac{3\alpha}{2}-\beta}\mathrm{B}(1-\beta, \alpha) \\ & +(\log \frac{t}{a})^{\frac{\alpha}{2}\left(1-\frac{N}{\rho q}\right)+\frac{\alpha}{2}-\beta}\mathrm{B}(1-\beta, \frac{\alpha}{2}(1-\frac{N}{\rho q}))\Big]\|\bar{u}\|_{\mathscr{C}}.\end{aligned} \tag{3.36}$$

Given that $u \in \mathscr{C}$, the continuity of Φu can be shown by using a similar argument as in Theorem 3.1. For $a < t_1 < t_2 < T$, the result follows from the following three estimates when $t_2 \to t_1$.

$$\begin{aligned}
\|I_1\|_{L^{\rho q}(\Omega)} &\le C(\log\frac{t_2}{a})^{-\beta}\int_{\frac{\log\frac{t_1}{a}}{\log\frac{t_2}{a}}}^{1}(1-s)^{\frac{\alpha}{2}-1}s^{-\beta-\frac{\alpha}{2}}\frac{\mathrm{d}s}{s},\\
\|I_2\|_{L^{\rho q}(\Omega)} &\le C\int_a^{t_1}\left|(\log\frac{t_2}{s})^{\alpha-1}-(\log\frac{t_1}{s})^{\alpha-1}\right|(\log\frac{t_2}{s})^{-\frac{\alpha}{2}}(\log\frac{s}{a})^{-\frac{\alpha}{2}-\beta}\frac{\mathrm{d}s}{s},\\
\|I_3\|_{L^{\rho q}(\Omega)} &\le C\int_a^{t_1}(\log\frac{t_1}{s})^{\alpha-1}(\log\frac{s}{a})^{-\beta-\frac{\alpha}{2}}\int_0^{\infty}\alpha\tau M_\alpha(\tau)\left(1+\tau^{-\frac{1}{2}}(\log\frac{t_1}{s})^{-\frac{\alpha}{2}}\right)\\
&\quad\times\left\|G\left(\tau\left((\log\frac{t_2}{s})^{\alpha}-(\log\frac{t_1}{s})^{\alpha}\right)\right)-I\right\|_{\mathscr{B}(L^{\rho q}(\Omega))}\mathrm{d}\tau\frac{\mathrm{d}s}{s},
\end{aligned}$$

where $\mathscr{B}(L^{\rho q}(\Omega))$ is a bounded linear operator space and the terms I_1, I_2, and I_3 are explicitly defined as follows,

$$\begin{aligned}
I_1 &= \int_{t_1}^{t_2}\left(\log\frac{t_2}{s}\right)^{\alpha-1}E_{\alpha,\alpha}\left((\log\frac{t_2}{s})^{\alpha}\Delta\right)\nabla\cdot(\bar{u}\nabla\bar{v})(s)\frac{\mathrm{d}s}{s},\\
I_2 &= \int_a^{t_1}\left[\left(\log\frac{t_2}{s}\right)^{\alpha-1}-\left(\log\frac{t_1}{s}\right)^{\alpha-1}\right]E_{\alpha,\alpha}\left((\log\frac{t_2}{s})^{\alpha}\Delta\right)\nabla\cdot(\bar{u}\nabla\bar{v})(s)\frac{\mathrm{d}s}{s},\\
I_3 &= \int_a^{t_1}\left(\log\frac{t_1}{s}\right)^{\alpha-1}\left[E_{\alpha,\alpha}\left((\log\frac{t_2}{s})^{\alpha}\Delta\right)-E_{\alpha,\alpha}\left((\log\frac{t_1}{s})^{\alpha}\Delta\right)\right]\nabla\cdot(\bar{u}\nabla\bar{v})(s)\frac{\mathrm{d}s}{s}.
\end{aligned}$$

Next, for $T < t < \overline{T}$, we have

$$\begin{aligned}
(\Phi\bar{u})(t)-u(T) &= \left(E_\alpha\left((\log\frac{t}{a})^{\alpha}\Delta\right)-E_\alpha\left((\log\frac{T}{a})^{\alpha}\Delta\right)\right)u_a\\
&\quad-\int_a^{T}\left((\log\frac{t}{s})^{\alpha-1}E_{\alpha,\alpha}\left((\log\frac{t}{s})^{\alpha}\Delta\right)-(\log\frac{T}{s})^{\alpha-1}E_{\alpha,\alpha}\left((\log\frac{T}{s})^{\alpha}\Delta\right)\right)\nabla\cdot(u\nabla v)(s)\frac{\mathrm{d}s}{s}\\
&\quad-\int_T^{t}(\log\frac{t}{s})^{\alpha-1}E_{\alpha,\alpha}\left((\log\frac{t}{s})^{\alpha}\Delta\right)\nabla\cdot(\bar{u}\nabla\bar{v})(s)\frac{\mathrm{d}s}{s}\\
&:= \mathscr{K}_1(t)+\mathscr{K}_2(t)+\mathscr{K}_3(t).
\end{aligned}$$

According to Lemma 3.1, it follows that $\mathscr{K}_1(t)$ tends to zero in the $L^{\rho q}$-norm as $t \to T^+$. Furthermore, by applying the Lebesgue dominated convergence theorem, we conclude that $\|\mathscr{K}_2(t)\|_{L^{\rho q}(\Omega)}$ also vanishes as $t \to T^+$. Taking into account inequalities (3.35) and (3.36), we arrive at

$$\begin{aligned}
\|\mathscr{K}_3(t)\|_{L^{\rho q}(\Omega)} &\le C\int_T^{t}(\log\frac{t}{s})^{\alpha-1}\left(1+(\log\frac{t}{s})^{-\frac{\alpha}{2}}\right)\|(\bar{u}\nabla\bar{v})(s)\|_{L^{\rho q}(\Omega)}\frac{\mathrm{d}s}{s}\\
&\le C\int_T^{t}(\log\frac{t}{s})^{\frac{\alpha}{2}-1}\|\bar{u}(s)\|_{L^{\rho q}(\Omega)}\|\nabla\bar{v}(s)\|_{L^{\infty}(\Omega)}\frac{\mathrm{d}s}{s}\\
&\le C\left(R+\|u(T)\|_{L^{\rho q}(\Omega)}\right)\sup_{t\in[a,\overline{T}]}(\log\frac{t}{a})^{\frac{\alpha}{2}}\|\nabla\bar{v}(t)\|_{L^{\infty}(\Omega)}\int_{\frac{\log\frac{T}{a}}{\log\frac{t}{a}}}^{1}(1-s)^{\frac{\alpha}{2}-1}s^{-\frac{\alpha}{2}}\mathrm{d}s\to 0
\end{aligned}$$

as $t \to T^+$. Therefore, we can take $\overline{T}$ so close to T such that $\|\mathscr{K}_i(t)\|_{L^{\rho q}(\Omega)} < R/3$, $i = 1, 2, 3$ and we have

$$\sup_{t\in[T,\overline{T}]}\|\Phi\bar{u}(t)-u(T)\|_{L^{\rho q}(\Omega)} < R.$$

Next, we prove that Φ is a contraction mapping. Let u^i be in $\mathscr{C}$, and define v^i by Eq. (3.6), $i = 1, 2$. It is crucial to analyze the contributions of the terms $\mathscr{J}_1$ and $\mathscr{J}_2$, as defined in expression (3.26). Using the inequality (3.36) yields

$$\begin{aligned}
(\log\frac{t}{a})^{\beta}\left\|\mathscr{J}_1(t)\right\|_{L^{\rho q}(\Omega)} \le& C(\log\frac{t}{a})^{\beta}\int_a^{t}(\log\frac{t}{s})^{\frac{\alpha}{2}-1}(\log\frac{s}{a})^{-\beta-\frac{\alpha}{2}}\frac{\mathrm{d}s}{s}\\
&\times\sup_{t\in[a,\overline{T}]}(\log\frac{t}{a})^{\frac{\alpha}{2}}\left\|\nabla v^1(t)\right\|_{L^{\infty}(\Omega)}\left\|u^1-u^2\right\|_{\mathscr{C}}\\
\le& C^2\mathrm{B}(1-\beta-\frac{\alpha}{2},\frac{\alpha}{2})\left(\|v_a\|_{L^{\infty}(\Omega)}+(\log\frac{\overline{T}}{a})^{\frac{\alpha}{2}\left(2-\frac{N}{\rho q}\right)-\beta}\mathrm{B}(1-\beta,\frac{\alpha}{2}(1-\frac{N}{\rho q}))\right.\\
&\left.\times(\log\frac{\overline{T}}{a})^{\beta}\left(R+\|u(T)\|_{L^{\rho q}(\Omega)}\right)\right)\left\|u^1-u^2\right\|_{\mathscr{C}}.
\end{aligned}\tag{3.37}$$

By considering the upper bound below,

$$\sup_{t\in(a,\overline{T})}(\log\frac{t}{a})^{\frac{\alpha}{2}}\left\|\nabla\left(v^1-v^2\right)(t)\right\|_{L^{\infty}(\Omega)} \le C(\log\frac{\overline{T}}{a})^{\frac{\alpha}{2}\left(2-\frac{N}{\rho q}\right)-\beta}\mathrm{B}\left(1-\beta,\frac{\alpha}{2}\left(1-\frac{N}{\rho q}\right)\right)\left\|u^1-u^2\right\|_{\mathscr{C}},$$

we conclude that

$$\begin{aligned}(\log\frac{t}{a})^{\beta}\left\|\mathscr{J}_2(t)\right\|_{L^{\rho q}(\Omega)} \le C^2(\log\frac{\overline{T}}{a})^{\frac{\alpha}{2}\left(2-\frac{N}{\rho q}\right)-\beta}(\log\frac{\overline{T}}{a})^{\beta}\left(R+\|u(T)\|_{L^{\rho q}(\Omega)}\right)\\ \times \mathrm{B}\left(1-\beta-\frac{\alpha}{2},\frac{\alpha}{2}\right)\mathrm{B}\left(1-\beta,\frac{\alpha}{2}\left(1-\frac{N}{\rho q}\right)\right)\left\|u^1-u^2\right\|_{\mathscr{C}}.\end{aligned} \tag{3.38}$$

By selecting $\|v_a\|_{L^\infty(\Omega)}$ and $\overline{T}$ appropriately, and utilizing the inequalities (3.37) and (3.38), it follows that Φ is a contraction.

Let u be the unique fixed point of Φ in $\mathscr{C}$, and define v by (3.6). A priori estimates below can be established as

$$\begin{aligned}\left\|\nabla E_{\alpha,\alpha}\left((\log\frac{t}{a})^{\alpha}\Delta\right)f\right\|_{L^q(\Omega)} &\le C\left(1+(\log\frac{t}{a})^{-\frac{\alpha}{2}}\right)\|f\|_{L^q(\Omega)},\quad t>a,\\ \left\|\nabla E_{\alpha}\left((\log\frac{t}{a})^{\alpha}(\Delta-\gamma)\right)v_a\right\|_{L^{\frac{\rho q}{\rho-1}}(\Omega)} &\le C\left\|\nabla v_a\right\|_{L^{\rho q}(\Omega)},\quad t>a,\\ \left\|\nabla E_{\alpha,\alpha}\left((\log\frac{t}{a})^{\alpha}(\Delta-\gamma)\right)f\right\|_{L^{\frac{\rho q}{\rho-1}}(\Omega)} &\le C(\log\frac{t}{a})^{-\frac{\alpha}{2}}\left((\log\frac{t}{a})^{\frac{\alpha}{2}}+1\right)\|f\|_{L^{\rho q}(\Omega)},\quad t>a,\\ \sup_{t\in[a,\overline{T}]}\|\nabla v(s)\|_{L^{\frac{\rho q}{\rho-1}}(\Omega)} &\le C\left(\left\|\nabla v_a\right\|_{L^\infty(\Omega)}+(\log\frac{\overline{T}}{a})^{\frac{\alpha}{2}-\beta}\mathrm{B}\left(1-\beta,\frac{\alpha}{2}\right)\left(R+(\log\frac{\overline{T}}{a})^{\beta}\|u(T)\|_{L^{\rho q}(\Omega)}\right)\right).\end{aligned}$$

Based on the preceding estimates, we get

$$\begin{aligned}\|u(t)-u_a\|_{L^q(\Omega)} &\le \left\|E_{\alpha}\left((\log\frac{t}{a})^{\alpha}\Delta\right)u_a-u_a\right\|_{L^q(\Omega)}\\ &\quad+C(\log\frac{t}{a})^{\frac{\alpha}{2}-\beta}\mathrm{B}\left(1-\beta,\frac{\alpha}{2}\right)\|u\|_{\mathscr{C}}\sup_{t\in[a,\overline{T}]}\|\nabla v(t)\|_{L^{\frac{\rho q}{\rho-1}}(\Omega)}\\ &\le \left\|E_{\alpha}\left((\log\frac{t}{a})^{\alpha}\Delta\right)u_a-u_a\right\|_{L^q(\Omega)}+C(\log\frac{t}{a})^{\frac{\alpha}{2}-\beta}.\end{aligned} \tag{3.39}$$

Now, we conclude that $u\in C\left([a,\overline{T}];L^q(\Omega)\right)$ from the inequality (3.39) and the continuous embedding $L^{\rho q}(\Omega)\hookrightarrow L^q(\Omega)$. Additionally, the fact that $v\in C\left([a,\overline{T}];L^q(\Omega)\right)$ can be established via Lemma 3.4. Consequently, the solution (u,v) satisfies the necessary conditions to be considered an L^q-mild solution, as stated in our theorem.

Let two L^q-mild solutions (u_1,v_1) and (u_2,v_2) belong to $C\left([a,\overline{T}];L^q(\Omega)\right)^2$ such that

$$\begin{aligned}u&=u_1=u_2,\quad t\in[a,T],\\ v&=v_1=v_2,\quad t\in[a,T].\end{aligned}$$

We shall prove that

$$u_1=u_2,\quad t\in[a,\overline{T}], \tag{3.40}$$

$$v_1=v_2,\quad t\in[a,\overline{T}]. \tag{3.41}$$

Let $t\in[a,\overline{T}]$. Considering inequalities (3.35) and (3.36) gives

$$\begin{aligned}\left\|u_1(t)-u_2(t)\right\|_{L^{\rho q}(\Omega)} \le& C\int_a^t(\log\frac{t}{s})^{\alpha-1}\left(1+(\log\frac{t}{s})^{-\frac{\alpha}{2}}\right)\left\|\left(\left(u_1-u_2\right)\nabla v_1+u_2\nabla\left(v_1-v_2\right)\right)(s)\right\|_{L^{\rho q}(\Omega)}\frac{\mathrm{d}s}{s}\\ \le& C\int_T^t(\log\frac{t}{s})^{\frac{\alpha}{2}\left(1-\frac{N}{\rho q}\right)-1}\left(\left\|\left(u_1-u_2\right)(s)\right\|_{L^{\rho q}(\Omega)}\left\|\nabla v_1(s)\right\|_{L^\infty(\Omega)}\right.\\ &\left.+\|u_2(s)\|_{L^{\rho q}(\Omega)}\left\|\nabla\left(v_1-v_2\right)(s)\right\|_{L^\infty(\Omega)}\right)\frac{\mathrm{d}s}{s}\\ \le& C\int_T^t(\log\frac{t}{s})^{\frac{\alpha}{2}\left(1-\frac{N}{\rho q}\right)-1}\left((\log\frac{s}{a})^{-\frac{\alpha}{2}}\left\|\left(u_1-u_2\right)(s)\right\|_{L^{\rho q}(\Omega)}\right.\\ &\left.+(\log\frac{s}{a})^{-\beta}\left\|\nabla\left(v_1-v_2\right)(s)\right\|_{L^\infty(\Omega)}\right)\frac{\mathrm{d}s}{s}\\ \le& C\int_T^t(\log\frac{t}{s})^{\frac{\alpha}{2}\left(1-\frac{N}{\rho q}\right)-1}\left(\left\|\left(u_1-u_2\right)(s)\right\|_{L^{\rho q}(\Omega)}+\left\|\nabla\left(v_1-v_2\right)(s)\right\|_{L^\infty(\Omega)}\right)\frac{\mathrm{d}s}{s}.\end{aligned} \tag{3.42}$$

Additionally, we have

$$\left\|\nabla\left(v_1-v_2\right)(t)\right\|_{L^\infty(\Omega)}\le C\int_T^t(\log\frac{t}{s})^{\frac{\alpha}{2}\left(1-\frac{N}{\rho q}\right)-1}\left\|\left(u_1-u_2\right)(s)\right\|_{L\rho q(\Omega)}\frac{\mathrm{d}s}{s}. \tag{3.43}$$

Now, let $\xi:[a,\overline{T}]\to[0,\infty)$ be defined by

$$\xi(t)=\left\|u_1(t)-u_2(t)\right\|_{L^{\rho q}(\Omega)}+\left\|\nabla\left(v_1-v_2\right)(t)\right\|_{L^\infty(\Omega)}.$$

From the estimates provided in (3.42) and (3.43), it follows that

$$\xi(t) \le C \int_a^t (\log \frac{t}{s})^{\frac{\alpha}{2}\left(1-\frac{N}{\rho q}\right)-1} \xi(s) \frac{\mathrm{d}s}{s}.$$

By applying Lemma 3.5 with $l(t) \equiv 0$, we deduce that $\xi(t) = 0$, leading to Eqs. (3.40) and (3.41). Consequently, the uniqueness of continuations is established.

(Blow-up). Suppose that $T_{\max} < \infty$ and that there exists a constant $K > 0$ such that for all $t \in [a, T_{\max})$ the inequality $\|u(t)\|_{L^{\rho q}(\Omega)} \le K$ holds. Thus, given a sequence of positive real numbers $t_n \to T_{\max}^-$, we want to show that $\left(u\left(t_n\right)\right)_{n\in\mathbb{N}}$ is a Cauchy sequence in $L^{\rho q}(\Omega)$. Indeed, for $a < t_m < t_n < T_{\max}$, we have

$$\begin{aligned}
&u\left(t_n\right) - u\left(t_m\right) \\
&= \left[E_\alpha\left((\log \frac{t_n}{a})^\alpha \Delta\right) - E_\alpha\left((\log \frac{t_m}{a})^\alpha \Delta\right)\right] u_a \\
&\quad - \int_a^{t_m} \left((\log \frac{t_n}{s})^{\alpha-1} E_{\alpha,\alpha}\left((\log \frac{t_n}{s})^\alpha \Delta\right) - (\log \frac{T_{\max}}{s})^{\alpha-1} E_{\alpha,\alpha}\left((\log \frac{T_{\max}}{s})^\alpha \Delta\right)\right) \nabla \cdot (u \nabla v)(s) \frac{\mathrm{d}s}{s} \\
&\quad + \int_a^{t_m} \left((\log \frac{t_m}{s})^{\alpha-1} E_{\alpha,\alpha}\left((\log \frac{t_m}{s})^\alpha \Delta\right) - (\log \frac{T_{\max}}{s})^{\alpha-1} E_{\alpha,\alpha}\left((\log \frac{T_{\max}}{s})^\alpha \Delta\right)\right) \nabla \cdot (u \nabla v)(s) \frac{\mathrm{d}s}{s} \\
&\quad - \int_{t_m}^{t_n} (\log \frac{t_n}{s})^{\alpha-1} E_{\alpha,\alpha}\left((\log \frac{t_n}{s})^\alpha \Delta\right) \nabla \cdot (u \nabla v)(s) \frac{\mathrm{d}s}{s}.
\end{aligned}$$

It follows that the right-hand items all converge to zero in the $L^{\rho q}$-norm as $n, m \to \infty$. Specifically,

$$\left\| \int_{t_m}^{t_n} (\log \frac{t_n}{s})^{\alpha-1} E_{\alpha,\alpha}\left((\log \frac{t_n}{s})^\alpha \Delta\right) \nabla \cdot (u \nabla v)(s) \frac{\mathrm{d}s}{s} \right\|_{L^{\rho q}(\Omega)} \le CK \int_{\frac{\log \frac{t_m}{s}}{\log \frac{t_n}{s}}}^1 (1-s)^{\frac{\alpha}{2}-1} s^{-\frac{\alpha}{2}} \mathrm{d}s.$$

Thus, we obtain that $\left\|u\left(t_n\right) - u\left(t_m\right)\right\|_{L^{\rho q}(\Omega)} \to 0$ as $n, m \to \infty$. Therefore, the limit $\lim_{n\to\infty} u(t_n)$ exists in $L^q(\Omega)$. By a similar argument, we can conclude that $\lim_{n\to\infty} v(t_n)$ exists in $L^q(\Omega)$. As a result, both $u(T_{\max})$ and $v(T_{\max})$ exist in $L^q(\Omega)$. This implies that the pair (u, v) can be extended, leading to a contradiction. The proof is complete. □

4. Numerical algorithm

In this part, we establish a numerical scheme based on the finite element method to solve the considered model, and the corresponding numerical analysis and computer simulations are displayed. Throughout this section, we assume that the numerical analysis is performed on a time interval $[a, T]$ strictly before the blow-up time, i.e., $T < T_{\max}$, guaranteeing sufficient regularity of the exact solution.

We denote $W^{m,p}(\Omega)$ as the Sobolev space endowed with the usual norm $\|\cdot\|_{W^{m,p}(\Omega)}$, and $H^m(\Omega) = W^{m,2}(\Omega)$. The L^2 inner product and L^2 norm are used as usual.

$$(v, w) = \int_\Omega vw \mathrm{d}x, \quad \|v\| = \sqrt{(v, v)}.$$

The weak formulation of problem (1.1) can be written as: $u, v \in H^1(\Omega)$ satisfy

$$\begin{cases}
\left({}_{CH}\mathrm{D}_{a,t}^\alpha u, w\right) + (\nabla u, \nabla w) - (u \nabla v, \nabla w) = 0, & \forall\, w \in H^1(\Omega), \\
\left({}_{CH}\mathrm{D}_{a,t}^\alpha v, w\right) + (\nabla v, \nabla w) + (\gamma v, w) = (u, w), & \forall\, w \in H^1(\Omega).
\end{cases} \tag{4.1}$$

Multiplying both sides of the second equation by u and substituting the result into the first equation yields

$$\left({}_{CH}\mathrm{D}_{a,t}^\alpha u, w\right) + (\nabla u, \nabla w) = \left(u^2, w\right) - (\gamma uv, w) - \left(u\, {}_{CH}\mathrm{D}_{a,t}^\alpha v, w\right). \tag{4.2}$$

Then, for $u, v \in H^1(\Omega)$, system (4.1) and Eq. (4.2) are equivalent.

4.1. Finite element analysis on a fixed mesh

A fixed mesh represents a mesh that does not change over time. Fixed meshes can be divided into two types: uniform meshes and nonuniform meshes. Fig. 1 shows the node distributions and mesh structures of two fixed meshes, including a graded mesh, a common type of nonuniform mesh. Graded meshes have shown their advantages in solving nonlinear reaction–diffusion equations [25,26].

Let $\mathscr{T}_h = \bigcup K$ denote a fixed mesh, and define the discretization parameter $h = \max_{K\in\mathscr{T}_h} h_K$ as the maximal diameter of the circumscribed ball over all elements, where h_K represents the diameter of the local element K. Let $V_h := \{\varphi \in C(\overline{\Omega}) | \varphi \in P^1(K), \forall K \in$

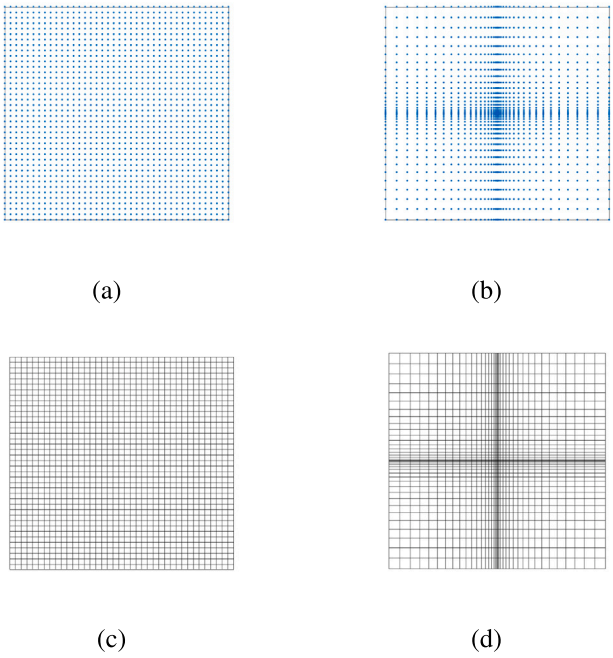


Fig. 1. (a) The nodes of the uniform mesh; (b) The nodes of the graded mesh. (c) Uniform mesh; (d) Graded mesh.

$\mathscr{T}_h\} \subset H^1(\Omega)$ be the standard finite element space, where $P^1(K)$ denotes the space of linear polynomials over the element K. The semi-discrete finite element scheme is given as follows: find $u_h,\ v_h \in V_h$ such that

$$\begin{cases} \left({}_{CH}\mathrm{D}^{\alpha}_{a,t}u_h, w_h\right) + \left(\nabla u_h, \nabla w_h\right) - \left(u_h \nabla v_h, \nabla w_h\right) = 0, & w_h \in V_h, \\ \left({}_{CH}\mathrm{D}^{\alpha}_{a,t}v_h, w_h\right) + \left(\nabla v_h, \nabla w_h\right) + \gamma\left(v_h, w_h\right) = \left(u_h, w_h\right), & w_h \in V_h. \end{cases} \tag{4.3}$$

Assume that the discretization parameters satisfy quasi-uniform condition, that is, there exists a positive constant c such that

$$\frac{h}{h_K} \le c, \quad \forall K \in \mathscr{T}_h.$$

Define the projection operator $R_h : H^1(\Omega) \to V_h$ as follows,

$$(\nabla u, \nabla w_h) = (\nabla R_h u, \nabla w_h), \quad w_h \in V_h.$$

Then, there exists a positive constant C, independent of h, such that [27]

$$\|u - R_h u\| \le Ch\|u\|_{H^1}, \quad \forall u \in H^1, \tag{4.4}$$

and

$$\|u - R_h u\| \le Ch^2\|u\|_{H^2}, \quad \forall u \in H^2. \tag{4.5}$$

Let $\{P_i\}_{i=1}^{M}$ be the set of all vertices of $\mathscr{T}_h$ with M being a positive integer. The Lagrange interpolation operator $\pi_h : C(\overline{\Omega}) \to V_h$ is defined by $\pi_h v(P_i) = v(P_i)$ for all $P_i \in \{P_i\}_{i=1}^{M}$. For any $K \in \mathscr{T}_h$, we have

$$\|\pi_h v - v\|_{L^p(K)} \le Ch_K^2\|v\|_{W^{2,p}(K)}, \quad p \in (d/2, \infty), v \in W^{2,p}(K).$$

The following lemmas will be used for error analysis later on.

Lemma 4.1. *Let $v(t)$ be absolutely continuous function on $[a, T]$. Then we have the inequality*

$$v(t)\,{}_{CH}\mathrm{D}^{\alpha}_{a,t}v(t) \ge \frac{1}{2}\,{}_{CH}\mathrm{D}^{\alpha}_{a,t}v^2(t).$$

Proof. To prove the inequality, it suffices to show that

$$\begin{aligned}
&v(t)\,{}_{CH}\mathrm{D}^{\alpha}_{a,t}v(t)-\frac{1}{2}\,{}_{CH}\mathrm{D}^{\alpha}_{a,t}v^2(t)\\
&=\frac{1}{\Gamma(1-\alpha)}v(t)\int_a^t\frac{\delta v(\tau)}{(\log\frac{t}{\tau})^{\alpha}}\frac{\mathrm{d}\tau}{\tau}-\frac{1}{2\Gamma(1-\alpha)}\int_a^t\frac{2v(\tau)\delta v(\tau)}{(\log\frac{t}{\tau})^{\alpha}}\frac{\mathrm{d}\tau}{\tau}\\
&=\frac{1}{\Gamma(1-\alpha)}\int_a^t\frac{(v(t)-v(\tau))\delta v(\tau)}{(\log\frac{t}{\tau})^{\alpha}}\frac{\mathrm{d}\tau}{\tau}\\
&=\frac{1}{\Gamma(1-\alpha)}\int_a^t\frac{\delta v(\tau)}{(\log\frac{t}{\tau})^{\alpha}}\left(\int_\tau^t\delta v(\eta)\frac{\mathrm{d}\eta}{\eta}\right)\frac{\mathrm{d}\tau}{\tau}\\
&=\frac{1}{\Gamma(1-\alpha)}\int_a^t\delta v(\eta)\left(\int_a^\eta\frac{\delta v(\tau)}{(\log\frac{t}{\tau})^{\alpha}}\frac{\mathrm{d}\tau}{\tau}\right)\frac{\mathrm{d}\eta}{\eta}\\
&\equiv I\geq 0.
\end{aligned}$$

In fact,

$$\begin{aligned}
I&=\frac{1}{\Gamma(1-\alpha)}\int_a^t(\log\frac{t}{\eta})^{\alpha}\frac{\delta v(\eta)}{(\log\frac{t}{\eta})^{\alpha}}\left(\int_a^\eta\frac{\delta v(\tau)}{(\log\frac{t}{\tau})^{\alpha}}\frac{\mathrm{d}\tau}{\tau}\right)\frac{\mathrm{d}\eta}{\eta}\\
&=\frac{1}{2\Gamma(1-\alpha)}\int_a^t(\log\frac{t}{\eta})^{\alpha}\delta\left(\int_a^\eta\frac{\delta v(\tau)}{(\log\frac{t}{\tau})^{\alpha}}\frac{\mathrm{d}\tau}{\tau}\right)^2\frac{\mathrm{d}\eta}{\eta}\\
&=\frac{\alpha}{\Gamma(1-\alpha)}\int_a^t(\log\frac{t}{\eta})^{\alpha-1}\left(\int_a^\eta\frac{\delta v(\tau)}{(\log\frac{t}{\tau})^{\alpha}}\frac{\mathrm{d}\tau}{\tau}\right)^2\frac{\mathrm{d}\eta}{\eta}\geq 0.
\end{aligned}$$

This proof is thus complete. □

The following lemma is a direct consequence of Lemma 1 in [28] and Lemma 3.2 in [29].

Lemma 4.2. *Let $u(\mathrm{x},\cdot)\in AC_{\delta}[a,T]$ for any x, $u(\cdot,t)\in C(\overline{\Omega})$ for any $t\in[a,T]$. Then, for $\alpha\in(0,1)$ and a continuous function $\Phi(\mathrm{x})$, there holds*

$$\int_\Omega {}_{CH}\mathrm{D}^{\alpha}_{a,t}u(\mathrm{x},t)\,\Phi(\mathrm{x})\mathrm{dx}={}_{CH}\mathrm{D}^{\alpha}_{a,t}\left(\int_\Omega u(\mathrm{x},t)\Phi(\mathrm{x})\mathrm{dx}\right).$$

Lemma 4.3. *Let a nonnegative absolutely continuous function $y(t)$ satisfy the inequality*

$${}_{CH}\mathrm{D}^{\alpha}_{a,t}y(t)\leq c_1y(t)+c_2(t),\quad 0<\alpha\leq 1$$

for almost all t in $[a,T]$, where $c_1>0$ and $c_2(t)$ is an integrable nonnegative function on $[a,T]$. Then

$$y(t)\leq y(a)E_{\alpha}\left(c_1(\log\frac{t}{a})^{\alpha}\right)+\Gamma(\alpha)E_{\alpha,\alpha}\left(c_1(\log\frac{t}{a})^{\alpha}\right){}_H\mathrm{D}^{-\alpha}_{a,t}c_2(t).$$

Proof. Let $g(t)$ be an integrable function such that ${}_{CH}\mathrm{D}^{\alpha}_{a,t}y(t)-c_1y(t)=g(t)$. According to formula (3.2) in [29], we have

$$y(t)=y(a)E_{\alpha}\left(c_1(\log\frac{t}{a})^{\alpha}\right)+\int_a^t(\log\frac{t}{\tau})^{\alpha-1}E_{\alpha,\alpha}\left(c_1(\log\frac{t}{\tau})^{\alpha}\right)g(\tau)\frac{\mathrm{d}\tau}{\tau}.$$

Based on the inequality $g(t)\leq c_2(t)$, the positivity of the Mittag-Leffler function $E_{\alpha,\alpha}$ for given parameters, and the asymptotic growth behavior of $E_{\alpha,\alpha}(t)$, we obtain

$$\begin{aligned}
y(t)&\leq y(a)E_{\alpha}\left(c_1(\log\frac{t}{a})^{\alpha}\right)+\int_a^t(\log\frac{t}{\tau})^{\alpha-1}E_{\alpha,\alpha}\left(c_1(\log\frac{t}{\tau})^{\alpha}\right)c_2(\tau)\frac{\mathrm{d}\tau}{\tau}\\
&\leq y(a)E_{\alpha}\left(c_1(\log\frac{t}{a})^{\alpha}\right)+\Gamma(\alpha)E_{\alpha,\alpha}\left(c_1(\log\frac{t}{a})^{\alpha}\right){}_H\mathrm{D}^{-\alpha}_{a,t}c_2(t).
\end{aligned}$$

This proof is ended. □

4.1.1. Error analysis of the semi-discrete finite element scheme

Write the error as a sum of two terms,

$$\begin{aligned}
u-u_h&=u-R_hu+R_hu-u_h=\theta+\eta,\\
v-v_h&=v-R_hv+R_hv-v_h=\rho+\beta.
\end{aligned}\tag{4.6}$$

The terms $\theta=u-R_hu$ and $\rho=v-R_hv$ represent the projection errors associated with the operator R_h. These projection errors are controllable. In contrast, the terms η and β will be the main object of the numerical analysis.

Remark 4.1. The optimal error estimates in the following finite element analysis require high spatial regularity of the exact solution, specifically $H^2(\Omega)$. While Section 3 guarantees the existence of L^q-mild solutions, we impose additional standard *a priori* assumptions in this section to ensure that the $H^2(\Omega)$-norm of the solution remains uniformly bounded over the entire interval $[a,T]$. Specifically, we assume that the initial data $u_a, v_a \in H^2(\Omega)$ satisfy the homogeneous Neumann boundary conditions, and that the boundary $\partial\Omega$ is sufficiently smooth.

Next, we provide the error analysis for the semi-discrete scheme (4.3).

Theorem 4.1. *Assume that the solution* $(u(\mathrm{x},\cdot), v(\mathrm{x},\cdot)) \in H^2(\Omega)$. *Then the semi-discrete finite element solutions* $\left(u_h, v_h\right)$ *of system* (4.3) *satisfy the following error estimate:*

$$\left\|u(t)-u_h(t)\right\| + \left\|v(t)-v_h(t)\right\| \le Ch^2, \tag{4.7}$$

where C *is a constant independent of the mesh size* h.

Proof. By subtracting the second equation in (4.3) from that in (4.1), one gets

$$\left({}_{CH}\mathrm{D}^{\alpha}_{a,t}\beta, w_h\right) + \left(\nabla(\rho+\beta), \nabla w_h\right) = -\gamma\left(\rho+\beta, w_h\right) - \left({}_{CH}\mathrm{D}^{\alpha}_{a,t}\rho, w_h\right) + \left(\theta+\eta, w_h\right). \tag{4.8}$$

Note that $\left(\nabla\rho, \nabla w_h\right) = \left(\nabla(v - R_h v), \nabla w_h\right) = 0$ and $\|{}_{CH}\mathrm{D}^{\alpha}_{a,t}\rho\| \le Ch^2$. Let $w_h = \beta$. And then apply Young's inequality and the interpolation estimate (4.5) to obtain

$$\left({}_{CH}\mathrm{D}^{\alpha}_{a,t}\beta, \beta\right) \le C\left(\|\beta\|^2 + h^4 + \|\eta\|^2\right). \tag{4.9}$$

It is also known from Lemmas 4.1 and 4.2 that

$$\begin{aligned}\left({}_{CH}\mathrm{D}^{\alpha}_{a,t}\beta, \beta\right) &= \int_{\Omega} \beta\, {}_{CH}\mathrm{D}^{\alpha}_{a,t}\beta\, d\mathrm{x} \\ &\ge \frac{1}{2}\int_{\Omega} {}_{CH}\mathrm{D}^{\alpha}_{a,t}\beta^2 d\mathrm{x} = \frac{1}{2}\,{}_{CH}\mathrm{D}^{\alpha}_{a,t}\|\beta\|^2.\end{aligned} \tag{4.10}$$

Since $\beta(a) = 0$, setting $y(t) = \|\beta\|^2$ in Lemma 4.3, it is immediately deduced that

$$\|\beta\| \le C\left(h^2 + \|\eta\|\right). \tag{4.11}$$

For the semi-discrete scheme (4.3), we multiply its second equation by u_h and substitute it into the first equation to obtain

$$\left({}_{CH}\mathrm{D}^{\alpha}_{a,t}u_h, w_h\right) + \left(\nabla u_h, \nabla w_h\right) = \left(\left(u_h\right)^2, w_h\right) - \gamma\left(u_h v_h, w_h\right) - \left(u_h\, {}_{CH}\mathrm{D}^{\alpha}_{a,t}v_h, w_h\right). \tag{4.12}$$

Moreover,

$$\begin{aligned} uv - u_h v_h &= u\left(v - v_h\right) + v_h\left(u - u_h\right) \\ &= u(\rho+\beta) + v_h(\theta+\eta), \\ u\ {}_{CH}\mathrm{D}^{\alpha}_{a,t}v - u_h\ {}_{CH}\mathrm{D}^{\alpha}_{a,t}v_h &= u\left({}_{CH}\mathrm{D}^{\alpha}_{a,t}v - {}_{CH}\mathrm{D}^{\alpha}_{a,t}v_h\right) + \left(u - u_h\right){}_{CH}\mathrm{D}^{\alpha}_{a,t}v_h \\ &= u\ {}_{CH}\mathrm{D}^{\alpha}_{a,t}(\rho+\beta) + (\theta+\eta)_{CH}\mathrm{D}^{\alpha}_{a,t}v_h. \end{aligned} \tag{4.13}$$

Note that $\left(\nabla\theta, \nabla w_h\right) = \left(\nabla(u - R_h u), \nabla w_h\right) = 0$. Let $w_h = \eta$, then subtracting (4.2) and (4.12) yields

$$\begin{aligned}\left({}_{CH}\mathrm{D}^{\alpha}_{a,t}\eta, \eta\right) + (\nabla\eta, \nabla\eta) = &-\left({}_{CH}\mathrm{D}^{\alpha}_{a,t}\theta, \eta\right) + \left(\left(u+u_h\right)(\theta+\eta), \eta\right) \\ &- \gamma\left(u(\rho+\beta), \eta\right) - \gamma\left(v_h(\theta+\eta), \eta\right) \\ &- \left(u\ {}_{CH}\mathrm{D}^{\alpha}_{a,t}(\rho+\beta) + (\theta+\eta)_{CH}\mathrm{D}^{\alpha}_{a,t}v_h, \eta\right).\end{aligned} \tag{4.14}$$

Since our numerical analysis is strictly restricted to the time interval $[a,T]$ with $T < T_{\max}$, the exact solutions u and v of (1.1) are non-negative and uniformly bounded on this interval. Consequently, the term $|{}_{CH}\mathrm{D}^{\alpha}_{a,t}v_h|$ is controlled. Using Young's inequality and interpolation estimate (4.5), we obtain

$$\begin{aligned}\left({}_{CH}\mathrm{D}^{\alpha}_{a,t}\eta, \eta\right) \le &C\frac{h^4 + \|\eta\|^2}{2} + C\frac{h^4 + 2\|\eta\|^2}{2} + C\frac{h^4 + \|\beta\|^2 + \|\eta\|^2}{2} \\ &+ C\frac{h^4 + 2\|\eta\|^2}{2} + C\frac{h^4 + \|\eta\|^2 + \|\beta\|^2}{2} + C\frac{h^4 + 2\|\eta\|^2}{2} \\ \le &C\left(\|\eta\|^2 + h^4 + \|\beta\|^2\right).\end{aligned} \tag{4.15}$$

Furthermore, by using (4.11) and Lemmas 4.1 and 4.3, we derive

$$\|\eta\| \le Ch^2. \tag{4.16}$$

Substituting (4.16) back into (4.11) gives

$$\|\beta\| \le Ch^2. \tag{4.17}$$

Finally, combining the interpolation estimate (4.5) with the triangle inequality, we conclude the proof. □

4.1.2. Stability and error estimation of the fully discrete scheme

Now, we derive the fully discrete scheme where the time fractional derivative is approximated by L1 scheme (2.1). Then, we present the following decoupled fully discrete scheme: For $n = 1, 2, \dots, N$, find $(u_h^n, v_h^n) \in V_h$ such that

$$\begin{cases} \left({}_{CH}\mathfrak{D}_{a,t}^{\alpha} u_h^n, w_h\right) + \left(\nabla u_h^n, \nabla w_h\right) - \left(u_h^n \nabla v_h^n, \nabla w_h\right) = 0, & w_h \in V_h, \quad n \geq 1, \\ \left({}_{CH}\mathfrak{D}_{a,t}^{\alpha} v_h^n, w_h\right) + \left(\nabla v_h^n, \nabla w_h\right) + \gamma\left(v_h^n, w_h\right) = \left(u_h^{n-1}, w_h\right), & w_h \in V_h, \quad n \geq 1, \end{cases} \tag{4.18}$$

where u_h^0 and v_h^0 are given. Let $u_h^n = \sum_{j=1}^{M} u_j^n \phi_j$, $v_h^n = \sum_{j=1}^{M} v_j^n \phi_j$ and $\{\phi_j\}_{j=1}^{M}$ denote the finite element basis functions. Then, substituting the basis expansions yields a vector system

$$\begin{cases} \left(b_{0,n}\mathrm{M} + \mathrm{K} + \mathrm{M}\right)\mathbf{v}^n = \mathrm{M}\mathbf{u}^{n-1} - \mathrm{M}\sum_{j=0}^{n-1} b_{n-j,n}\mathbf{v}^j, \quad n \geq 1, \\ \left(b_{0,n}\mathrm{M} + \mathrm{K} - \mathrm{N}(\mathbf{v}^n)\right)\mathbf{u}^n = -\mathrm{M}\sum_{j=0}^{n-1} b_{n-j,n}\mathbf{u}^j, \quad n \geq 1, \end{cases}$$

where $\mathbf{u}^n$ and $\mathbf{v}^n$ represent the coefficient vectors of $\sum_{j=1}^{M} u_j^n \phi_j$ and $\sum_{j=1}^{M} v_j^n \phi_j$, mass matrix M, stiffness matrix K and nonlinear matrix N are respectively represented as

$$\mathrm{M}_{ij} = (\phi_j, \phi_i),$$

$$\mathrm{K}_{ij} = (\nabla\phi_j, \nabla\phi_i),$$

$$\mathrm{N}_{ij}(\mathbf{v}^n) = \sum_{m=1}^{M} v_m^n (\phi_j \nabla\phi_m, \nabla\phi_i).$$

In the process of solving the discrete system, we first apply an explicit scheme to the second equation to obtain the intermediate solution v_h^n. This result is then substituted into the first equation, which is likewise formulated in explicit form, thereby enabling the determination of the solution u_h^n.

Algorithm 1 Fully discrete scheme for the time-fractional Keller–Segel system

Initialize: Discretize initial conditions $u_h^0 \to \mathbf{u}^0$, $v_h^0 \to \mathbf{v}^0$.

for $n = 1, 2, \dots, N$ **do**

Step 1: Solve for $\mathbf{v}^n$

- ▷ Assemble RHS: $\mathbf{b}_v^n = \mathrm{M}\mathbf{u}^{n-1} - \mathrm{M}\sum_{j=0}^{n-1} b_{n-j,n}\mathbf{v}^j$
- ▷ Solve linear system: $(b_{0,n}\mathrm{M} + \mathrm{K} + \mathrm{M})\mathbf{v}^n = \mathbf{b}_v^n$

Step 2: Solve for $\mathbf{u}^n$

- ▷ Construct matrix $\mathrm{N}(\mathbf{v}^n)$ using the updated $\mathbf{v}^n$.
- ▷ Assemble RHS: $\mathbf{b}_u^n = -\mathrm{M}\sum_{j=0}^{n-1} b_{n-j,n}\mathbf{u}^j$
- ▷ Solve linear system: $(b_{0,n}\mathrm{M} + \mathrm{K} - \mathrm{N}(\mathbf{v}^n))\mathbf{u}^n = \mathbf{b}_u^n$

end for

Lemma 4.4. *Let $\xi_h^n, \eta_h^n \in V_h$ for $n = 0, 1, \dots, N$. Assume that the sequence of norms $\{\|\eta_h^n\|\}_{n=0}^{N}$ is nondecreasing, and suppose the discrete Caputo–Hadamard derivative satisfies*

$${}_{CH}\mathfrak{D}_{a,t}^{\alpha}\|\xi_h^n\|^2 \leq C_0\left(\|\xi_h^n\|^2 + \|\eta_h^{n-1}\|^2\right), \; n = 1, \dots, N. \tag{4.19}$$

Then there exists a constant $\tau^* > 0$ such that for $\tau < \tau^*$, the following estimate holds,

$$\|\xi_h^n\| \leq C_1\left(\|\xi_h^0\| + \|\eta_h^{n-1}\|\right), \; n = 1, \dots, N. \tag{4.20}$$

Here, C_0 and C_1 are constants independent of τ and n.

Proof. Combining the L1 formula and (4.19), we have

$$a_{n,n}\|v_h^n\|^2 - a_{1,n}\|v_h^0\|^2 + \sum_{j=1}^{n-1}(a_{j,n} - a_{j+1,n})\|v_h^j\|^2 \leq C_0\left(\|v_h^n\|^2 + \|u_h^{n-1}\|^2\right). \tag{4.21}$$

According to Lemma 2.1, the summation term is negative. By rearranging the terms, we can rewrite (4.21) as

$$a_{n,n}\|v_h^n\|^2 \le C_0\|v_h^n\|^2 + C_0\|u_h^{n-1}\|^2 + a_{1,n}\|v_h^0\|^2 + \sum_{j=1}^{n-1}(a_{j+1,n} - a_{j,n})\|v_h^j\|^2, \tag{4.22}$$

and then we have

$$(a_{n,n} - C_0)\|v_h^n\|^2 \le C_0\|u_h^{n-1}\|^2 + a_{1,n}\|v_h^0\|^2 + \sum_{j=1}^{n-1}(a_{j+1,n} - a_{j,n})\|v_h^j\|^2. \tag{4.23}$$

We know $a_{n,n} > a_{1,n} > 0$ by Lemma 2.1. When τ is sufficiently small, coefficient $a_{n,n} \sim \tau^{-\alpha}$ becomes significantly large, but we have

$$\frac{\sum_{j=1}^{n-1}(a_{j+1,n} - a_{j,n})}{a_{n,n} - C_0} = \frac{a_{n,n} - a_{1,n}}{a_{n,n} - C_0} \le C_1.$$

Therefore, using the discrete Gronwall inequality and the above bound, we derive the following inequality for $\tau < \tau^*$,

$$\|v_h^n\| \le C_1\left(\|v_h^0\| + \|u_h^{n-1}\|\right). \quad \square \tag{4.24}$$

Next, we give the numerical stability analysis of the fully discrete scheme (4.18) under the $L^2(\Omega)$ norm.

Theorem 4.2. *For $n = 1, 2, \ldots, N$, there exists a constant τ^* such that when $\tau < \tau^*$, the fully discrete scheme (4.18) satisfies*

$$\left\|u_h^n\right\| + \left\|v_h^n\right\| \le C\left(\left\|u_h^0\right\| + \left\|v_h^0\right\|\right), \tag{4.25}$$

where the constant C is independent of the mesh size h and the time stepsize τ.

Proof. In the second equation of the fully discrete scheme (4.18), let $w_h = v_h^n$. We obtain

$$\left({}_{CH}\mathfrak{D}_{a,t}^{\alpha} v_h^n, v_h^n\right) + \left(\nabla v_h^n, \nabla v_h^n\right) + \gamma\left(v_h^n, v_h^n\right) = \left(u_h^{n-1}, v_h^n\right). \tag{4.26}$$

Note that

$$\begin{aligned}\left({}_{CH}\mathfrak{D}_{a,t}^{\alpha} v_h^n, v_h^n\right) &= \left(a_{n,n}v_h^n - \sum_{j=1}^{n-1}(a_{j+1,n} - a_{j,n})v_h^j - a_{1,n}v_h^0, v_h^n\right) \\ &\ge a_{n,n}\|v_h^n\|^2 - \sum_{j=1}^{n-1}(a_{j+1,n} - a_{j,n})\frac{\|v_h^j\|^2 + \|v_h^n\|^2}{2} - a_{1,n}\frac{\|v_h^0\|^2 + \|v_h^n\|^2}{2} \\ &= \frac{1}{2}{}_{CH}\mathfrak{D}_{a,t}^{\alpha}\|v_h^n\|^2.\end{aligned} \tag{4.27}$$

Applying Young's inequality together with the estimate in (4.27), we obtain

$${}_{CH}\mathfrak{D}_{a,t}^{\alpha}\left\|v_h^n\right\|^2 \le C\left(\left\|v_h^n\right\|^2 + \left\|u_h^{n-1}\right\|^2\right). \tag{4.28}$$

Hence, using Lemma 4.4, we conclude that there exists a constant τ^* such for all $\tau < \tau^*$,

$$\left\|v_h^n\right\| \le C\left(\left\|v_h^0\right\| + \left\|u_h^{n-1}\right\|\right). \tag{4.29}$$

Similarly, we multiply both sides of the second equation of the fully discrete scheme (4.18) by u_h^n and substitute it into the first equation of the fully discrete scheme to obtain

$$\left({}_{CH}\mathfrak{D}_{a,t}^{\alpha} u_h^n, w_h\right) + \left(\nabla u_h^n, \nabla w_h\right) = \left(u_h^n u_h^{n-1}, w_h\right) - \gamma\left(u_h^n v_h^n, w_h\right) - \left(u_h^n\, {}_{CH}\mathfrak{D}_{a,t}^{\alpha} v_h^n, w_h\right). \tag{4.30}$$

Let $w_h = u_h^n$. Since u_h^{n-1} and ${}_{CH}\mathfrak{D}_{a,t}^{\alpha} v_h^n$ are bounded, the above equation can be transformed into

$$\begin{aligned}\left({}_{CH}\mathfrak{D}_{a,t}^{\alpha} u_h^n, u_h^n\right) + \left(\nabla u_h^n, \nabla u_h^n\right) &= \left(u_h^n u_h^{n-1}, u_h^n\right) - \gamma\left(u_h^n v_h^n, u_h^n\right) - \left(u_h^n\, {}_{CH}\mathfrak{D}_{a,t}^{\alpha} v_h^n, u_h^n\right) \\ &\le C_1\left(u_h^n, u_h^n\right) + C_2\left(v_h^n, u_h^n\right) + C_3\left(u_h^n, u_h^n\right),\end{aligned} \tag{4.31}$$

where C_1, C_2, C_3 are positive constants. Next, by using (4.27) and Young's inequality again, we derive

$${}_{CH}\mathfrak{D}_{a,t}^{\alpha}\left\|u_h^n\right\|^2 \le C\left(\left\|u_h^n\right\|^2 + \left\|v_h^n\right\|^2\right). \tag{4.32}$$

Then, applying (4.29) and Lemma 4.4 yields

$$\left\|u_h^n\right\| \le C\left(\left\|u_h^0\right\| + \left\|v_h^0\right\|\right). \tag{4.33}$$

Finally, substituting the above result into (4.29) completes the proof. $\square$

Remark 4.2. The stability threshold τ^* in Theorem 4.2 is determined by the condition $a_{n,n} > C$ (see proof of Lemma 4.4), where $a_{n,n} \sim \tau^{-\alpha}$. Hence, for sufficiently small τ, the scheme is stable.

We present the following error estimate for the fully discrete scheme (4.18) in the $L^2(\Omega)$ norm.

Theorem 4.3. *Assume $(u(x,t), v(x,t)) \in C^2([a,T]; L^2(\Omega)) \cap C^1([a,T]; H^2(\Omega))$. For $n = 1, 2, \dots, N$, there exists a constant τ^* such that when $\tau < \tau^*$, the fully discrete scheme (4.18) satisfies*

$$\left\|u(t^n) - u_h^n\right\| + \left\|v(t^n) - v_h^n\right\| \le C\left(\tau + h^2\right), \tag{4.34}$$

where the constant C is independent of the mesh size h.

Proof. Let

$$E_u^n = u_h(t_n) - u_h^n, \quad E_v^n = v_h(t_n) - v_h^n. \tag{4.35}$$

First, subtract the second equation of the fully discrete scheme (4.18) from the second equation of the semi-discrete scheme (4.3) to obtain

$$\begin{aligned}\left({}_{CH}\mathfrak{D}_{a,t}^{\alpha} E_v^n, w_h\right) + \left(\nabla E_v^n, \nabla w_h\right) = &-\gamma\left(E_v^n, w_h\right) + \left({}_{CH}\mathfrak{D}_{a,t}^{\alpha} v_h(t_n) - {}_{CH}\mathrm{D}_{a,t}^{\alpha} v_h(t_n), w_h\right) \\ &+ \left(E_u^n + u_h^n - u_h^{n-1}, w_h\right).\end{aligned} \tag{4.36}$$

Since $(u_h, v_h) \in C^2[a,T]$, it follows that

$$\left|{}_{CH}\mathfrak{D}_{a,t}^{\alpha} v_h(t_n) - {}_{CH}\mathrm{D}_{a,t}^{\alpha} v_h(t_n)\right| \le C\tau^{2-\alpha},$$

and

$$|u_h^n - u_h^{n-1}| = |\tau\, \partial_t u(\xi)| \le C\tau, \quad \xi \in (t_{n-1}, t_n).$$

Let $w_h = E_v^n$ in Eq. (4.36). According to (4.27), one has

$${}_{CH}\mathfrak{D}_{a,t}^{\alpha} \left\|E_v^n\right\|^2 \le C(\left\|E_v^n\right\|^2 + \left\|E_u^n\right\|^2 + \tau^2).$$

Hence, from Lemma 4.4, we get

$$\left\|E_v^n\right\| \le C\left(\left\|E_u^n\right\| + \tau\right). \tag{4.37}$$

Next, subtracting (4.30) from (4.12), we obtain

$$\begin{aligned}&\left({}_{CH}\mathfrak{D}_{a,t}^{\alpha} E_u^n, w_h\right) + \left(\nabla E_u^n, \nabla w_h\right) \\ =&\left({}_{CH}\mathfrak{D}_{a,t}^{\alpha} u_h\left(t_n\right) - {}_{CH}\mathrm{D}_{a,t}^{\alpha} u_h\left(t_n\right), w_h\right) + \left(\left(u_h\left(t_n\right) + u_h^n\right) E_u^n, w_h\right) \\ &+ \left(u_h^n\left(u_h^n - u_h^{n-1}\right), w_h\right) - \gamma\left(u_h\left(t_n\right) E_v^n + v_h^n E_u^n, w_h\right) - \left(E_u^n\, {}_{CH}\mathfrak{D}_{a,t}^{\alpha} v_h\left(t_n\right), w_h\right) \\ &- \left(u_h\left(t_n\right)\left({}_{CH}\mathrm{D}_{a,t}^{\alpha} v_h\left(t_n\right) - {}_{CH}\mathfrak{D}_{a,t}^{\alpha} v_h\left(t_n\right)\right), w_h\right) - \left(u_h^n\, {}_{CH}\mathfrak{D}_{a,t}^{\alpha} E_v^n, w_h\right).\end{aligned}$$

Let $w_h = E_u^n$. Then, using Young's inequality and (4.27), one has

$${}_{CH}\mathfrak{D}_{a,t}^{\alpha} \left\|E_u^n\right\|^2 \le C\left(\left\|E_u^n\right\|^2 + \left\|E_v^n\right\|^2 + \tau^2\right).$$

Therefore, using Lemma 4.4 and (4.37), we get

$$\left\|E_u^n\right\| \le C\tau.$$

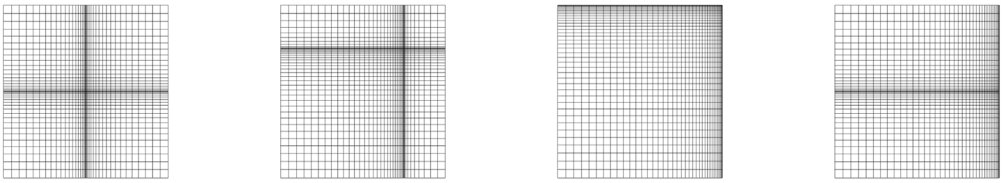
Substituting this back into (4.37) leads to

$$\left\|E_v^n\right\| \le C\tau.$$

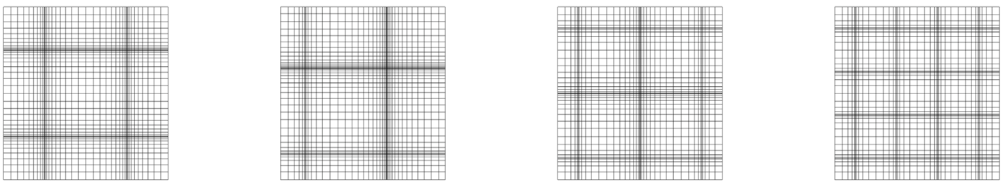
Finally, by applying the triangle inequality and the semi-discrete error estimate (4.7), the conclusion is shown. □

Remark 4.3. The H^2 regularity is essential for the standard finite element method to achieve optimal spatial convergence, while the C^2 regularity is required to bound the local truncation error of the temporal L1 scheme.

The theoretical error estimates for fixed meshes in this section rely on the spatial regularity $u, v \in H^2(\Omega)$, which holds only for $t < T_{\max}$. As $t \to T_{\max}^-$, this regularity is lost, causing the error constants in Theorems 4.1 and 4.3 to become unbounded. Consequently, fixed-mesh simulations deteriorate near blow-up and may fail to resolve the sharp profile. This motivates the use of adaptive moving meshes, which concentrate nodes in regions of steep gradients, thereby compensating for the loss of regularity and enabling more accurate resolution of the blow-up behavior.



(a) One blow-up point at the center of the domain. (b) One blow-up point in the lower left domain. (c) One blow-up point on the upper right corner. (d) One blow-up point on the right central edge.



(e) Four blow-up points. (f) Four shifted blow-up points. (g) Nine blow-up points. (h) Sixteen blow-up points.

Fig. 2. Moving graded meshes for single or multiple blow-up points.

4.2. Auxiliary moving mesh

As mentioned earlier, the blow-up position in the chemotaxis model can be estimated through analytical methods or preliminary computational experiments. This provides the capability to pre-design a moving mesh through the construction of auxiliary functions.

In the following, we introduce an auxiliary adaptive graded mesh. It preserves parallelism in the mesh lines along the spatial direction, thereby ensuring that all mesh cells retain a strictly rectangular geometry. Such adaptive grids are similar to the tensor-product grids described in [30], while offering the advantage of a simple, undistorted structure.

4.2.1. Auxiliary moving mesh I: moving graded mesh

Consider the blow-up problem in a rectangular domain $\Omega_p : [a_1, b_1] \times [a_2, b_2]$. Assume there is only one blow-up point with coordinate $(p_1, p_2) \in \Omega_p \backslash \partial\Omega_p$. We map the domain Ω_p to the domain $\Omega_c : [-1, 1]^2$ through an affine transformation and map the blow-up point to the origin. This affine transformation is defined as

$$\boldsymbol{\Phi} : (\eta_1, \eta_2) = \begin{cases} \left(\dfrac{\xi_1 - p_1}{p_1 - a_1}, \dfrac{\xi_2 - p_2}{p_2 - a_2} \right), \ \xi_1 \le p_1, \ \xi_2 \le p_2, \\ \left(\dfrac{\xi_1 - p_1}{b_1 - p_1}, \dfrac{\xi_2 - p_2}{b_2 - p_2} \right), \ \xi_1 > p_1, \ \xi_2 > p_2, \end{cases} \tag{4.38}$$

for every $(\xi_1, \xi_2) \in [a_1, b_1] \times [a_2, b_2]$ and $(\eta_1, \eta_2) \in [-1, 1]^2$, where the transformation $\boldsymbol{\Phi}$ is applied componentwise to the coordinates. Our next goal is to generate a graded mesh that is increasingly refined near the center. For this purpose, we define an auxiliary moving mesh function (AMMF),

$$(X_1(t), X_2(t)) = (\text{sign}(\eta_1)|\eta_1|^{c_1 + \sin(c_2(t-a))}, \text{sign}(\eta_2)|\eta_2|^{c_1 + \sin(c_2(t-a))}), \ t \in [a, T], \tag{4.39}$$

where $c_1 \ge 1$, $c_2 = \tau_c \times \frac{\pi}{2(T-a)}$ is an aggregation parameter, and $\tau_c \in (0, 1]$ represents a parameter related to the velocity of movement. Specifically, $\tau_c = 0$ corresponds to a fixed mesh, and a larger value of τ_c indicates a higher speed of movement. The parameter c_1 determines the initial mesh configuration. When $c_1 = 1$, the initial mesh is uniform. Finally, the domain Ω_c is mapped to the domain Ω_p through the inverse transformation $\boldsymbol{\Phi}^{-1}$. For $(Y_1, Y_2) \in \Omega_p$,

$$\boldsymbol{\Phi}^{-1} : (Y_1, Y_2) = \begin{cases} ((p_1 - a_1)X_1 + p_1, (p_2 - a_2)X_2 + p_2), \ -1 \le X_1 \le 0, \ -1 \le X_2 \le 0, \\ ((b_1 - p_1)X_1 + p_1, (b_2 - p_2)X_2 + p_2), \ 0 < X_1 \le 1, \ 0 < X_2 \le 1. \end{cases} \tag{4.40}$$

For the case of multiple blow-up points, simply divide the domain into small areas centered around the blow-up points, then use the same method to move the meshes of the small areas, and finally combine them. The above method is also applicable to the case of boundary blow-up points. We provide moving graded meshes for various scenarios, as illustrated in Fig. 2. Subfigures 2(a)-2(d) show meshes at different locations for a single blow-up point, while 2(e)-2(h) show cases with multiple blow-up points.

The primary motivation for using moving graded meshes is their structural simplicity and remarkably low computational overhead. Unlike traditional moving mesh methods that require solving a highly nonlinear moving mesh partial differential equation (MMPDE) system iteratively, the graded mesh utilizes a predefined, explicit analytical mapping (Eqs. (4.38)–(4.39)). While a practical limitation of this approach is that it requires prior knowledge of the approximate blow-up location, in practice, this location can often be reliably estimated either from the symmetry of the initial data or by conducting a computationally inexpensive "pilot run" on a coarse uniform mesh.

The advantage of this method is that it can effectively handle difference discretization of operators, due to the parallel mesh lines of each spatial component. Unfortunately, this method can only provide a mesh with a number of aggregation points that is an integer power of 2. For example, it is currently unable to generate a graded mesh with three central clusters, which requires further improvement. However, for the problem of a single blow-up point, this method has specific advantages.

4.2.2. Auxiliary moving mesh II: moving triangle mesh

If some information about the blow-up points' coordinates is known in advance, we can also generate the required mesh by designing auxiliary functions combined with known moving mesh methods. The auxiliary function will replace the solution in generating the moving mesh. This method is more flexible and computationally efficient than traditional moving mesh methods. Before detailing our proposed method, it is necessary to consider an existing moving mesh strategy that forms the conceptual basis for our approach. In the following, we briefly introduce this method.

Let Ω and Ω_c in $\mathbb{R}^2$ represent the physical and computational domains, respectively. Both domains are assumed to be bounded, simply connected, and polygonal. Generally speaking, Ω_c can be chosen to be the same as Ω. Convex domains are often selected because they help avoid singularity in the coordinate transformation [31]. We also assume that a symmetric and uniformly positive definite metric tensor $\mathbb{M} = \mathbb{M}(\mathbf{x})$ defined in Ω is given, which provides information about the size and shape of mesh elements. Typically, $\mathbb{M}$ is defined in a mesh adaptation process based on the physical solution, solution error, or other physical considerations.

Let x and $\boldsymbol{\xi}$ represent the coordinates in the domains Ω and Ω_c, respectively. The coordinate transformation is given by $\mathrm{x} = \mathrm{x}(\boldsymbol{\xi}) : \Omega_c \to \Omega$, with the inverse transformation being denoted as $\boldsymbol{\xi} = \boldsymbol{\xi}(\mathrm{x}) : \Omega \to \Omega_c$. Meshing functionals typically use the inverse transformation, since this formulation more effectively avoids singularities, as noted in [31].

We consider a general meshing functional

$$I[\boldsymbol{\xi}] = \int_{\Omega} G(\mathbb{J}, \det(\mathbb{J}), \mathbb{M}, \mathrm{x})\mathrm{dx}, \tag{4.41}$$

where $\mathbb{J} = \frac{\partial \boldsymbol{\xi}}{\partial \mathrm{x}}$ is the Jacobian matrix of the transformation $\boldsymbol{\xi} = \boldsymbol{\xi}(\mathrm{x})$, and G is a given smooth function. Let G be a smooth function with continuous derivatives up to the third order with respect to all its arguments. We assume that the Jacobian satisfies $\|\mathbb{J}\| < \infty$ and $|\det(\mathbb{J})| < \infty$ for all $\mathrm{x} \in \Omega$, where $\|\cdot\|$ denotes the matrix and vector 2-norm. Since the Jacobian matrix is nonsingular, the functional in (4.41) is mathematically equivalent to

$$I[\mathrm{x}] = \int_{\Omega_c} \frac{G(\mathbb{J}, \det(\mathbb{J}), \mathbb{M}, \mathrm{x})}{\det(\mathbb{J})}\mathrm{d}\boldsymbol{\xi}. \tag{4.42}$$

The formulation in (4.41) is quite general and encompasses many existing meshing functionals. We consider two representative examples in the following.

The first example is a generalization of the Winslow's variable diffusion functional,

$$I[\boldsymbol{\xi}] = \int_{\Omega} \mathrm{tr}\left(\mathbb{J}\mathbb{M}^{-1}\mathbb{J}^{T}\right)\mathrm{dx}, \tag{4.43}$$

where $\mathrm{tr}(\cdot)$ denotes the trace of a matrix. This functional admits a unique minimizer, as proved in [14].

The second example is Huang's functional [32],

$$I[\boldsymbol{\xi}] = \theta \int_{\Omega} \sqrt{\det(\mathbb{M})}\left(\mathrm{tr}\left(\mathbb{J}\mathbb{M}^{-1}\mathbb{J}^{T}\right)\right)^{\frac{dp}{2}}\mathrm{dx} + (1-2\theta)d^{\frac{dp}{2}} \int_{\Omega} \sqrt{\det(\mathbb{M})}\left(\frac{\det(\mathbb{J})}{\sqrt{\det(\mathbb{M})}}\right)^{p}\mathrm{dx}, \tag{4.44}$$

where $0 \le \theta \le 1$ and $p > 0$ are dimensionless parameters. This functional incorporates terms that enforce alignment and equidistribution conditions, respectively. For $0 < \theta \le \frac{1}{2}$, $dp \ge 2$, and $p \ge 1$, the functional is coercive, polyconvex, and admits a minimizer [14]. In particular, for $\theta = \frac{1}{2}$ and $dp = 2$, it reduces to

$$I[\boldsymbol{\xi}] = \theta \int_{\Omega} \sqrt{\det(\mathbb{M})}\,\mathrm{tr}\left(\mathbb{J}\mathbb{M}^{-1}\mathbb{J}^{T}\right)\mathrm{dx},$$

which is the energy functional for a harmonic mapping from Ω to Ω_c. Moreover, (4.44) and Winslow's functional (4.43) coincide when $\theta = \frac{1}{2}$, $dp = 2$, and $\mathbb{M} = I$. Huang's functional is used in our moving mesh method.

A common approach in variational methods for computing coordinate transformations is to discretize and solve the corresponding Euler–Lagrange equation. Following the standard mathematical framework described in [14], the Euler–Lagrange equation corresponding to (4.41) can be derived and is given by

$$\frac{\delta I}{\delta \boldsymbol{\xi}} \equiv -\nabla \cdot \left(\frac{\partial G}{\partial \mathbb{J}} + \frac{\partial G}{\partial r}\det(\mathbb{J})\mathbb{J}^{-1}\right) = 0, \tag{4.45}$$

where $\frac{\delta I}{\delta \xi}$ denotes the functional derivative of $I[\xi]$, and $\frac{\partial G}{\partial \mathbb{J}}$ and $\frac{\partial G}{\partial r} = \frac{\partial G}{\partial \det(\mathbb{J})}$ are the derivatives of G with respect to its first and second arguments. This equation is defined for the inverse coordinate transformation ξ. Since the computational mesh of Ω_c is generally known, the physical mesh of Ω needs to be determined. It is common practice to exchange the roles of the independent variable x and the dependent variable ξ in the mesh Eq. (4.45), and then discretize it on the computational mesh using finite difference or finite element methods. The resulting nonlinear algebraic system can then be solved to obtain the physical mesh.

In general, Eq. (4.45) is highly nonlinear. An effective strategy for solving such a nonlinear system is to employ a time-varying or MMPDE approach, which is particularly useful in dynamic mesh adaptation. An MMPDE is defined as a gradient flow equation of the functional (4.41), i.e.,

$$\frac{\partial \xi}{\partial t} = -\frac{P}{\tau_c}\frac{\delta I}{\delta \xi}, \tag{4.46}$$

where t denotes a quasi-time variable, $\tau_c > 0$ is a constant parameter that controls the scale of mesh movement, and P is a positive balancing function used to make the equation to have some invariance properties. When the goal is to compute the physical coordinates directly, Eq. (4.46) can be coupled with the identity

$$\frac{\partial \mathrm{x}}{\partial t} + \mathbb{J}^{-1}\frac{\partial \xi}{\partial t} = 0.$$

This gives

$$\frac{\partial \mathrm{x}}{\partial t} = \frac{P}{\tau_c}\mathbb{J}^{-1}\frac{\partial I}{\partial \xi}.$$

Then, using the x-formulation, we have

$$\frac{\partial \mathrm{x}}{\partial t} = -\frac{P}{\tau_c}\frac{\delta I}{\delta \mathrm{x}}. \tag{4.47}$$

To guarantee the invariance of the MMPDE under the scaling transformations of $\mathbb{M}$ for the current functional, a selection of P is

$$P = \det(\mathbb{M})^{\frac{p-1}{2}}.$$

Discretizing Eq. (4.47) yields a system of equations governing the nodal velocities of the physical mesh. The solution of this equation is the minimizer of the mesh functional, whose existence and uniqueness have been established. One approach for computing this solution, as adopted in [33], is the direct discretization of the functional (4.41).

In the computational process, the rezoning approach involves alternating between solving the physical PDE and updating the mesh. The process involves three steps: firstly, estimating the solution error or mesh quality; secondly, adjusting (or moving) the mesh based on this estimate; and finally, advancing the PDE solution on the updated mesh. This auxiliary function evolves in a manner similar to the physical solution, exhibiting sharp growth at certain locations over time. For the Keller–Segel equation with a single blow-up point (p_1, p_2) in domain $\Omega = [a_1, b_1] \times [a_2, b_2]$, we define the following auxiliary function:

$$\tilde{u} = [c_1 + c_2(t-a)]\exp\left\{-[c_1 + c_2(t-a)][(x_1-p_1)^2 + (x_2-p_2)^2]\right\}, (x_1, x_2) \in \Omega, \tag{4.48}$$

where $c_1 > 0$, $c_2 \geq 0$ are aggregation parameters. We can choose $c_1 = 100$ and $c_2 = \frac{c_1 N_t}{T-a}$, where N_t denotes the number of time steps, and T is terminal time. Fig. 3 shows moving triangle meshes that adapt to single or multiple blow-up points. Subfigures 3(a)-3(d) display meshes at different positions for a single blow-up point, while 3(e)-3(h) present cases with multiple blow-up points.

Remark 4.4. In our numerical experiments, we primarily consider initial data with symmetric structures. Since the solution of the Keller–Segel system tends to preserve this symmetry during evolution, it allows us to naturally and precisely deduce the blow-up locations in advance. For general initial data where the blow-up locations are completely unknown *a priori*, we recommend a practical two-step strategy. First, one can conduct a computationally inexpensive "pilot run" on a coarse uniform mesh. Since the Keller–Segel system develops sharp gradients relatively early, this pilot run will quickly capture the approximate regions of gradient aggregation. Once these locations are estimated, the global domain can be partitioned into several smaller sub-domains, ensuring that each sub-domain contains only one independent aggregation point. Finally, the proposed auxiliary moving mesh methods can be applied locally to each sub-domain, which are then combined to form a globally adaptive mesh.

4.3. Finite element discretization on the moving mesh

Assuming that the moving mesh is obtained by auxiliary moving mesh II. Given the computational coordinate and physical coordinate:

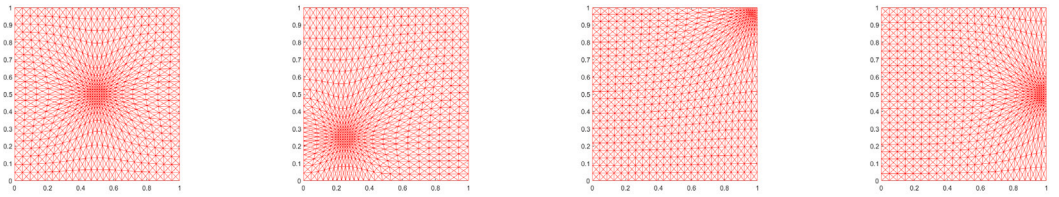
$$t = \tau,\ \mathrm{x} = \mathrm{x}(\xi, \tau), \quad \tau = t,\ \xi = \xi(\mathrm{x}, t).$$

Then, the time partial derivative in the physical equations can be expressed as

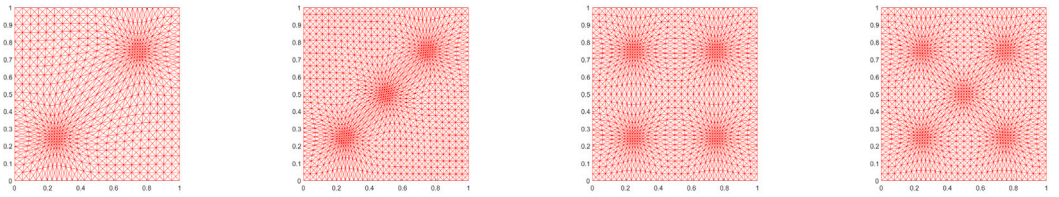
$$u_t = \frac{\partial u}{\partial t} = \dot{u} + \xi_t \cdot \nabla_\xi u, \quad v_t = \frac{\partial v}{\partial t} = \dot{v} + \xi_t \cdot \nabla_\xi v, \tag{4.49}$$

or

$$u_t = \frac{\partial u}{\partial t} = \dot{u} - \dot{\mathrm{x}} \cdot \nabla u, \quad v_t = \frac{\partial v}{\partial t} = \dot{v} - \dot{\mathrm{x}} \cdot \nabla v, \tag{4.50}$$



(a) One blow-up point at the center of the domain. (b) One blow-up point in the lower left domain. (c) One blow-up point on the upper right corner. (d) One blow-up point on the right central edge.



(e) Two blow-up points. (f) Three blow-up points. (g) Four blow-up points. (h) Five blow-up points.

Fig. 3. Moving triangle meshes for single or multiple blow-up points.

where

$$u_t(\mathrm{x},t)=u_t=\left.\frac{\partial u}{\partial t}\right|_{\mathrm{x}},\quad \dot{u}(\xi,\tau)=\dot{u}=\left.\frac{\partial u}{\partial \tau}\right|_{\xi}.$$

Substituting (4.50) into (2.1) yields

$$\begin{aligned}
&{}_{CH}\mathrm{D}^{\alpha}_{a,t}g(\mathrm{x},t)\Big|_{t=t_n}=\frac{1}{\Gamma(1-\alpha)}\int_a^{t_n}\left(\log\frac{t_n}{s}\right)^{-\alpha}\delta g(\mathrm{x},t)\frac{\mathrm{d}s}{s}\\
&=\frac{1}{\Gamma(1-\alpha)}\int_a^{t_n}\left(\log\frac{t_n}{s}\right)^{-\alpha}(\delta g-\delta\mathrm{x}\cdot\nabla g)\frac{\mathrm{d}s}{s}\\
&=\frac{1}{\Gamma(1-\alpha)}\sum_{k=1}^{n}\int_{t_{k-1}}^{t_k}\left(\log\frac{t_n}{s}\right)^{-\alpha}(\delta g-\delta\mathrm{x}\cdot\nabla g)\frac{\mathrm{d}s}{s}\\
&=\frac{1}{\Gamma(1-\alpha)}\sum_{k=1}^{n}\left[\frac{g\left(t_k\right)-g\left(t_{k-1}\right)}{\log\frac{t_k}{t_{k-1}}}-\frac{\mathrm{x}(t_k)-\mathrm{x}(t_{k-1})}{\log\frac{t_k}{t_{k-1}}}\cdot\nabla g(t_{k-1})\right]\int_{t_{k-1}}^{t_k}\left(\log\frac{t_n}{s}\right)^{-\alpha}\frac{\mathrm{d}s}{s}+\widetilde{R}^k\\
&=\sum_{k=1}^{n}a_{k,n}\left[g\left(t_k\right)-g\left(t_{k-1}\right)-\left(\mathrm{x}\left(t_k\right)-\mathrm{x}\left(t_{k-1}\right)\right)\cdot\nabla g\left(t_{k-1}\right)\right]+\widetilde{R}^k
\end{aligned}$$

$$a_{k,n}=\frac{1}{\Gamma(2-\alpha)}\frac{1}{\log\frac{t_k}{t_{k-1}}}\left(\left(\log\frac{t_n}{t_{k-1}}\right)^{1-\alpha}-\left(\log\frac{t_n}{t_k}\right)^{1-\alpha}\right),$$

and

$$\begin{aligned}
\widetilde{R}^k=&\frac{1}{\Gamma(1-\alpha)}\sum_{k=1}^{n}\int_{t_{k-1}}^{t_k}\left(\log\frac{t_n}{s}\right)^{-\alpha}\left(\delta g(s)-\frac{g\left(t_k\right)-g\left(t_{k-1}\right)}{\log\frac{t_k}{t_{k-1}}}\right)\frac{\mathrm{d}s}{s}\\
&+\frac{1}{\Gamma(1-\alpha)}\sum_{k=1}^{n}\int_{t_{k-1}}^{t_k}\left(\log\frac{t_n}{s}\right)^{-\alpha}\left(\frac{\mathrm{x}(t_k)-\mathrm{x}(t_{k-1})}{\log\frac{t_k}{t_{k-1}}}\cdot\nabla g(t_{k-1})-\delta\mathrm{x}\cdot\nabla g\right)\frac{\mathrm{d}s}{s}.
\end{aligned}$$

Therefore, the discretization of system (1.1) on a moving mesh is given as follows:

$$\begin{cases}
\left(\sum_{k=1}^{n}a_{k,n}\left[u_h^k-u_h^{k-1}-\left(\mathrm{x}^k-\mathrm{x}^{k-1}\right)\cdot\nabla u_h^{k-1}\right],w_h\right)+\left(\nabla u_h^n,\nabla w_h\right)-\left(u_h^n\nabla v_h^n,\nabla w_h\right)=0,\\
\left(\sum_{k=1}^{n}a_{k,n}\left[v_h^k-v_n^{k-1}-\left(\mathrm{x}^k-\mathrm{x}^{k-1}\right)\cdot\nabla v_h^{k-1}\right],w_h\right)+\left(\nabla v_h^n,\nabla w_h\right)+\gamma\left(v_h^n,w_h\right)=\left(u_h^{n-1},w_h\right).
\end{cases}\tag{4.51}$$

Set

$$u_h^n = \sum_{j=1}^{M} U_j^n \phi_j(\mathrm{x}), \quad v_h^n = \sum_{j=1}^{M} V_j^n \phi_j(\mathrm{x}), \tag{4.52}$$

where U_j^n and V_j^n are numerical solutions at (x_j, t_n). Combining (4.51) and (4.52), we obtain

$$\begin{cases} \sum_{k=1}^{n} a_{k,n} \left[\sum_{j=1}^{M} \left(U_j^k - U_j^{k-1} \right) (\phi_j, \phi_i) - \sum_{j=1}^{M} \left(\mathrm{x}^k - \mathrm{x}^{k-1} \right) U_j^{k-1} \cdot (\nabla \phi_j, \phi_i) \right] \\ \quad + \sum_{j=1}^{M} U_j^n (\nabla \phi_j, \nabla \phi_i) - \sum_{j=1}^{M} U_j^n \left(\phi_j \sum_{\beta=1}^{M} V_\beta^n \nabla \phi_\beta, \nabla \phi_i \right) = 0, \\ \sum_{k=1}^{n} a_{k,n} \left[\sum_{j=1}^{M} \left(V_j^k - V_j^{k-1} \right) (\phi_j, \phi_i) - \sum_{j=1}^{M} \left(\mathrm{x}^k - \mathrm{x}^{k-1} \right) V_j^{k-1} (\nabla \phi_j, \phi_i) \right] \\ \quad + \sum_{j=1}^{M} V_j^n (\nabla \phi_j, \nabla \phi_i) + \gamma \sum_{j=1}^{M} V_j^n (\phi_j, \phi_i) = \sum_{j=1}^{M} U_j^{n-1} (\phi_j, \phi_i). \end{cases} \tag{4.53}$$

Rearranging Eqs. (4.53) yields

$$\begin{cases} \sum_{j=1}^{M} a_{n,n} U_j^n (\phi_j, \phi_i) + \sum_{j=1}^{M} U_j^n (\nabla \phi_j, \nabla \phi_i) - \sum_{j=1}^{M} U_j^n \left(\phi_j \sum_{\beta=1}^{M} V_\beta^n \nabla \phi_\beta, \nabla \phi_i \right) \\ \quad = \sum_{k=2}^{n} (a_{k,n} - a_{k-1,n}) \sum_{j=1}^{M} U_j^{k-1} (\phi_j, \phi_i) + \sum_{j=1}^{M} a_{1,n} U_j^0 (\phi_j, \phi_i) \\ \quad + \sum_{k=1}^{n} a_{k,n} \sum_{j=1}^{M} \left(\mathrm{x}^k - \mathrm{x}^{k-1} \right) U_j^{k-1} \cdot (\nabla \phi_j, \phi_i), \\ \sum_{j=1}^{M} a_{n,n} V_j^n (\phi_j, \phi_i) + \sum_{j=1}^{M} V_j^n (\nabla \phi_j, \nabla \phi_i) + \gamma \sum_{j=1}^{M} V_j^n (\phi_j, \phi_i) \\ \quad = \sum_{k=2}^{n} (a_{k,n} - a_{k-1,n}) \sum_{j=1}^{M} V_j^{k-1} (\phi_j, \phi_i) + \sum_{j=1}^{M} a_{1,n} V_j^0 (\phi_j, \phi_i) \\ \quad + \sum_{k=1}^{n} a_{k,n} \sum_{j=1}^{M} \left(\mathrm{x}^k - \mathrm{x}^{k-1} \right) V_j^{k-1} \cdot (\nabla \phi_j, \phi_i) + \sum_{j=1}^{M} U_j^{n-1} (\phi_j, \phi_i). \end{cases} \tag{4.54}$$

The above equations are equivalent to the vector system below,

$$\begin{cases} \left(a_{nn} \mathrm{M} + \mathrm{A} - \mathrm{H} \right) U^n = \sum_{k=2}^{n} \left(a_{k,n} - a_{k-1} \right) \mathrm{M} U^{k-1} + a_{1,n} \mathrm{M} U^0 + \sum_{k=1}^{n} \mathrm{B}^k U^{k-1}, \\ \left(a_{n,n} \mathrm{M} + \mathrm{A} + \gamma \, \mathrm{M} \right) V^n = \sum_{k=2}^{n} \left(a_{kn} - a_{k-1,n} \right) \mathrm{M} V^{k-1} + a_{1,n} \mathrm{M} V^0 + \sum_{k=1}^{n} \mathrm{B}^k V^{k-1} + \mathrm{M} U^{n-1}, \end{cases} \tag{4.55}$$

where

$$\begin{aligned} & U^n = [U_1^n, U_2^n, \ldots, U_M^n]', \ V^n = [V_1^n, V_2^n, \ldots, V_M^n]', \ n = 1, 2, \ldots, N, \\ & \mathrm{M}_{ij} = (\phi_j, \phi_i) = \int_\Omega \phi_j \phi_i \mathrm{d}\Omega, \\ & \mathrm{A}_{ij} = (\nabla \phi_j, \nabla \phi_i) = \int_\Omega \nabla \phi_j \cdot \nabla \phi_i \mathrm{d}\Omega, \\ & \mathrm{H}_{ij} = \sum_{\beta=1}^{M} v_\beta^n (\phi_j \nabla \phi_\beta, \nabla \phi_i) = \sum_{\beta=1}^{M} v_\beta^n \int_\Omega \phi_j \nabla \phi_\beta \cdot \nabla \phi_i \mathrm{d}\Omega, \\ & \mathrm{B}_{ij}^k = a_{k,n} \left((\mathrm{x}^k - \mathrm{x}^{k-1}) \cdot \nabla \phi_j, \phi_i \right) = a_{k,n} \int_\Omega \left(\mathrm{x}^k - \mathrm{x}^{k-1} \right) \cdot \nabla \phi_j \phi_i \mathrm{d}\Omega. \end{aligned}$$

Finally, we present the finite element algorithm for system (1.1) on a moving triangular mesh:

Table 1
The L^∞- and L^2-norm errors of the solution.

Uniform mesh			Moving graded mesh			Moving triangle mesh		
N	L^∞ error	L^2 error	N	L^∞ error	L^2 error	N	L^∞ error	L^2 error
$2\times10\times10$	−−	−−	$2\times20\times20$	3.682×10^{-1}	6.601×10^{-2}	$4\times10\times10$	1.192×10^{-1}	2.788×10^{-2}
$2\times20\times20$	1.425	3.227×10^{-1}	$2\times30\times30$	1.723×10^{-1}	3.021×10^{-2}	$4\times20\times20$	8.049×10^{-2}	6.768×10^{-3}
$2\times40\times40$	2.463×10^{-1}	8.867×10^{-3}	$2\times40\times40$	1.025×10^{-1}	1.717×10^{-2}	$4\times30\times30$	6.257×10^{-2}	7.385×10^{-3}
$2\times80\times80$	1.008×10^{-1}	2.958×10^{-3}	$2\times50\times50$	6.754×10^{-2}	1.122×10^{-2}	$4\times40\times40$	2.905×10^{-2}	3.680×10^{-3}

Finite element algorithm on a moving triangular mesh

for $k = 0, 1, \ldots, n$ **do**

Step 1: Evaluate the mesh functional using $\tilde{u}(t_k)$ as defined in (4.48), and substitute it into the MMPDE discretization to compute the physical mesh $\mathrm{x}(t_k)$ at time t_k.

Step 2: Discretize and solve the physical PDE system on the updated mesh to obtain U^{k+1} and V^{k+1}.

end for

The finite element algorithm for system (1.1) on a moving graded mesh is given as follows:

Finite element algorithm on a moving graded mesh

for $k = 0, 1, \ldots, n$ **do**

Step 1: Compute the mesh coordinates $(Y_1(t_k), Y_2(t_k))$ at time t_k using Eqs. (4.38)–(4.40).

Step 2: Discretize and solve the physical PDE system on the updated mesh to obtain U^{k+1} and V^{k+1}.

end for

4.4. Numerical simulations

This subsection examines the key parameters influencing the blow-up behavior of the fractional chemotaxis model through numerical experiments, in which the solutions obtained using both fixed and moving meshes are also compared. The parameter N is the total number of elements, where $N = 2\times\cdot\times\cdot$ and $N = 4\times\cdot\times\cdot$ denote the division of each rectangular cell into two or four triangular elements, respectively. Unless stated otherwise, Huang's functional with parameters $p = 1.5$ and $\theta = \frac{1}{3}$ is employed as the mesh functional in the computational framework. In the numerical calculations, a fixed, uniform time step size τ (e.g., $\tau = 10^{-6}$) is employed. In contrast, for the mesh adaptation process, the MMPDE (4.47) is integrated using `ode15s`, which inherently utilizes an adaptive variable time-stepping strategy to ensure stability and accuracy when tracking the rapidly moving mesh nodes.

Before presenting the specific examples, it is worth noting that we intentionally employ initial data with symmetric structures or specific analytic forms in our numerical experiments. This design guarantees that the exact blow-up locations are known in advance, providing a reliable benchmark to rigorously validate the accuracy, stability, and mesh-aggregation capabilities of our proposed moving mesh algorithms. For general asymmetric initial data, the preliminary coarse-mesh precomputation strategy discussed in Remark 4.4 can be employed to identify the aggregation points before the full adaptive simulation.

To evaluate the effectiveness of the two moving mesh methods, we consider a test problem with an exact solution that exhibits a rapidly intensifying gradient near a localized region as time progresses.

Example 4.1. Consider the following semilinear problem:

$$\begin{cases} {}_{CH}\mathrm{D}^{\alpha}_{a,t}u - \Delta u - u^2 = f(x,y,t),\ (x,y)\in(0,1)^2,\ t\in\times(a,T], \\ u(x,y,a) = 0,\ (x,y)\in[0,1]^2, \\ u(0,y,t) = u(1,y,t) = u(x,0,t) = u(x,1,t) = 0,\ t\in[a,T], \end{cases} \tag{4.56}$$

where $a = 1, T = 2.1$. The exact solution of the problem (4.56) is given by

$$u(x,y,t) = 100(\log t)^2\left[\exp\left(-\frac{\left(x-\frac{1}{2}\right)^2+\left(y-\frac{1}{2}\right)^2}{\varepsilon}\right) - \exp\left(-\frac{1}{4\varepsilon}\right)\right].$$

This is a sharp solution with a peak [34]. The source term is constructed accordingly and takes the form

$$f(x,y,t) = \frac{200(\log t)^{2-\alpha}}{\Gamma(3-\alpha)}\left[\exp\left(-\frac{\left(x-\frac{1}{2}\right)^2+\left(y-\frac{1}{2}\right)^2}{\varepsilon}\right)-\exp\left(-\frac{1}{4\varepsilon}\right)\right]+100(\log t)^2$$
$$\times\left\{\frac{4}{\varepsilon}\exp\left(-\frac{\left(x-\frac{1}{2}\right)^2+\left(y-\frac{1}{2}\right)^2}{\varepsilon}\right)-\frac{4\left[\left(x-\frac{1}{2}\right)^2+\left(y-\frac{1}{2}\right)^2\right]}{\varepsilon^2}\exp\left(-\frac{\left(x-\frac{1}{2}\right)^2+\left(y-\frac{1}{2}\right)^2}{\varepsilon}\right)\right\}$$
$$-100^2(\log t)^4\left[\exp\left(-\frac{\left(x-\frac{1}{2}\right)^2+\left(y-\frac{1}{2}\right)^2}{\varepsilon}\right)-\exp\left(-\frac{1}{4\varepsilon}\right)\right]^2.$$

In the numerical calculations, we set the parameters as $\alpha = 0.5$, $N_t = 100$, and $\varepsilon = 10^{-3}$. The finite element method is employed to solve the equation under three mesh configurations: a uniform mesh, a moving graded mesh, and a moving triangle mesh. To examine the impact of these mesh strategies on numerical accuracy, we configure the moving graded mesh with parameters $\tau_c = 0.01$ and $c_1 = 1.4$, and the moving triangle mesh with $\tau_c = 0.01$ and $c_1 = 500$. The L^∞ and L^2 norm errors of the computed solution at the final time are evaluated under varying numbers of mesh elements, as summarized in Table 1. Because these three methods employ different mesh structures, and the fact that moving meshes do not simply yield higher accuracy by increasing the number of elements, we cannot configure them with the exact same element count. Nevertheless, we ensure a fair comparison. On the one hand, the moving mesh methods can achieve significantly higher accuracy even with fewer elements. On the other hand, we maintain closely matched total element counts; for example, the moving graded mesh with $N = 2\times40\times40$ yields 3200 triangular elements, which is highly comparable to the 3600 elements in the moving triangle mesh with $N = 4\times30\times30$. Furthermore, to better illustrate the spatial distribution of numerical errors, we present the surface plot of the exact solution, along with scatter plots of the pointwise absolute errors at nodal locations for the three mesh types, as shown in Fig. 4.

In addition, to simulate the case of multiple blow-up points, we choose the exact solutions with multiple peaks as

$$u(x,y,t) = 100(\log t)^2\left[\exp\left(-\frac{\left(x-\frac{1}{4}\right)^2+\left(y-\frac{1}{4}\right)^2}{\varepsilon}\right)+\exp\left(-\frac{\left(x-\frac{3}{4}\right)^2+\left(y-\frac{3}{4}\right)^2}{\varepsilon}\right)-\exp\left(-\frac{1}{4\varepsilon}\right)\right]$$

and

$$u(x,y,t) = 100(\log t)^2\left[\exp\left(-\frac{\left(x-\frac{1}{4}\right)^2+\left(y-\frac{1}{4}\right)^2}{\varepsilon}\right)+\exp\left(-\frac{\left(x-\frac{3}{4}\right)^2+\left(y-\frac{3}{4}\right)^2}{\varepsilon}\right)\right.$$
$$\left.+\exp\left(-\frac{\left(x-\frac{1}{4}\right)^2+\left(y-\frac{3}{4}\right)^2}{\varepsilon}\right)+\exp\left(-\frac{\left(x-\frac{3}{4}\right)^2+\left(y-\frac{1}{4}\right)^2}{\varepsilon}\right)-\exp\left(-\frac{1}{4\varepsilon}\right)\right].$$

We set $\alpha = 0.5$, $N_t = 100$, and $\varepsilon = 10^{-3}$. The moving graded mesh method uses parameters $\tau_c = 0.01$ and $c_1 = 2$, whereas the moving triangle mesh method uses $\tau_c = 0.01$ and $c_1 = 5000$. Figs. 5 and 6 present a visual comparison between the surface of the exact solution and the absolute errors of the numerical solution computed on the three types of meshes.

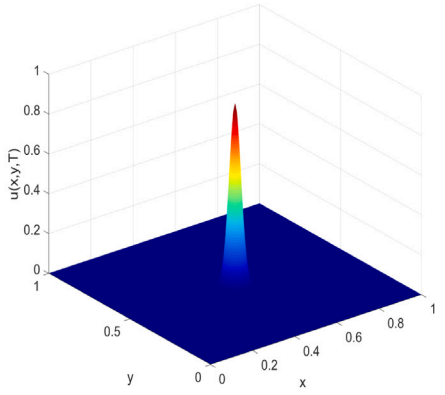
Example 4.1 shows that the two moving mesh methods effectively simulate peak-type solutions, indicating their potential applications for blow-up problems. More importantly, Table 1 and Figs. 4–6 demonstrate that even with the same and relatively small number of nodes, moving mesh methods achieve significantly higher accuracy. Fixed uniform meshes suffer from severe spurious oscillations near sharp gradients, whereas moving meshes effectively reduce both L^∞ and L^2 errors. As noted in Remark 4.3, the solution loses its high spatial regularity ($H^2(\Omega)$) as it approaches the blow-up time. By dynamically aggregating nodes around the singularity, moving meshes successfully compensate for this severe regularity degradation, thereby preserving numerical stability and precisely resolving the sharp profile.

Example 4.2. Consider the following time-fractional Keller–Segel system with $\alpha \in (0,1)$ in a square domain:

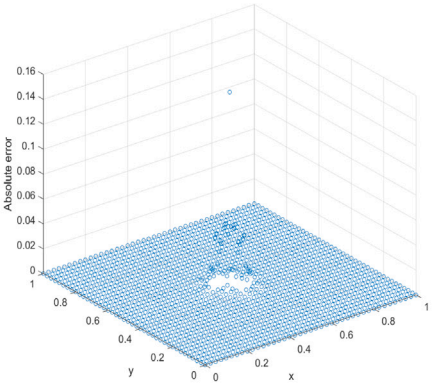
$$\begin{cases} {}_{CH}\mathrm{D}^{\alpha}_{a,t}u = \Delta u - \nabla\cdot(u\nabla v), & \mathrm{x}\in\Omega=(-0.5,0.5)^2,\ t>a=1,\\ {}_{CH}\mathrm{D}^{\alpha}_{a,t}v = \Delta v - \gamma v + u, & \mathrm{x}\in\Omega=(-0.5,0.5)^2,\ t>a=1,\\ \dfrac{\partial u}{\partial \mathbf{n}} = \dfrac{\partial v}{\partial \mathbf{n}} = 0, & \mathrm{x}\in\partial\Omega,\ t>a=1. \end{cases} \tag{4.57}$$

The physical parameter γ is chosen to be equal to 1. The initial conditions are given by

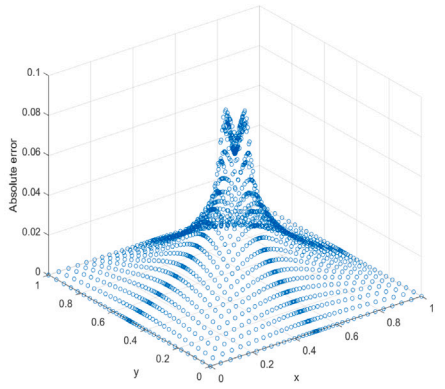
$$\begin{cases} u(x,y,0) = 400\exp(-40(x^2+y^2)),\\ v(x,y,0) = 50\exp(-5(x^2+y^2)). \end{cases}$$



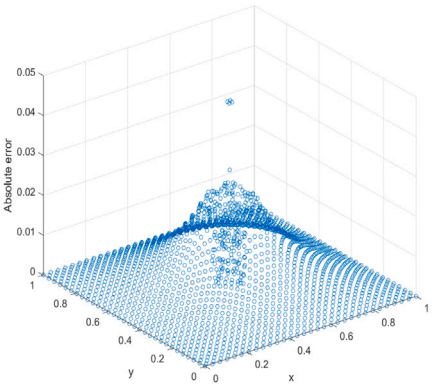
(a) Exact solution at T.



(b) Absolute error of the numerical solution on the uniform mesh at T with $N = 2 \times 40 \times 40$.



(c) Absolute error of the numerical solution on the moving graded mesh at T with $N = 2 \times 40 \times 40$.

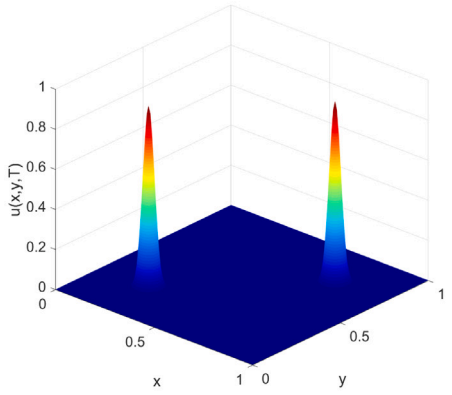


(d) Absolute error of the numerical solution on the moving triangle mesh at T with $N = 4 \times 30 \times 30$.

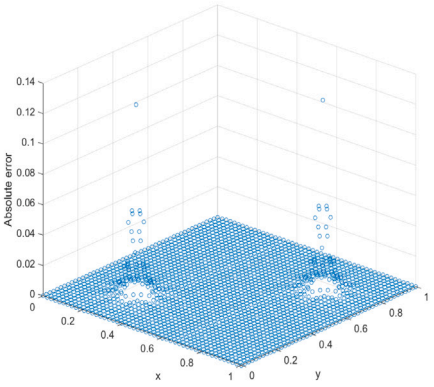
Fig. 4. Exact solution of Eq. (4.56) with one peak and absolute errors at T on three meshes.

We evaluate the numerical solution for $\alpha = 0.5$ using three types of meshes. The uniform mesh with $N = 2 \times 128 \times 128$ and $\tau = 2 \times 10^{-7}$. The solution is shown in Fig. 7, which displays the initial solutions and the numerical solution u at $t = 1 + 5 \times 10^{-6}$, $t = 1 + 1 \times 10^{-5}$, $1 + 2 \times 10^{-5}$, $1 + 3 \times 10^{-5}$ and $t = 1 + 4 \times 10^{-5}$, and v at $t = 1 + 4 \times 10^{-5}$. The solutions on moving graded mesh with $N = 2 \times 48 \times 48$ and moving triangle mesh with $N = 4 \times 40 \times 40$ and $\tau = 1 \times 10^{-6}$, where time is taken as $t = 1 + 3 \times 10^{-5}$. Their images are shown in Fig. 8. In the moving graded mesh method, we choose the parameters $\tau_c = 7.5 \times 10^{-3}$, $c_1 = 1.4$. In the moving triangle mesh, we choose the parameters $\tau_c = 1.5 \times 10^{-4}$, $c_1 = 500$.

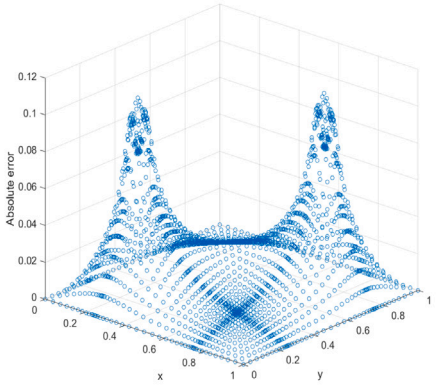
To capture the evolution progression of the solution, we show the variation of the numerical solution $u(0, y, t)$ on an adaptive mesh with $t = 1 + 1 \times 10^{-5}$, $t = 1 + 2 \times 10^{-5}$, $t = 1 + 3 \times 10^{-5}$, $t = 1 + 4 \times 10^{-5}$ and $t = 1 + 5 \times 10^{-5}$. The simulation is conducted under the parameter setting: $\alpha = 0.5$, $\tau = 1 \times 10^{-6}$, $N = 4 \times 36 \times 36$, $\tau_c = 10^{-2}$ and $c_1 = 5000$. The numerical results are shown in Fig. 9. An important physical property of the Keller–Segel system with homogeneous Neumann boundary conditions is the conservation of total mass. Preserving and monitoring this mass conservation is a valuable diagnostic tool in our numerical experiments, particularly as the solution approaches blow-up. Therefore, we continuously monitor the conservation of total mass $M^n = \int_\Omega u_h^n \mathrm{dx}$ during the numerical evolution. The maximum relative mass error $|M^n - M^0|/M^0$ ($< 1.2 \times 10^{-4}$), as illustrated in Fig. 10, is actually a combined result of the time-fractional approximation, the nonlinear treatment, and the standard rezoning interpolation. Importantly, this strategy, combined with the peak profile of the initial data, causes the mesh movement to progressively decrease over time until it



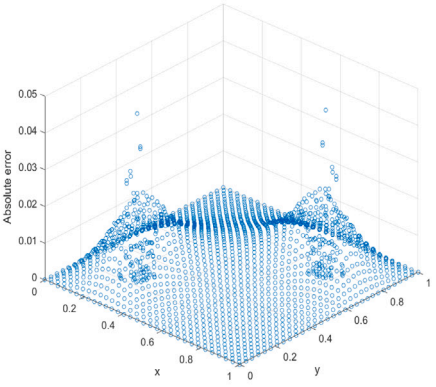
(a) Exact solution at T.



(b) Absolute error of the numerical solution on the uniform mesh at T with $N = 2 \times 48 \times 48$.



(c) Absolute error of the numerical solution on the moving graded mesh at T with $N = 2 \times 48 \times 48$.



(d) Absolute error of the numerical solution on the moving triangle mesh at T with $N = 4 \times 30 \times 30$.

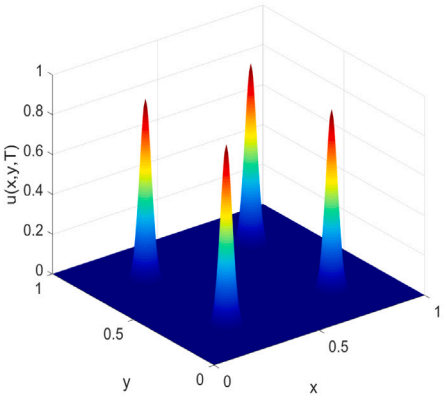
Fig. 5. Exact solution of Eq. (4.56) with two peaks and absolute errors at T on three meshes.

stops completely, because the maximum mesh density is controlled. As a result, the interpolation error introduced at each step is practically negligible.

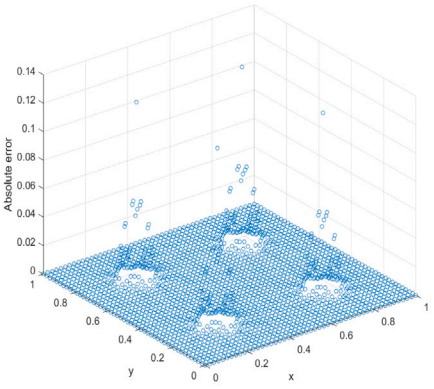
We examine how different values of α affect the blow-up time T of the solution. The blow-up threshold is numerically defined as the solution reaches a magnitude of 1×10^4. The relationship between the blow-up time and α (ranging from 0.1 to 0.9) is illustrated in Fig. 11, where the red region indicates the blow-up zone and the blue region represents the stable zone. As α increases, the blow-up time is progressively delayed. This observation effectively validates our theoretical premise regarding the influence of the fractional derivative. Unlike standard integer-order models, the Caputo–Hadamard fractional derivative incorporates a historical memory effect into the chemotaxis system. By tuning the fractional order α, the onset of the finite time blow-up predicted in Theorem 3.2 can be quantitatively controlled and delayed, which proves that our fractional model is highly capable of capturing anomalous and delayed chemotactic behaviors in biological processes.

The initial conditions also play a pivotal role in determining the onset time of blow-up. To examine this influence, we construct a parameterized initial values

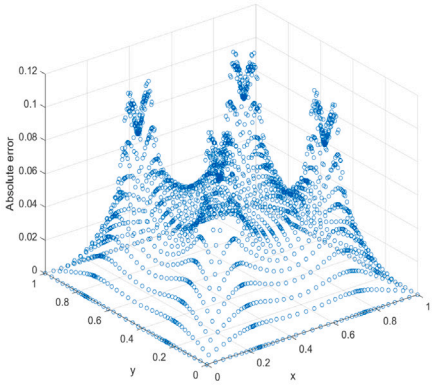
$$\begin{cases} u(x, y, 0) = 100p \exp(-10p(x^2 + y^2)), \\ v(x, y, 0) = 10p \exp(-p(x^2 + y^2)), \end{cases}$$



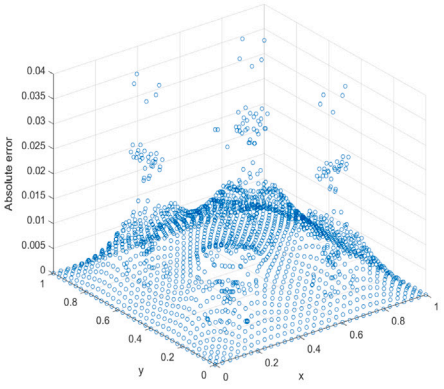
(a) Exact solution at T.



(b) Absolute error of the numerical solution on the uniform mesh at T with $N = 2 \times 48 \times 48$.



(c) Absolute error of the numerical solution on the moving graded mesh at T with $N = 2 \times 48 \times 48$.



(d) Absolute error of the numerical solution on the moving triangle mesh at T with $N = 4 \times 30 \times 30$.

Fig. 6. Exact solution of Eq. (4.56) with four peaks and absolute errors at T on three meshes.

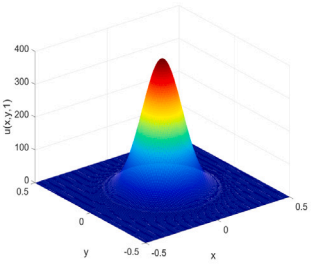
where the parameter p is systematically varied within the range from 2 to 10. For each parameter setting, we monitor the evolution of the numerical solution U and record the time at which it first exceeds the critical threshold of 1×10^4 (as blow-up time). Their relationship is shown in Fig. 12. This approach allows us to quantitatively assess how variations in initial conditions affect the dynamic and time of blow-up response, offering insights into the sensitivity of the system to initial perturbations.

In addition, we test numerical solutions with multiple blow-up points using different meshes. The parameter $\alpha = 0.5$ is fixed. Firstly, we compute the numerical solution on a uniform mesh with $N = 2 \times 128 \times 128$ and $\tau = 1 \times 10^{-6}$. The resulting 3D surface plots and their corresponding 2D contour plots for two and four blow-up points are shown in Fig. 13.

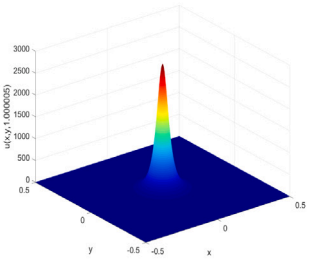
In the case of two blow-up points, we use the moving graded method with the parameters $N = 2 \times 50 \times 50$, $\tau_c = 0.025$, $c_1 = 1.5$, and the moving triangle method with the parameters $N = 4 \times 45 \times 45$, $\tau_c = 10^{-4}$, $c_1 = 5000$. Their 3D and 2D contour results are shown in Fig. 14.

In the case of four blow-up points, we use the moving graded method with the parameters $N = 2 \times 50 \times 50$, $\tau_c = 0.01$, $c_1 = 1.4$, and the moving triangle method with the parameters $N = 4 \times 42 \times 42$, $\tau_c = 10^{-3}$, $c_1 = 2000$. The corresponding results are shown in Fig. 15.

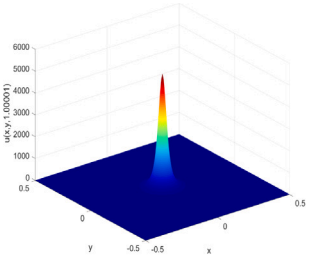
To improve the readability of these multi-point blow-up cases, we have additionally provided 2D contour plots in Figs. 13(d)–(e), 14(e)–(f), and 15(e)–(f). Compared to the traditional 3D surface plots, these 2D representations more intuitively and quantitatively



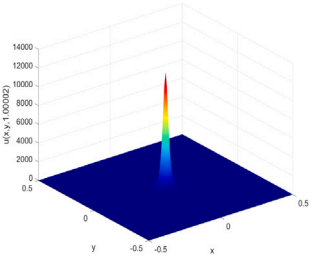
(a) Initial value of u.



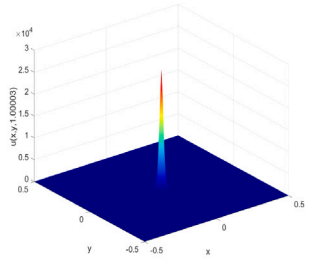
(b) u at $t = 1 + 5 \times 10^{-6}$.



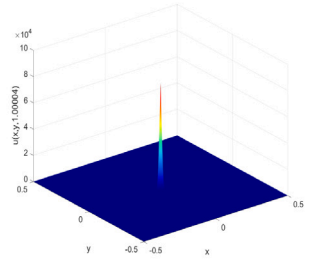
(c) u at $t = 1 + 1 \times 10^{-5}$.



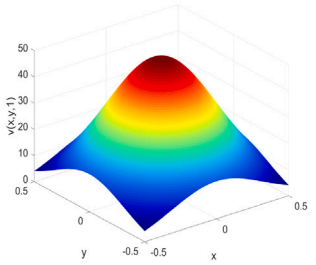
(d) u at $t = 1 + 2 \times 10^{-5}$.



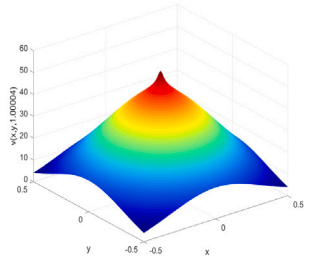
(e) u at $t = 1 + 3 \times 10^{-5}$.



(f) u at $t = 1 + 4 \times 10^{-5}$.

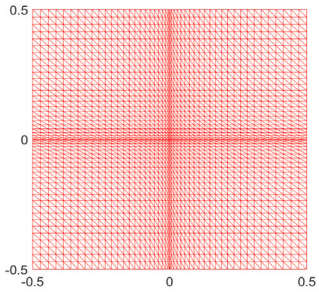


(g) Initial value of v.

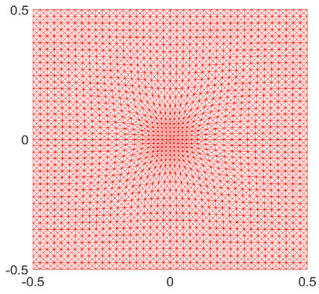


(h) v at $t = 1 + 3.75 \times 10^{-5}$.

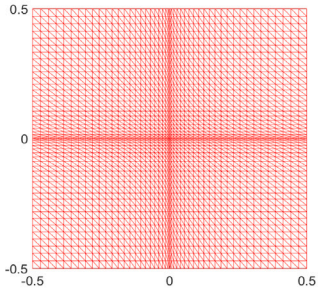
Fig. 7. Numerical solutions of (4.57) with $N = 2 \times 128 \times 128$, $\tau = 2 \times 10^{-7}$ and $\alpha = 0.5$. (a) $u(x, y, t)$ at $t = 1$, (b) $u(x, y, t)$ at $t = 1 + 1 \times 10^{-6}$, (c) $u(x, y, t)$ at $t = 1 + 1 \times 10^{-5}$, (d) $u(x, y, t)$ at $t = 1 + 2 \times 10^{-5}$, (e) $u(x, y, t)$ at $t = 1 + 3 \times 10^{-5}$, (f) $u(x, y, t)$ at $t = 1 + 4 \times 10^{-5}$, (g) $v(x, y, t)$ at $t = 1$, (h) $v(x, y, t)$ at $t = 1 + 4 \times 10^{-5}$.



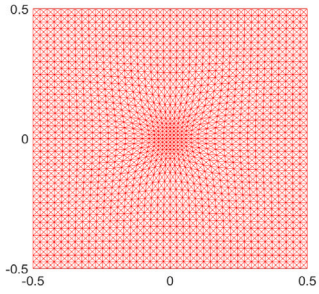
(a) Moving graded mesh at initial time.



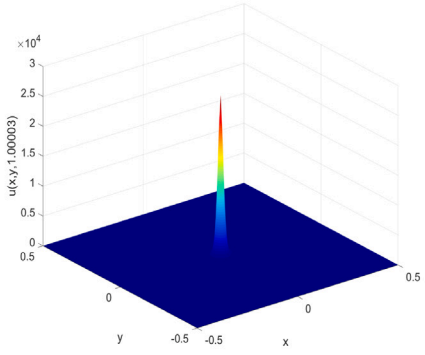
(b) Moving triangle mesh at initial time.



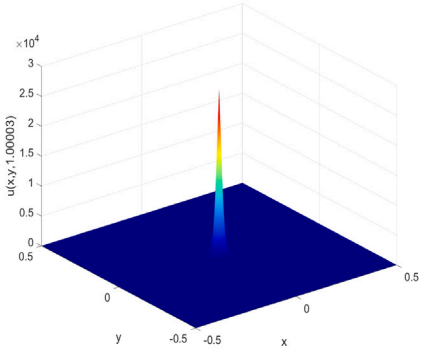
(c) Moving graded mesh at $t = 1 + 3 \times 10^{-5}$.



(d) Moving triangle mesh at $t = 1 + 3 \times 10^{-5}$.



(e) The numerical solution of (4.57) on the moving graded mesh.



(f) The numerical solution of (4.57) on the moving triangle mesh.

Fig. 8. (a) Moving graded mesh at initial time with $N = 2 \times 48 \times 48$, (b) Moving triangle mesh at initial time with $N = 4 \times 40 \times 40$. (c) Moving graded mesh at $t = 1+3\times10^{-5}$ with $N = 2\times48\times48$, (d) Moving triangle mesh at $t = 1+3\times10^{-5}$ with $N = 4\times40\times40$. (e) $u(x, y, t)$ at $t = 1+3\times10^{-5}$ on mesh (c) and $\tau = 1 \times 10^{-6}$, (f) $u(x, y, t)$ at $t = 1 + 3 \times 10^{-5}$ on mesh (d) and $\tau = 1 \times 10^{-6}$.

illustrate the precise spatial coordinates of the multiple blow-up points. Furthermore, for the adaptive mesh methods, the contour plots clearly demonstrate how the mesh elements highly concentrate exactly at these isolated aggregation regions, successfully avoiding any visual overlapping or obstruction caused by 3D perspective effects.

Numerical experiments validate our theoretical findings on the factors influencing the blow-up phenomenon. As confirmed in Figs. 11 and 12, the blow-up time is fundamentally governed by the initial conditions and the fractional order α. Specifically, the

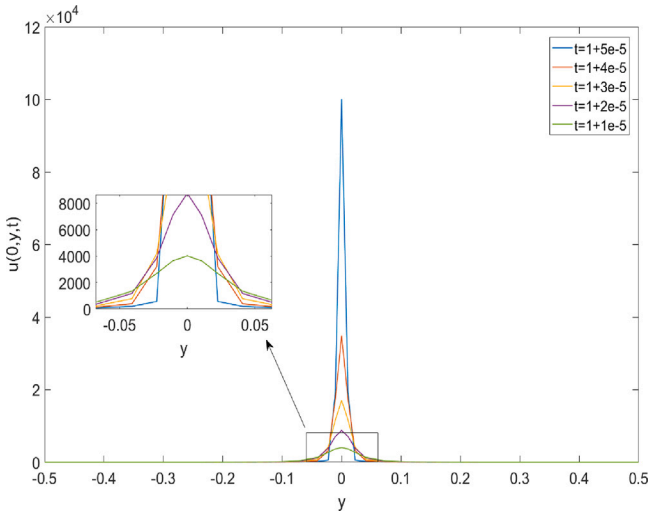


Fig. 9. The evolution of solution $u(0, y, t)$ for Eq. (4.57) with $N = 4 \times 36 \times 36$ and $\tau = 10^{-6}$.

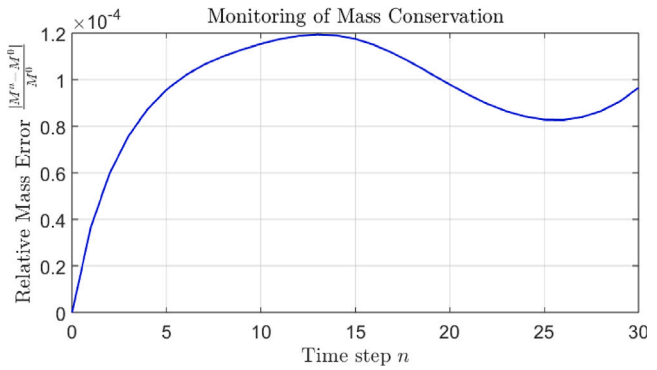


Fig. 10. Monitoring of mass conservation: evolution of the maximum relative mass error $|M^n - M^0|/M^0$ on the moving mesh over the time interval $t \in [1, 1 + 3 \times 10^{-5}]$.

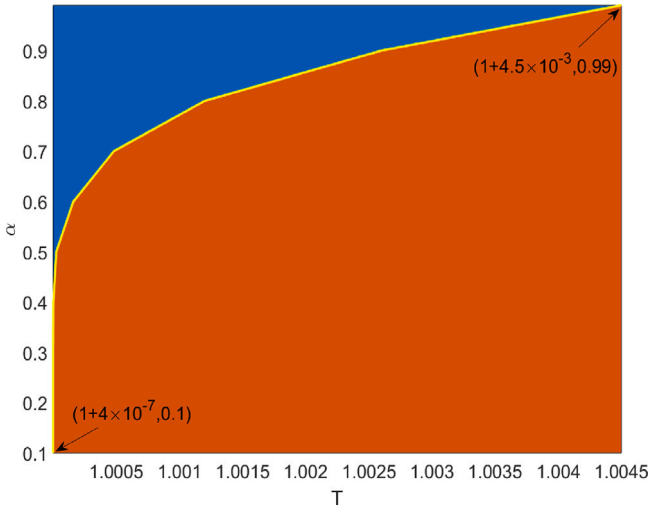


Fig. 11. The blow-up zone (red) and the stable zone (blue) on an adaptive mesh. (For interpretation of the references to color in this figure legend, the reader is referred to the web version of this article.)

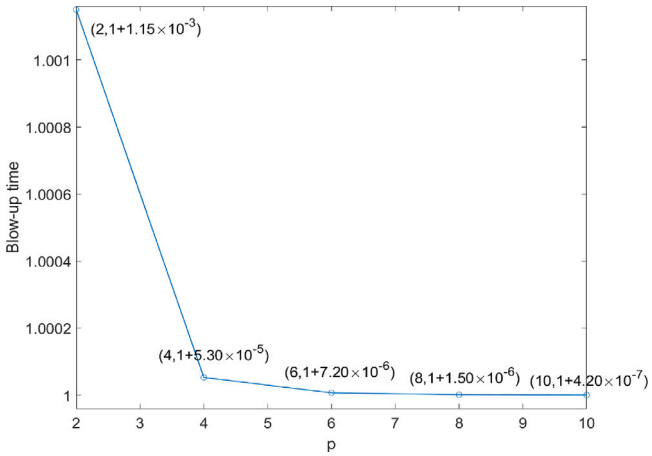


Fig. 12. Blow-up time vs. parameter p.

initial data dictate the system's sensitivity, while a larger α strengthens the memory effect of the Caputo–Hadamard derivative, effectively delaying the blow-up. Overall, these consistent results strongly demonstrate the effectiveness and robustness of the proposed moving mesh methods in simulating complex fractional chemotaxis systems with severe singularities.

5. Conclusion

This article investigates well-posedness and blow-up of Caputo–Hadamard time-fractional Keller–Segel system and presents effective moving mesh methods for single or multi-point blow-up problems. The proof of existence is based on $L^p - L^q$ estimates of the Mittag-Leffler type operators. Theoretical analysis indicates that both the solution behavior and the blow-up time are affected by the initial condition and the order of the fractional derivative, which is supported by numerical simulations. In addition, the two proposed moving mesh methods have been validated to be effective, providing more ideas for solving fractional blow-up problems.

CRediT authorship contribution statement

Dingding Cao: Writing – review & editing, Writing – original draft, Visualization, Methodology. **Changpin Li:** Writing – review & editing, Writing – original draft, Visualization, Supervision, Methodology. **Paul Andries Zegeling:** Writing – review & editing, Supervision, Methodology.

Ethics approval and consent to participate

This declaration is not applicable.

Funding

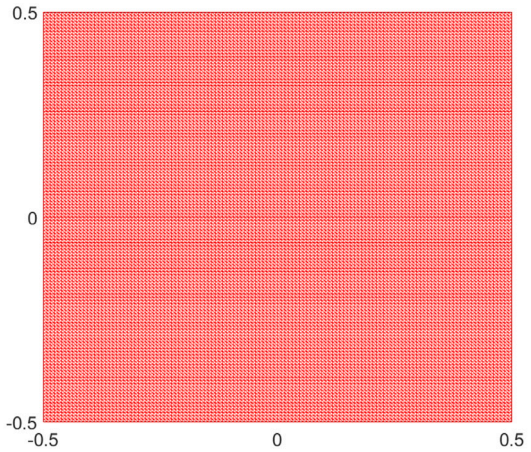
This work was partially supported by National Natural Science Foundation of China under Grant No. 12271339.

Declaration of competing interest

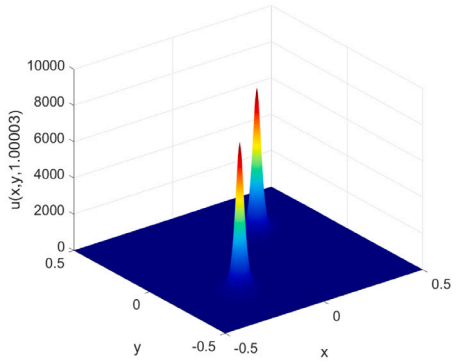
The authors declare that they have no conflict of interest.

Data availability

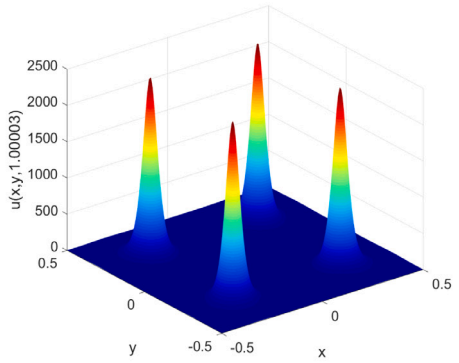
Data will be made available on reasonable request.



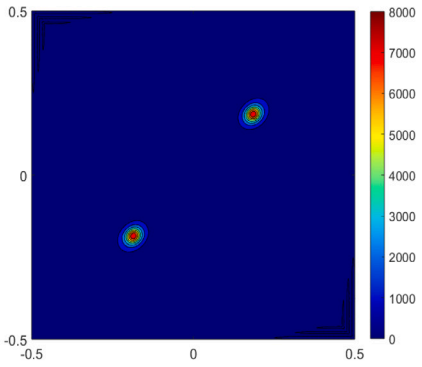
(a) Uniform mesh with $N = 2 \times 128 \times 128$.



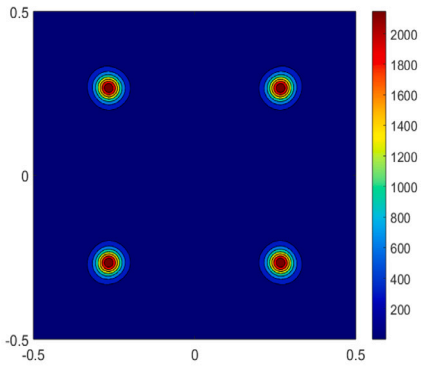
(b) The numerical solution with two blow-up points on a uniform mesh.



(c) The numerical solution with four blow-up points on a uniform mesh.

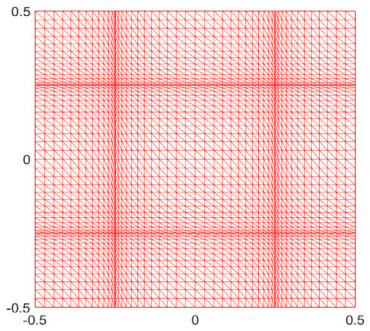


(d) The contour of the solution in (b).

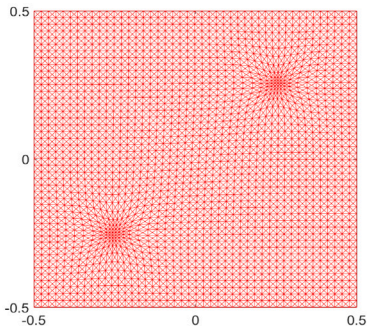


(e) The contour of the solution in (c).

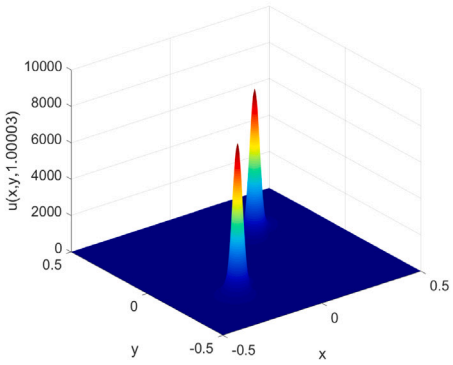
Fig. 13. The numerical solutions on a uniform mesh. (a) Uniform mesh with $N = 2 \times 128 \times 128$; (b) 3D surface plot of $u(x, y, t)$ of two blow-up points at $t = 1 + 3 \times 10^{-5}$; (c) 3D surface plot of $u(x, y, t)$ of four blow-up points at $t = 1 + 3 \times 10^{-5}$; (d) 2D contour plot corresponding to the two blow-up points in (b); (e) 2D contour plot corresponding to the four blow-up points in (c).



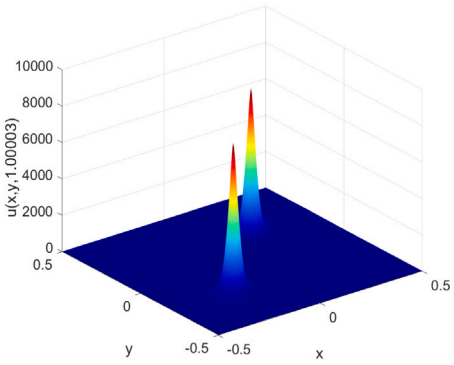
(a) Moving graded mesh at $t = 1 + 3 \times 10^{-5}$.



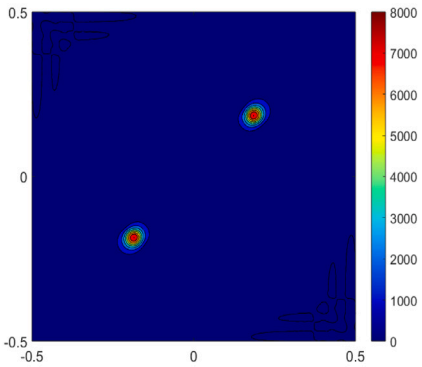
(b) Moving triangle mesh at $t = 1 + 3 \times 10^{-5}$.



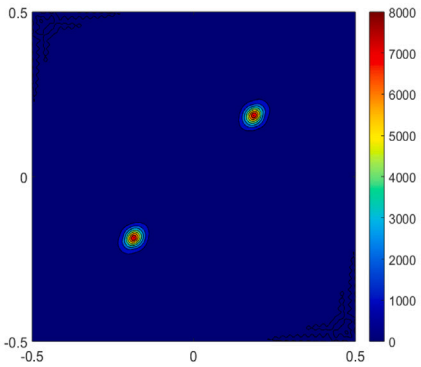
(c) The numerical solution on the moving graded mesh.



(d) The numerical solution on the moving triangle mesh.

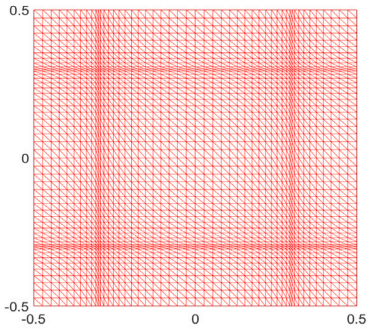


(e) The contour of the solution in (c).

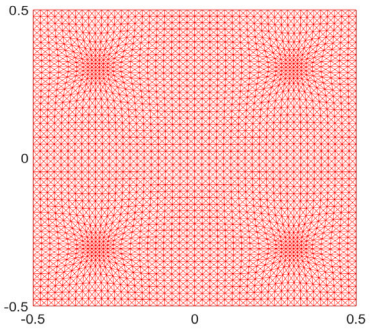


(f) The contour of the solution in (d).

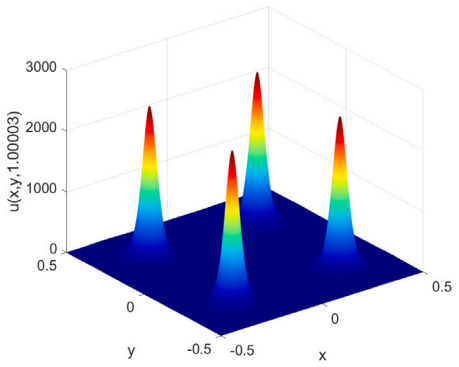
Fig. 14. (a) Moving graded mesh at initial time with $N = 2 \times 50 \times 50$; (b) Moving triangle mesh at initial time with $N = 4 \times 45 \times 45$. (c) 3D surface plot of $u(x, y, t)$ at $t = 1 + 3 \times 10^{-5}$ on the moving grade mesh with $N = 2 \times 50 \times 50$; (d) 3D surface plot of $u(x, y, t)$ at $t = 1 + 3 \times 10^{-5}$ on the moving triangle mesh with $N = 4 \times 45 \times 45$; (e) 2D contour plot corresponding to the solution in (c); (f) 2D contour plot corresponding to the solution in (d).



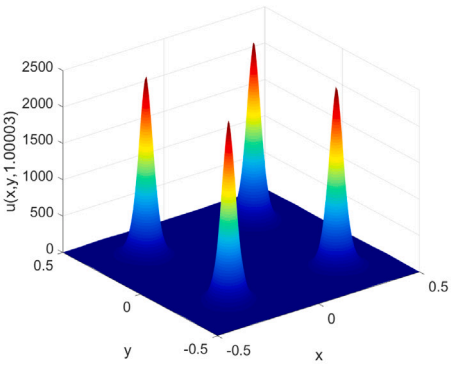
(a) Moving graded mesh at $t = 1 + 3 \times 10^{-5}$.



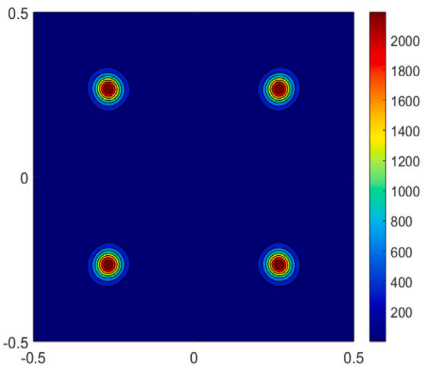
(b) Moving triangle mesh at $t = 1 + 3 \times 10^{-5}$.



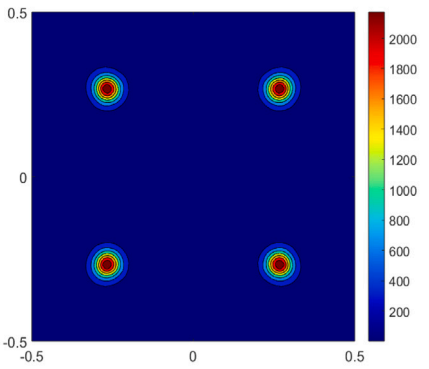
(c) The numerical solution on the moving graded mesh.



(d) The numerical solution on the moving triangle mesh.



(e) The contour of the solution in (c).



(f) The contour of the solution in (d).

Fig. 15. (a) Moving graded mesh at initial time with $N = 2 \times 50 \times 50$; (b) Moving triangle mesh at initial time with $N = 4 \times 42 \times 42$. (c) 3D surface plot of $u(x, y, t)$ at $t = 1 + 3 \times 10^{-5}$ on the moving graded mesh with $N = 2 \times 50 \times 50$; (d) 3D surface plot of $u(x, y, t)$ at $t = 1 + 3 \times 10^{-5}$ on the moving triangle mesh with $N = 4 \times 42 \times 42$; (e) 2D contour plot corresponding to the solution in (c); (f) 2D contour plot corresponding to the solution in (d).

References

[1] E.F. Keller, L.A. Segel, Initiation of slime mold aggregation viewed as an instability, J. Theoret. Biol. 26 (3) (1970) 399–415.
[2] S.I. Dejak, D. Egli, P.M. Lushnikov, I.M. Sigal, On blow up dynamics in the Keller–Segel model of chemotaxis, St. Petersburg Math. J. 25 (4) (2014) 547–574.
[3] S.G. Samko, A.A. Kilbas, O.I. Marichev, Fractional Integrals and Derivatives: Theory and Applications, Gordon and Breach Science Publishers, Amsterdam, 1993.
[4] A.A. Kilbas, H.M. Srivastava, J.J. Trujillo, Theory and Applications of Fractional Differential Equations, Elsevier, Amsterdam, 2006.
[5] C.P. Li, M. Cai, Theory and Numerical Approximations of Fractional Integrals and Derivatives, SIAM, Philadelphia, USA, 2019.
[6] V. Nanjundiah, Chemotaxis, signal relaying and aggregation morphology, J. Theoret. Biol. 42 (1) (1973) 63–105.
[7] J. Azevedo, C. Cuevas, E. Henríquez, Existence and asymptotic behaviour for the time-fractional Keller–Segel model for chemotaxis, Math. Nachr. 292 (3) (2019) 462–480.
[8] C. Cuevas, C. Silva, H. Soto, On the time-fractional Keller–Segel model for chemotaxis, Math. Methods Appl. Sci. 43 (2) (2020) 769–798.
[9] A. Akilandeeswari, J. Tyagi, Nonnegative solutions to time fractional Keller–Segel system, Math. Methods Appl. Sci. 44 (2) (2021) 1812–1830.
[10] N.A. Tuan, N.H. Tuan, C. Yang, On Cauchy problem for fractional parabolic–elliptic Keller–Segel model, Adv. Nonlinear Anal. 12 (1) (2023) 97–116.
[11] M. Costa, C. Cuevas, C. Silva, H. Soto, Well-posedness and blow-up of the fractional Keller–Segel model on domains, Math. Nachr. 296 (12) (2023) 5569–5592.
[12] Z. Jiang, L.Z. Wang, Existence and asymptotic stability of mild solution to fractional Keller–Segel-Navier–Stokes system, Math. Methods Appl. Sci. 47 (12) (2024) 9814–9833.
[13] F. Gao, L.J. Guo, X.Y. Xie, H. Zhan, Global existence, uniqueness and L^{∞}-bound of weak solutions of fractional time-space Keller–Segel system, Fract. Calc. Appl. Anal. 28 (1) (2025) 232–275.
[14] W.Z. Huang, R.D. Russell, Adaptive Moving Mesh Methods, Springer, New York, 2011.
[15] C.J. Budd, W.Z. Huang, R.D. Russell, Adaptivity with moving grids, Acta Numer. 18 (2009) 111–241.
[16] W.Z. Huang, L. Kamenski, A geometric discretization and a simple implementation for variational mesh generation and adaptation, J. Comput. Phys. 301 (2015) 322–337.
[17] C.P. Li, Z.Q. Li, Asymptotic behaviours of solution to Caputo-Hadamard fractional partial differential equation with fractional Laplacian, Int. J. Comput. Math. 98 (2) (2021) 305–339.
[18] M. Gohar, C.P. Li, Z.Q. Li, Finite difference methods for Caputo-Hadamard fractional differential equations, Mediterr. J. Math. 17 (6) (2020) 194.
[19] A. Alsaedi, B. Ahmad, M. Kirane, R. Lassoued, Global existence and large time behavior of solutions of a time fractional reaction diffusion system, Fract. Calc. Appl. Anal. 23 (2) (2020) 390–407.
[20] M. Winkler, Aggregation vs, Global diffusive behavior in the higher-dimensional Keller–Segel model, J. Differ. Equ. 248 (12) (2010) 2889–2905.
[21] R.N. Wang, D.H. Chen, T.J. Xiao, Abstract fractional Cauchy problems with almost sectorial operators, J. Differential Equations 252 (1) (2012) 202–235.
[22] T. Kato, Strong solutions of the Navier–Stokes equations in Morrey-spaces, Bol. Soc. Bras. Mat. 22 (2) (1992) 127–155.
[23] J. Dixon, S. McKee, Weakly singular discrete Grönwall inequalities, Z. Angew. Math. Mech. 66 (11) (1986) 535–544.
[24] J.R.L. Webb, A fractional Grönwall inequality and the asymptotic behaviour of global solutions of Caputo fractional problems, Electron. J. Differential Equations 2021 (80) (2021) 1–22.
[25] M.A. Beauregard, Q. Sheng, An adaptive splitting approach for the quenching solution of reaction–diffusion equations over nonuniform grids, J. Comput. Appl. Math. 241 (2013) 30–44.
[26] J.L. Padgett, Q. Sheng, Numerical solution of degenerate stochastic Kawarada equations via a semi-discretized approach, Appl. Math. Comput. 325 (2018) 210–226.
[27] N. Saito, Error analysis of a conservative finite-element approximation for the Keller–Segel system of chemotaxis, Commun. Pure Appl. Anal. 11 (1) (2012) 339–364.
[28] Y.F. Xu, Z.S. Zheng, Quenching phenomenon of a time-fractional diffusion equation with singular source term, Math. Methods Appl. Sci. 40 (16) (2017) 5750–5759.
[29] D.D. Cao, C.P. Li, Quenching phenomenon in the Caputo-Hadamard time-fractional Kawarada problem: analysis and computation, Math. Comput. Simulation 233 (2025) 21–38.
[30] P.A. Zegeling, Tensor-product adaptive grids based on coordinate transformations, J. Comput. Appl. Math. 166 (1) (2004) 343–360.
[31] A.S. Dvinsky, Adaptive grid generation from harmonic maps on Riemannian manifolds, J. Comput. Phys. 95 (2) (1991) 450–476.
[32] W.Z. Huang, Variational mesh adaptation: isotropy and equidistribution, J. Comput. Phys. 174 (2) (2001) 903–924.
[33] W.Z. Huang, L. Kamenski, On the mesh nonsingularity of the moving mesh PDE method, Math. Comp. 87 (312) (2018) 1887–1911.
[34] E.Y. Fan, C.P. Li, The moving mesh finite element methods for solving Caputo-Hadamard fractional evolution equations: from sharp solution to blow-up solution, J. Nonlinear Sci. 35 (5) (2025) 101.